BAW-1283, Ca-7
AEC R&D Report
TID-4500, 23rd Ed.
UC-80

SPECTRAL SHIFT CONTROL REACTOR BASIC PHYSICS PROGRAM

Measurement of k_∞ and Other Lattice Parameters by the Small Lattice Experiment Technique

November 1963

By

T. C. Engelder, N. L. Snidow, D. M. Roberts, and G. T. Fairburn

Critical Experiment Laboratory
Research & Development Division

and

D. H. Roy
Engineering Department
Atomic Energy Division

Submitted to
THE UNITED STATES ATOMIC ENERGY COMMISSION
by
THE BABCOCK & WILCOX COMPANY
Nuclear Development Center
Lynchburg, Virginia

DISCLAIMER

ACKNOWLEDGMENT

The authors thank D. B. Wehmeyer for assistance in developing the theoretical basis for these experiments, and K. E. Roach for the interpretation of the initial results. We are also highly indebted to J. M. Doederlein, on loan from the Institute for Atomic Energy, Kjeller, Norway, who performed all of the nuclear design calculations and actively participated in fundamental design decisions during the formative stages of this program.

The Babcock & Wilcox Company
Nuclear Development Center
Report BAW-1283

ABSTRACT

The Small Lattice Experiment (SLE) is a technique for measuring k_∞ and other infinite-medium lattice parameters using much less test fuel than is required for equivalent critical or exponential experiments. The theoretical basis for applying such an experiment to epithermal lattices is discussed, an analysis of spectral mismatch error is given, and the facility for the measurements is described. SLE measurements are compared to those in an equivalent critical assembly to test the validity of the technique. In an epithermal lattice of 4.02%-enriched UO_2 fuel rods having a nonmoderator-to-moderator volume ratio of 1.0 and moderated by a D_2O-H_2O mixture containing 70% D_2O, values of k_∞, $\overline{\phi}_m/\overline{\phi}_f$, δ_{25}, and ρ_{28} agree within statistical errors (0.5 to 1%). The SLE technique was also used to measure these parameters in two similar epithermal lattices containing (U-235-ThO_2) fuel rods ($N_{Th}/N_{25} = 15$).

CONTENTS

CONTENTS (Cont'd)

List of Tables

List of Figures

Figures (Cont'd)

Page

Figure

1. INTRODUCTION

The small lattice experiment (SLE) is a method of measuring k_∞ and other infinite medium lattice parameters, such as $\overline{\phi}_m/\overline{\phi}_f$, and δ_{25}, and ρ_{28}, using much less test fuel than is required for equivalent critical or exponential experiments. The procedures developed here represent an extension to epithermal systems of the original Physical Constant Test Reactor (PCTR)[1] technique for thermal reactor studies. Similar thermal reactor measurements have also been made in the Pawling Lattice Test Rig (PLATR).[2]

The facility in which these experiments are performed is a three-region critical assembly. The central test region, containing the medium of fuel and moderator to be studied, is surrounded by a buffer region having similar but not necessarily identical nuclear properties. The outer driver region is loaded with sufficient fuel of any convenient type to make the entire assembly critical. If the nuclear properties of the buffer region can be adjusted such that an asymptotic neutron spectrum is established throughout the test region, then the lattice parameters of the test region can be measured by standard techniques. Futhermore, the k_∞ of the test region medium can be derived from the quantity of poison that reduces the k_∞ to unity. This condition occurs when the reactivity difference between the poisoned test region and a void (k_∞ = 1.00) is zero.

Although the validity of the small lattice experiment technique for thermal assemblies has been firmly established as a result of extensive PCTR and PLATR experience, the SLE extension to epithermal systems involves additional considerations and requires confirmation. Therefore, the objective of the program described here was twofold: (1) to develop a more general theory of the technique applicable to both thermal and epithermal systems and (2) to confirm the approach by comparing small lattice and critical experiment measurements in the same epithermal

lattice. The reference lattice consisted of 4.02%-enriched UO_2 fuel rods having a nonmoderator-to-moderator volume ratio (M/W) of 1.0 and moderated by a D_2O-H_2O mixture containing 70% D_2O. Approximately 50% of the fissions and 90% of the U-238 absorptions in this lattice were epithermal.

The theoretical basis for k_∞ measurements, the facility for small lattice experiments, the experimental techniques, and the results of the measurements in the reference lattice are given in the following sections of this report. Since good agreement between small lattice experiment and critical experiment results was obtained for the reference lattice, the small lattice experiment technique was then employed for measurements on two epithermal lattices of 93%-enriched UO_2-ThO_2 (N_{Th}/N_{25} = 15) fuel rods. These data are also included for completeness.

The work described in this report constitutes one phase of the Spectral Shift Control Reactor (SSCR) Basic Physics Program, an AEC-supported study of the physics of slightly enriched uranium (and thorium) lattices moderated by D_2O-H_2O mixtures.[3,4] The small lattice experiment technique was developed under this program as a means of reducing the quantity of fuel required for useful experiments and in preparation for eventual studies of U-233 fueled lattices. Whereas critical experiments of the SSCR type require about 5000 slightly enriched UO_2 rods containing 150 to 300 kg of U-235, equivalent small lattice experiments can be performed with less than 1% of this fuel. Availability of U-233 is so limited that large critical experiments using this fuel are impractical, and minimum inventory techniques, such as the small lattice experiment, must be employed.

2. THEORETICAL BASIS

The infinite medium multiplication factor k_∞ can be defined as:

$$k_\infty = \frac{\text{total neutrons from fission}}{\text{total neutrons absorbed}} \tag{2-1}$$

Several four-factor representations of k_∞ are possible if the factors are properly defined to form a consistent set. For U-235-fueled systems in which nonthermal fissions must be considered, k_∞ can be written as:

$$k_\infty = \eta_{25}^{th} f \epsilon p (1 + \delta_{25}^{\infty}) \tag{2-2}$$

This expression is exact providing the factors are defined for an infinite medium as follows:

$$\eta_{25}^{th} = \frac{\text{fission neutrons from thermal absorptions in U-235}}{\text{thermal neutrons absorbed in U-235}}$$

$$f = \frac{\text{thermal neutrons absorbed in U-235}}{\text{total thermal neutrons absorbed}}$$

$$\epsilon = \frac{\text{total fission neutrons from U-235 and U-238}}{\text{total fission neutrons from U-235}}$$

$$p = \frac{\text{total thermal neutrons absorbed}}{\text{total neutrons absorbed}}$$

$$1 + \delta_{25}^{\infty} = \frac{\text{total fission neutrons from U-235}}{\text{fission neutrons from thermal absorptions in U-235}}$$

In an idealized small lattice experiment it is assumed that, when the test region is poisoned so that a null-reactivity condition exists between the poisoned test region and a void, k_∞ of the poisoned test region is exactly equal to that of a void, i.e., unity. This assumption implies that the spectrum in the poisoned test region is that of an infinite poisoned medium and that there is a detailed neutron balance in space, energy, and angle over the surface of the test region. This condition corresponds to a flat flux and perfect spectral match with no net leakage over the entire test region.

The consequences of mismatch are discussed in Appendix A. However, if ideal conditions are achieved, Equation 2-2 for the poisoned test region becomes

$$1 = (\eta_{25}^{th} f \epsilon p)_p (1 + \delta_{25}^{\infty})_p \tag{2-3}$$

where the subscript p refers to the poisoned medium. Then the infinite medium multiplication factor of the unpoisoned medium is simply

$$k_\infty = \left(\frac{\eta^{th}}{\eta_p^{th}}\right)\left(\frac{f}{f_p}\right)\left(\frac{\epsilon}{\epsilon_p}\right)\left(\frac{p}{p_p}\right)\frac{(1 + \delta_{25}^{\infty})}{(1 + \delta_{25}^{\infty})_p} \tag{2-4}$$

In these experiments the change in η^{th} due to the shift in the thermal spectrum when the medium is poisoned is negligibly small, because η for U-235 is essentially constant over the thermal range. Therefore, Equation 2-4 can be written

$$k_\infty = \left(\frac{f}{f_p}\right)\left(\frac{\epsilon}{\epsilon_p}\right)\left(\frac{p}{p_p}\right)\frac{(1 + \delta_{25}^{\infty})}{(1 + \delta_{25}^{\infty})_p} \tag{2-5}$$

Another modification to Equation 2-4 can be made. As will be shown below, one approach to the derivation of k_∞ from small lattice experiments involves the measurement of δ_{25}, the ratio of the epithermal to thermal fission rate in the unpoisoned and poisoned test medium. δ_{25} is derived from C_{25}, the measured U-235 cadmium ratio, through the relation, $\delta_{25} = 1/(C_{25} - 1)$. Since the infinite medium δ_{25} cannot be measured in a practical experiment of finite dimensions, the finite medium δ_{25} is used in Equation 2-4, and a small correction L is applied to account for the difference between δ_{25}^{∞} and δ_{25}. Thus,

$$k_\infty = \left(\frac{f}{f_p}\right)\left(\frac{\epsilon}{\epsilon_p}\right)\left(\frac{p}{p_p}\right)\frac{(1 + \delta_{25})}{(1 + \delta_{25})_p} L \tag{2-6}$$

where

$$L = \left(\frac{1 + P_{NL}^{th} \delta_{25}}{1 + \delta_{25}}\right)\left(\frac{1 + \delta_{25}}{1 + P_{NL}^{th} \delta_{25}}\right)_p \tag{2-7}$$

In this expression, δ_{25} is the experimental quantity measured in the finite system and P_{NL}^{th} is the nonleakage probability of thermal neutrons in the system in which δ_{25} is measured.

The correction L can be derived by using the modified two-group formulation

$$k_\infty = \eta^{th} f \epsilon p + \eta^r \epsilon p_{28} (1 - p_{25}).$$

In a finite system the epithermal and thermal fission rates are

$$\Sigma^r \phi^r p_{28}(1 - p_{25})\eta^r/\nu \quad \text{and} \quad \Sigma_{25}^{th} \phi^{th} \eta^{th}/\nu .$$

Since $\Sigma^r \phi^r$ is the rate at which neutrons are slowed down into the resonance region and $\Sigma_{25}^{th} \phi^{th}$ is the thermal fission rate in U-235, the two terms are related as follows:

$$\Sigma_{25}^{th} \phi^{th} = \Sigma^r \phi^r P_{NL}^{th} fp$$

Therefore, the ratio of the epithermal to thermal fission rate is

$$\delta_{25} = \frac{p_{28}(1 - p_{25})\eta^r}{fp\, P_{NL}^{th} \eta^{th}}$$

The same equation with $P_{NL}^{th} = 1$ applies to the infinite system, so

$$\delta_{25}(\text{infinite}) = P_{NL}^{th}\, \delta_{25}(\text{finite})$$

Although, in principle, each of the ratios in Equation 2-6 could be measured and a purely experimental value of k_∞ could be obtained, some of the ratios can be computed much more accurately than they can be measured. This is possible because the two media are nearly identical, differing only in that the poisoned test medium contains a small concentration of poison. Thus systematic errors due to uncertainties in cross sections and other nonmeasured input parameters tend to cancel in the computation of the ratios in Equation 2-6; and, in addition, the effects of computational errors on k_∞ diminish as the ratios approach unity. Therefore, the error in k_∞ derived from small lattice experiments can be minimized by supplementing measurements with calculations wherever conservative estimates of errors definitely establish that calculations are more accurate.

One approach to the derivation of k_∞ from small lattice experiments is illustrated in Table 2-1, where predicted values and estimated errors for the parameters appearing in Equation 2-6 are given for a typical epithermal lattice (4.02%-enriched UO_2, M/W= 1.0, 70% D_2O). The following measurements are made; their assumed experimental errors are shown in parentheses:

N_B Poison (boron) concentration in test region for null-reactivity condition (1%)

$\bar{\phi}_m/\bar{\phi}_f$ Ratio of average thermal flux in moderator to average thermal flux in fuel (2%)

$\bar{\phi}_p/\bar{\phi}_f$ Ratio of average thermal flux in poison to average thermal flux in fuel (2%)

C_{25} Cadmium ratio of U-235 in fuel of unpoisoned test region (0.5%)

$(C_{25})_p$ Cadmium ratio of U-235 in fuel of poisoned test region (0.5%)

The unpoisoned and poisoned thermal utilizations (f and f_p) are derived from measurements of N_B, $\bar{\phi}_m/\bar{\phi}_f$, and $\bar{\phi}_p/\bar{\phi}_f$. The estimated error in f/f_p includes a 0.3% uncertainty due to cross sections and number densities. The $(1 + \delta_{25})$ terms are obtained from C_{25} measurements in the unpoisoned and poisoned test regions. Since this parameter enters as a ratio, systematic errors in the measurement should tend to cancel, and a precision of ±0.5% in C_{25} should be attainable.

Table 2-1. Typical Values of Parameters in Equation 2-6

Parameter	Unpoisoned	Poisoned	Ratio	Estimated error in ratio
f	0.845	0.731	1.156	±0.004
ϵ	1.085	1.097	0.989	±0.002
p	0.327	0.306	1.069	±0.003
$1 + \delta_{25}$	1.720	1.859	0.925	±0.006
L	--	--	0.995	±0.003
k_∞	--	--	1.125	±0.009

The changes in the thermal nonleakage probability and in ϵ due to poison addition are very small and can be computed with negligible error. Although absolute values of p are usually difficult to calculate, changes in p can be computed much more accurately. This is particularly true when the change in p arises exclusively from the addition of poison, in this case boron, which has a well-known 1/v cross section. Since, within the multigroup framework used in the analysis, more than 80% of

the change in p is directly attributable to absorptions in the boron, p/p_p can be derived accurately from the measured N_B. Spectral effects on p_{25} and p_{28} constitute the remainder of the total change in p and make the largest contribution to the assigned error in p/p_p.

There is an alternate expression that can be used to determine k_∞ with less error than Equation 2-6 in certain types of lattices. As can be seen from Table 2-1, the largest contributor to the total error is the measurement of $(1 + \delta_{25})/(1 + \delta_{28})_p$. Furthermore, the p ratio is very nearly equal to the reciprocal of the $(1 + \delta_{25})$ ratio. This suggests that both ratios contain the same fundamental nuclear properties and that the measurement of $1 + \delta_{25}$ may be partially redundant. Therefore, some cancellation of error may occur if k_∞ is expressed as

$$k_\infty = \frac{f}{f_p}(1 - \Gamma) \tag{2-8}$$

where

$$(1 - \Gamma) \equiv \left(\frac{\epsilon}{\epsilon_p}\right)\left(\frac{p}{p_p}\right)\frac{(1 + \delta_{25}^{\infty})}{(1 + \delta_{25}^{\infty})_p} \tag{2-9}$$

and Γ is a number very close to zero. The definition of Γ follows from the fundamental definition of k_∞ (Equation 2-1), i.e.,

$$\Gamma = \left[\left(T_p - \frac{f_p}{f}T\right) + \left(E_p - \frac{f_p}{f}E\right)\right]\frac{1}{T_p + E_p} \tag{2-10}$$

where T is the number of neutrons produced from thermal fissions and E is the number of neutrons produced from nonthermal fissions. Note that Γ vanishes for the special case of a pure thermal system, i.e., $E = E_p = 0$, $T = \eta^{th} f p$, and $p_p = p$. Thus Γ may be considered as an index of epithermality.

It is difficult to derive a simple analytical expression for Γ that can be used as a basis for verifying and generalizing the hypothesis that Γ is small and can be computed with little error. However, the validity of this hypothesis can be demonstrated, at least for the specific lattices under study in this program, within the multigroup framework of Equation 2-10. Table 2-2 lists the results of infinite medium multigroup calculations for large variations in three important input parameters: the thermal cutoff energy, the effective resonance integral of the fertile material, and the volume of moderator displaced by the poison foils in

the poisoned test region. Although these input variations affect absolute values of p and $(1 + \delta_{25}^{\infty})$ by as much as 20% and the ratios (p/p_p) and $(1 + \delta_{25}^{\infty})/(1 + \delta_{25}^{\infty})_p$ by as much as 4%, the maximum change in $1 - \Gamma$ is only about 0.2%.

The choice between Equations 2-6 and 2-8 for the analysis of a particular small lattice experiment depends on the following considerations. In both approaches f/f_p is obtained through measurements of N_B, the poison concentration for null-reactivity, and the flux ratios. For those lattices in which the change in p is small and primarily due to boron absorptions, p/p_p can be computed with good accuracy from N_B. Then, if $(1 + \delta_{25})/(1 + \delta_{25})_p$ can be measured with comparable accuracy, k_∞ can be derived with less error from Equation 2-6. If, however, the change in p is large or more difficult to compute because of spectral effects, uncertainties in the correct cutoff energy, or other complications, then Γ can be computed from the measured N_B, and Equation 2-8 will give a more accurate value of k_∞. Equation 2-8 is also preferable when accurate measurements of $(1 + \delta_{25}^{\infty})/(1 + \delta_{25}^{\infty})_p$ are complicated by local heterogeneities, fuel inaccessibility, or other factors. Thus the better approach can be predetermined for each experiment on the basis of a careful analysis and evaluation of all sources of error, both experimental and calculational.

Both approaches require the calculation of certain parameters using measured quantities as inputs. The BPG code[5] and its latest revision BPG-II[3], which were developed in the SSCR Basic Physics Program, were used for this purpose. These codes have matched a variety of data from critical experiment lattices differing in enrichment, M/W ratio, and D_2O concentration.[3,6] The BPG code is essentially the same as the latest of the MUFT series (MUFT-5). It utilizes the Greuling-Goertzel slowing-down model in the B_1 approximation; it calculates the multiplication constant for a bare reactor in which the leakage is characterized by a single buckling; and it computes a complete neutron balance in 39 energy groups. For the calculation of L and for certain exploratory studies described in the appendixes, multiregion calculations simulating the geometry of the experiments are required. For these purposes, standard four-group, one- and two-dimensional diffusion codes with BPG-generated input coefficients were used.

Table 2-2. Typical Values of Parameters in Equation 2-8

Thermal cutoff, ev	Resonance integral, barns	Moderator displaced, cm^3	ϵ/ϵ_p	p	p_p	$1 + \delta_{25}^{\infty}$	$(1 + \delta_{25}^{\infty})_p$	$1 - \Gamma$
4.02%-Enriched UO_2, 69.7% D_2O								
0.400	16.54	229	0.98866	0.32737	0.29818	1.82838	2.04334	0.97126
0.625	16.54	229	0.98881	0.34990	0.32311	1.71206	1.89021	0.96985
0.400	20.39	229	0.98781	0.29206	0.26530	1.87052	2.09881	0.96918
0.400	16.54	200	0.98888	0.32737	0.29946	1.82838	2.03730	0.97019
UO_2-ThO_2, 70.4% D_2O								
0.400	13.99	212	0.99671	0.37100	0.30847	1.88875	2.35889	0.95980
0.625	13.99	212	0.99675	0.40103	0.34333	1.74949	2.12720	0.95755
0.400	15.99	212	0.99658	0.35533	0.29479	1.89808	2.37478	0.96011
0.400	13.99	183	0.99672	0.37100	0.30864	1.88875	2.35615	0.96043
UO_2-ThO_2, 80.4% D_2O								
0.400	13.47	174	0.99731	0.29374	0.24445	2.24634	2.81055	0.95784
0.625	13.47	174	0.99734	0.32410	0.27778	2.03863	2.48184	0.95585

3. DESIGN OF FACILITY

Major features of the facility for small lattice experiments are shown in Figures 3-1 through 3-3 and are discussed in the following sections. Additional details are available in the facility Hazards Report[7] and in the relevant Quarterly Technical Reports[8-11].

3.1. Driver Region

The driver region is a vertical honeycomb of 160 four-inch-square (0.34-inch-wall) by 8-foot-long hollow graphite channels arranged to form a 56-inch-square matrix with a 24-inch-square cavity in the center. The loading is adjusted for criticality with each buffer and test region configuration by filling the appropriate number of graphite channels with 1.6-inch-square by 12-inch-long graphite bars. In some cases it is necessary to increase the reactivity of the driver by taping 1.6-inch-wide by 12-inch-long by 0.010-inch-thick foils of 93%-enriched U-Al alloy (18 wt % U) to the sides of some of the graphite bars. For the case illustrated by Figures 3-2 and 3-3 (poisoned test and buffer regions), 44 channels were filled with U-Al and graphite over a length of 6 feet capped with 1-foot-thick top and bottom graphite reflectors, and the outer 92 channels were filled only with graphite to form an additional radial reflector. The mass of U-235 in this loading was approximately 3.5 kg.

Seven control rods are located in the inner row of graphite channels. The rods are 2.5-inch-diameter by 8-foot-long aluminum cylinders wrapped with 0.020-inch-thick cadmium sheet. They move vertically in 3-inch-OD aluminum guide tubes permanently mounted in the graphite channels. Normally the three pairs of ganged rods are fully withdrawn and act as safety rods. Rod No. 2 is used as the regulating rod.

The graphite channels are mounted on a split-bed assembly, consisting of fixed and movable 5-foot by 10-foot steel tables. This arrangement permits separation of the driver during major loading changes and

provides access to the buffer and test regions for radial flux measurements. The tables can be separated 48 inches by a lead-screw operated by a combined electric and pneumatic table drive mechanism. Table-closing speeds vary from 12 to 0.5 in./min, depending on the separation. The closed position, indicated by four linear potentiometers, is reproducible to ± 0.001 inch.

The instrumentation and control system is of conventional design and is fully described in the Hazards Report[7].

3.2. Core Tank and Moderator System

The buffer and test regions are assembled in a 22-7/8-inch-ID by 76-inch-high aluminum core tank having a 3/8-inch-thick wall. The 1-1/4-inch-thick aluminum cover is provided with an O-ring seal so that the tank can be hermetically sealed to minimize moderator degradation by exchange with light water vapor in the atmosphere. Small access ports are located at the midplane (for foil holders) and near the base (to facilitate loading fuel rods). The core tank is centered in the driver cavity and mounted on a 1-foot-high aluminum platform.

The moderator, a D_2O-H_2O mixture containing 70 or 80% D_2O, is stored in a small (110 gal) dump tank between runs. On startup, the moderator is pumped into the core tank using conventional equipment and procedures for liquid-moderated critical assemblies[7]. The moderator is always dumped for shutdown. In most cases this provides sufficient shutdown margin to obviate table separation between runs. The buffer and test regions are moderated by the same D_2O-H_2O mixture.

3.3. Fuel Rods

Two types of fuel rods were used in the buffer and test regions, as described in Table 3-1. The 4.02%-enriched UO_2 fuel rods were swaged in stainless steel tubes, and the UO_2-ThO_2 fuel rods consisted of sintered pellets of blended 93%-enriched UO_2 and ThO_2 ($N_{Th}/N_{25} = 15$) in aluminum tubes.

Table 3-1. Properties of Fuel Rods

Property	4.02%-enriched UO_2	UO_2-ThO_2
Outer diameter, in.	0.4755 ± 0.0015	0.308 ± 0.001
Wall thickness, in.	0.0160 ± 0.0005	0.014 ± 0.001
Wall material	# 304 steel	# 1100 aluminum
Fuel diameter, in.	0.444 ± 0.002	0.260 ± 0.002
Total length, in.	≈71.5	62.0 ± 0.2
Active (fuel) length, in.	66.7 ± 0.3	60.0 ± 0.1
Weight of fuel, gm/rod	1600 ± 2	434.6 ± 0.2
Wt U/wt UO_2, %	88.01 ± 0.02	- -
Weight of ThO_2, gm/rod	- -	405.0 ± 0.2
Weight of U-235, gm/rod	56.61 ± 0.10	24.04 ± 0.02
Enrichment, wt U-235/wt U, %	4.020 ± 0.005	- -
Atoms Th ÷ atoms U-235	- -	15.00 ± 0.05
Bulk fuel density, gm/cm³	9.46 ± 0.10	8.33 ± 0.14
Σ_a (impurities), cm²/cm³ oxide	$<5 \times 10^{-4}$	$<6 \times 10^{-3}$

3.4. Buffer Region

The function of the buffer region is to produce an asymptotic neutron spectrum throughout the test region, so that errors due to spectral mismatch are minimized when the buffer is identical to the test region. However, calculations suggest that the error in k_∞ due to imperfect asymptotic conditions may not be serious even if a substantial part of the buffer region differs from the test region. To test this prediction, the buffer region in the first set of experiments (4.02%-enriched UO_2 in test region) was divided into two regions: an inner buffer identical to the test region and an outer buffer having dissimilar nuclear properties. As will be shown, satisfactory results were obtained with the dissimilar buffer. Although a dissimilar outer buffer could have been used in the second set of experiments (UO_2-ThO_2 fuel in test region), sufficient fuel was available to simplify the experiments by making the entire buffer region identical to the test region.

3.4.1. 4.02%-Enriched UO_2 Experiments

For the experiments in which the test region contained 4.02%-enriched UO_2 fuel rods, the inner buffer was an identical uniform lattice of these fuel rods on a pitch of 0.595 inch (M/W = 1.006), and the outer buffer was a uniform lattice of UO_2-ThO_2 fuel rods on a pitch of 0.387 inch (M/W = 0.990). The effective radius of the buffer lattice was 11.0 inches. The fuel rods were aligned at the top and bottom by 22-inch-diameter by 1-inch-thick drilled aluminum grid plates having an 8.3-inch-square hole in the center for the test insert. Since the UO_2-ThO_2 fuel rods were approximately 1 foot shorter than the 4.02%-enriched UO_2 fuel rods, the grid plates were mounted approximately 6 inches above the base of the core tank and 6 inches below the top. Figure 3-4 shows the buffer grid plates in the core tank and some of the fuel rods loaded in the outer buffer.

3.4.2. UO_2-ThO_2 Experiments

For the experiments in which the test region contained UO_2-ThO_2 fuel rods, the entire buffer region was an identical lattice of these fuel rods on a pitch of 0.387 inch (M/W = 0.990). The effective radius of the buffer lattice was 11.0 inches. The fuel rods were aligned by egg-crate grid plates constructed of 0.071-inch-thick by 1-inch-wide aluminum strips that interlocked on a 0.387-inch pitch. Additional alignment was obtained at elevations corresponding to the top and bottom of the test region by using similar grid plates with alternate strips removed to facilitate loading. The intermediate grid plates covered only the area around the test region and along the diameter where the flux traverses were made.

All four grid plates were provided with a 6.6-inch-square hole at the center for the test insert. Four aluminum angles (1 in. × 1 in. × 1/16 in.) were mounted in the corners of the hole to serve as guides for the insertion of the test insert. The grid plates were aligned and supported by 3/8-inch-diameter threaded stainless steel rods located at the periphery of the buffer region. Since the UO_2-ThO_2 rods were only 5 feet long, axial symmetry was provided by supporting them on an aluminum shelf approximately 6 inches above the base of the tank.

The arrangement of the internal structure for the UO_2 - ThO_2 experiments is illustrated in Figures 3-5 and 3-6.

3.5. Test Insert and Test Region

The test region, i.e., the region that is replaced by a void in the null-reactivity measurements, is located in the center of a removable section of the lattice called the test insert. The test insert is approximately the same total length as the fuel rods in the buffer region and fits in the square hole in the center of the buffer region. It can be removed from the buffer region lattice to provide access to the test region for poisoning and void replacement. Since the test region should be surrounded by buffer material axially as well as radially, the top and bottom sections of the test insert are indentical to the middle (test region) section and form the axial buffers. The test insert is also surrounded radially by one or two rows of full length fuel rods, which actually constitute part of the inner buffer. These full length rods are included in the test insert for two reasons. First, they serve as structural members to hold the three sections together, since the lattices are so tightly packaged that the introduction of extraneous material for structural puposes is prohibited. Second, by using the same grid plates that hold the test region to align the first row of inner buffer rods, the lattice spacing can be controlled more accurately. The shorter fuel rods in the test insert are cut to the proper length from full length rods and resealed with thin epoxy-cemented aluminum end caps.

3.5.1. 4.02%-Enriched UO_2 Experiments

The test insert for these experiments, shown in Figure 3-7, was an 8.33-inch-square by 6-foot-long lattice of 196 (14 × 14) 4.02%-enriched UO_2 fuel rods on a pitch of 0.595 inch (M/W = 1.006). The central 18-inch-long section contained the test region, and the top and bottom 27-inch-long sections formed the axial buffers. Each section was provided with 1/4-inch-thick aluminum grid plates at the top and bottom, and three rods at each corner were epoxy-cemented to the grid plates so that the sections could be handled separately. Figure 3-8 shows the central section before the cut fuel rods were loaded.

The test region itself was a sublattice of 144 (12 × 12) fuel rods. Thus, the outer row of 52 full length fuel rods in the test

insert actually formed part of the inner buffer. The three sections of the test insert were held together by studs that were threaded into the end plugs of eight full length rods and bolted to the top grid plate of the top buffer and to the bottom grid plate of the bottom buffer.

3.5.2. UO_2-ThO_2 Experiments

The test insert for these experiments (see Figures 3-5 and 3-6) was a 6.58-inch-square by 62-inch-long lattice of 289 (17 × 17) UO_2-ThO_2 fuel rods on a pitch of 0.387 inch (M/W = 0.990). The central 18-inch-long section contained the test region, and the top and bottom 22-inch-long sections formed the axial buffers. The fuel rods in the end buffers were supported by thin (1/4- to 1/2-inch-thick) stainless steel grid plates.

The test region itself was a sublattice of 169 (13 × 13) fuel rods, held at the top and bottom by aluminum grid plates, 5/16- and 1/2-inch thick respectively. Thus, the two outer rows of full length fuel rods in the test insert actually formed part of the inner buffer. The three sections of the test insert were held together by four 0.25-inch-diameter stainless steel tie rods, which replaced the corner full length fuel rods. The test region was removable as a unit without disassembling the test insert, as was necessary in the preceding experiments, by withdrawing the two rows of full length fuel rods on one side of the test insert and moving the test region through this opening.

3.6. Void Can

The void that replaces the poisoned test region in the null-reactivity measurements is simulated by a hollow, air-filled aluminum can having exactly the same outer dimensions as the test region. Since these lattices are very undermoderated, the void can is divided internally into a number of watertight compartments by thin aluminum plates to reduce the nuclear hazards of flooding. The end plates are designed to match the test region end grid plates as closely as possible so that their reactivity effects cancel. However, a small correction is required for neutron absorptions in the aluminum walls and internal divider plates. Absorptions in the nitrogen in the air are negligible in comparison.

3.6.1. 4.02%-Enriched UO_2 Experiments

In these experiments, the void can had outer dimensions of 7.140 inches (12 × 0.595 in.) square by 18 inches long and a wall thickness of 0.163 inch. It was divided into eight compartments by 0.081-inch-thick plates. The volume of aluminum in the walls and dividers was 79.4 $in.^3$ and 27.2 $in.^3$, respectively, so that aluminum occupied 12.0 vol % of the test region disregarding the end plates. The active length of the test region and void was 17.50 ± 0.01 inches. Figure 3-9 is a view of the void can, and Figure 3-10 shows the test insert assembled with the test region and a second view with the void can in place.

3.6.2. UO_2-ThO_2 Experiments

In these experiments, the void can had outer dimensions of 5.031 inches (13 × 0.387 in.) square by 18 inches long and a wall thickness of 0.140 inch. It was divided into six compartments by 0.081-inch-thick plates. The volume of aluminum in the walls and dividers was 47.1 $in.^3$ and 9.0 $in.^3$, respectively, so that aluminum occupied 12.9 vol % of the test region disregarding the end plates. The active length of the test region and void was 17.20 ± 0.01 inches.

3.7. Poisons

The test region is poisoned with 0.0102 ± 0.002-inch-thick foils of Binal, a homogeneous mixture of natural B_4C and aluminum containing 2.53 ± 0.02 wt % boron and having a density of 2.62 gm/cm^3. The foils are inserted vertically between rows of fuel rods and are trimmed as necessary to fit the test region dimensions. Some of the foils are perforated to reduce their weight and to permit a more uniform poison distribution.

In some cases it is necessary to flatten the flux distribution by adding poison to the buffer region after the test region has been poisoned. Binal foils were used in the end buffer regions and in that part of the inner buffer included with the test insert. Additional poisoning was achieved by taping 0.050-inch-diameter silver (90% Ag-10% Cu) wires to some of the buffer fuel rods.

Figure 3-1. Facility for Small Lattice Experiments

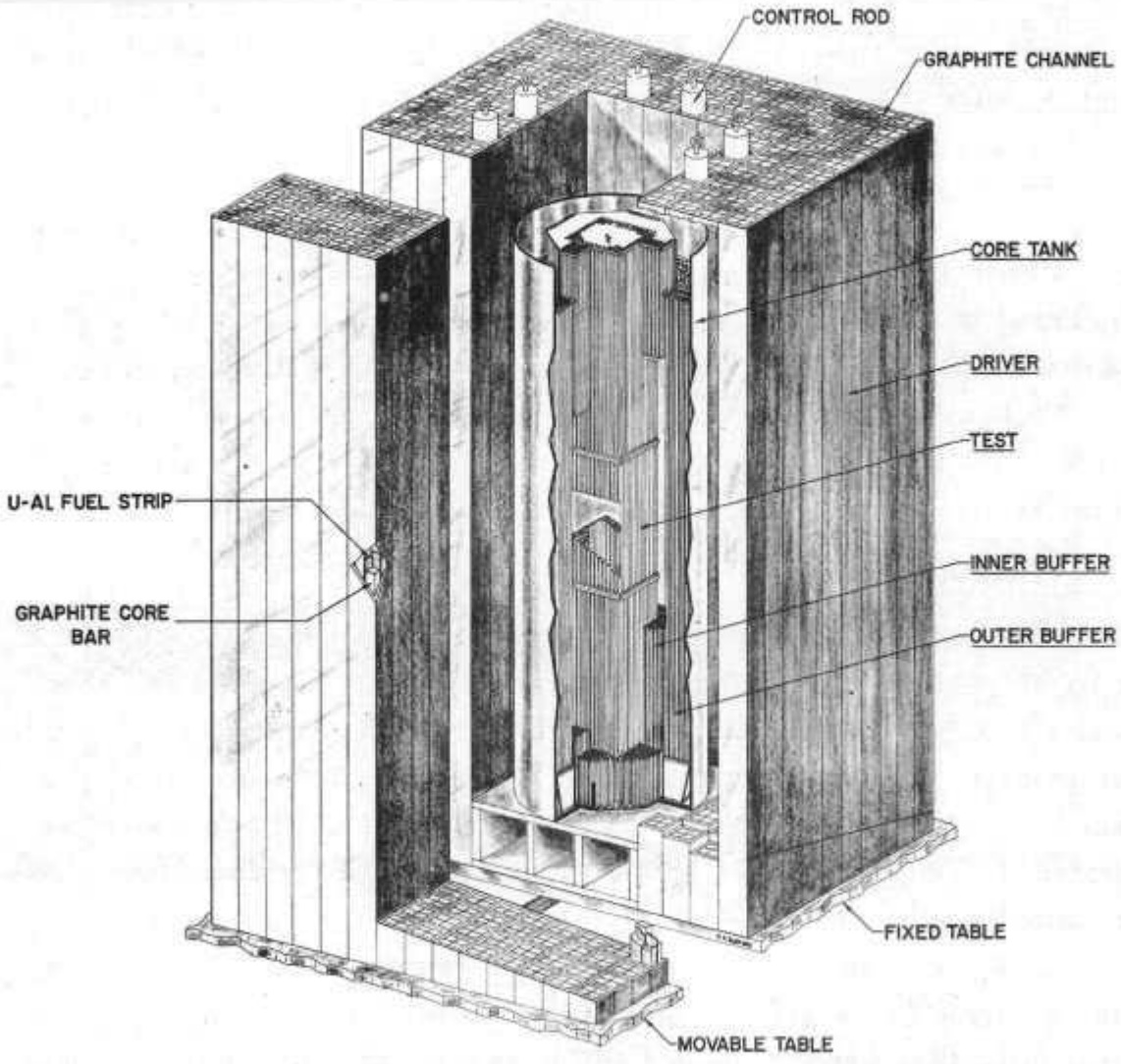

Figure 3-2. Assembly Plan (4.02%-Enriched UO_2 Experiments)

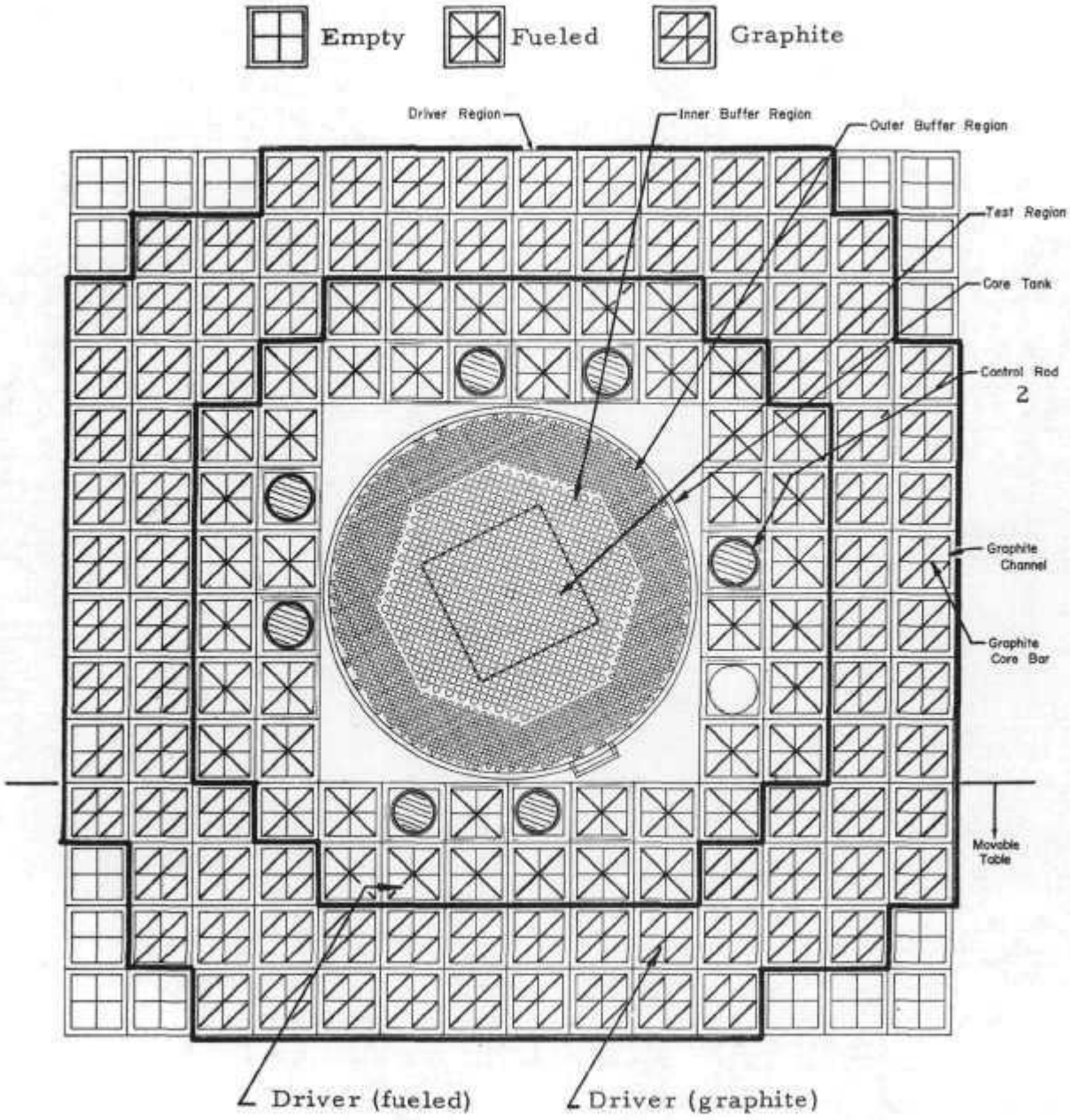

Figure 3-3. Assembly Elevation (4.02%-Enriched UO_2 Experiments)

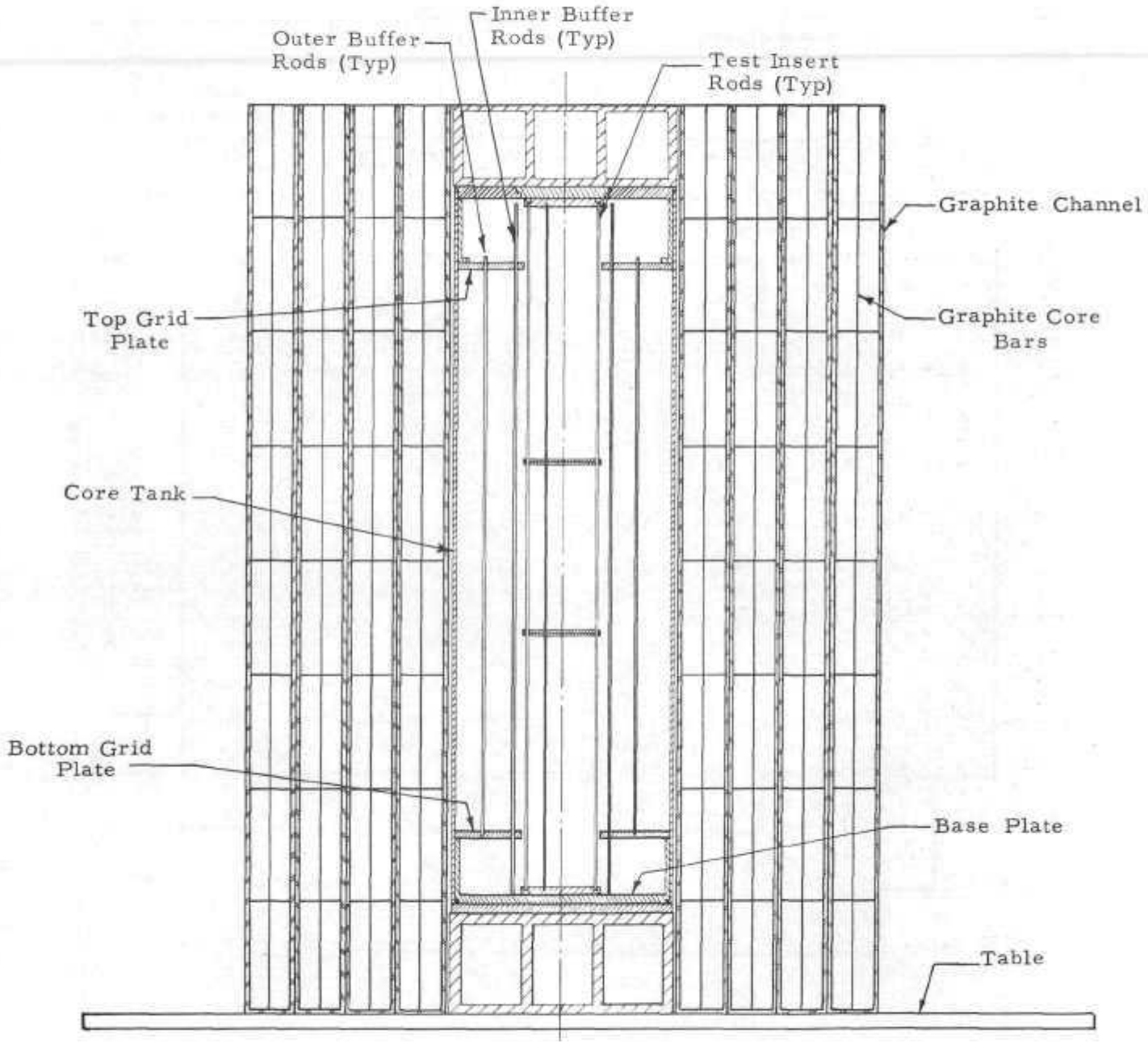

Figure 3-4. Core Tank and Buffer Region (4.02%-Enriched UO_2 Experiments)

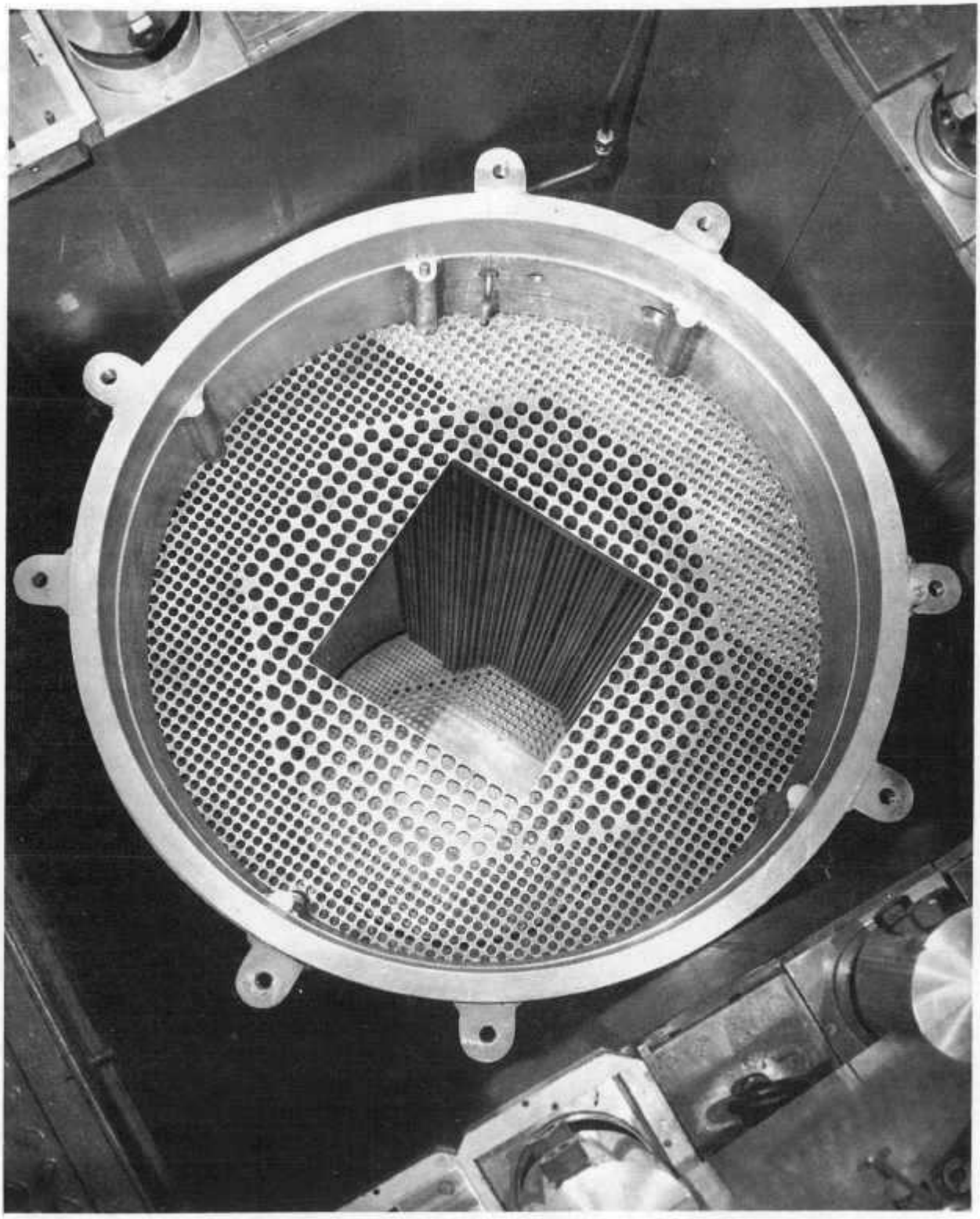

Figure 3-5. Test and Buffer Region Plan (UO_2 - ThO_2 Experiments)

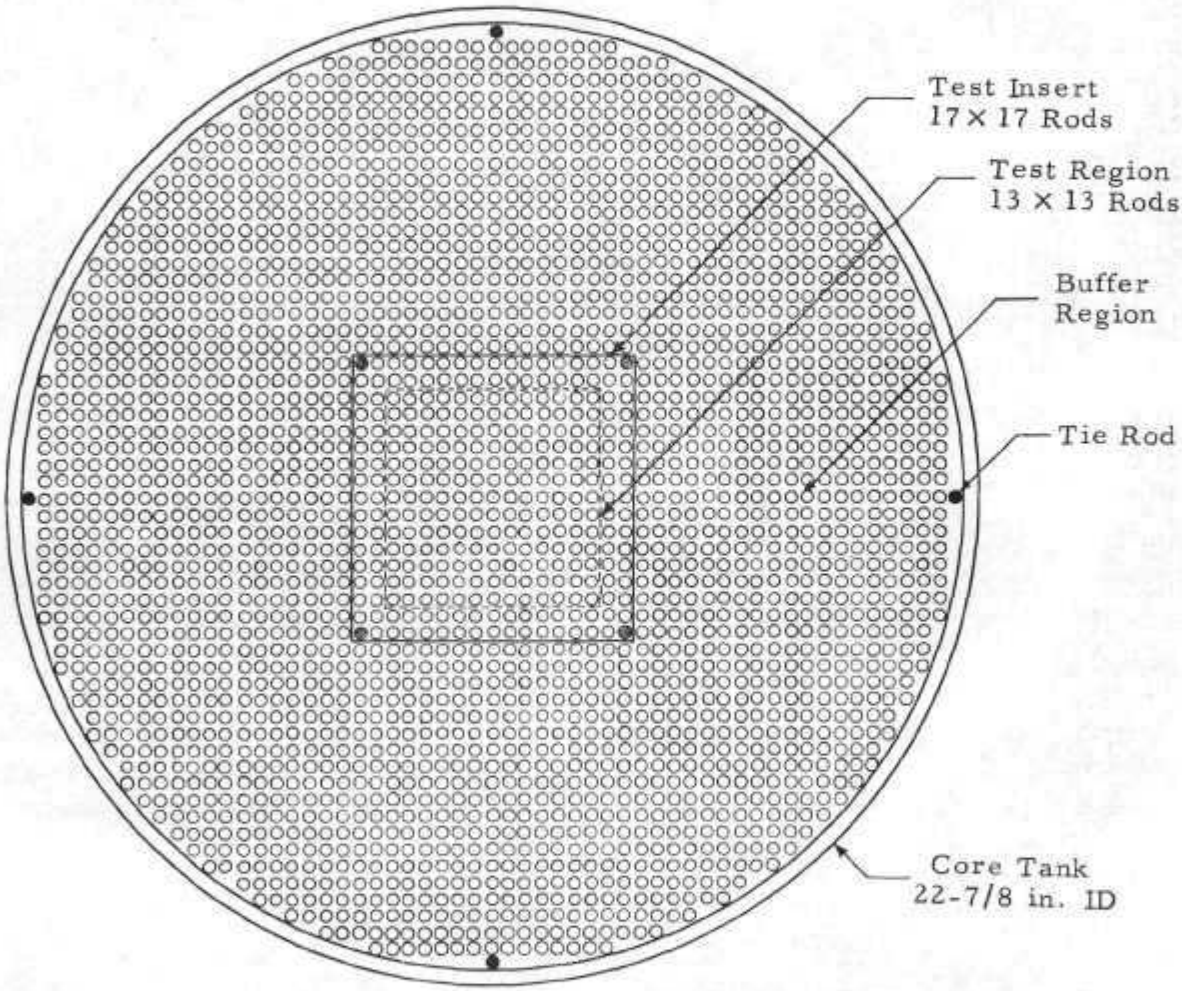

Figure 3-6. Test and Buffer Region Elevation (UO_2 - ThO_2 Experiments)

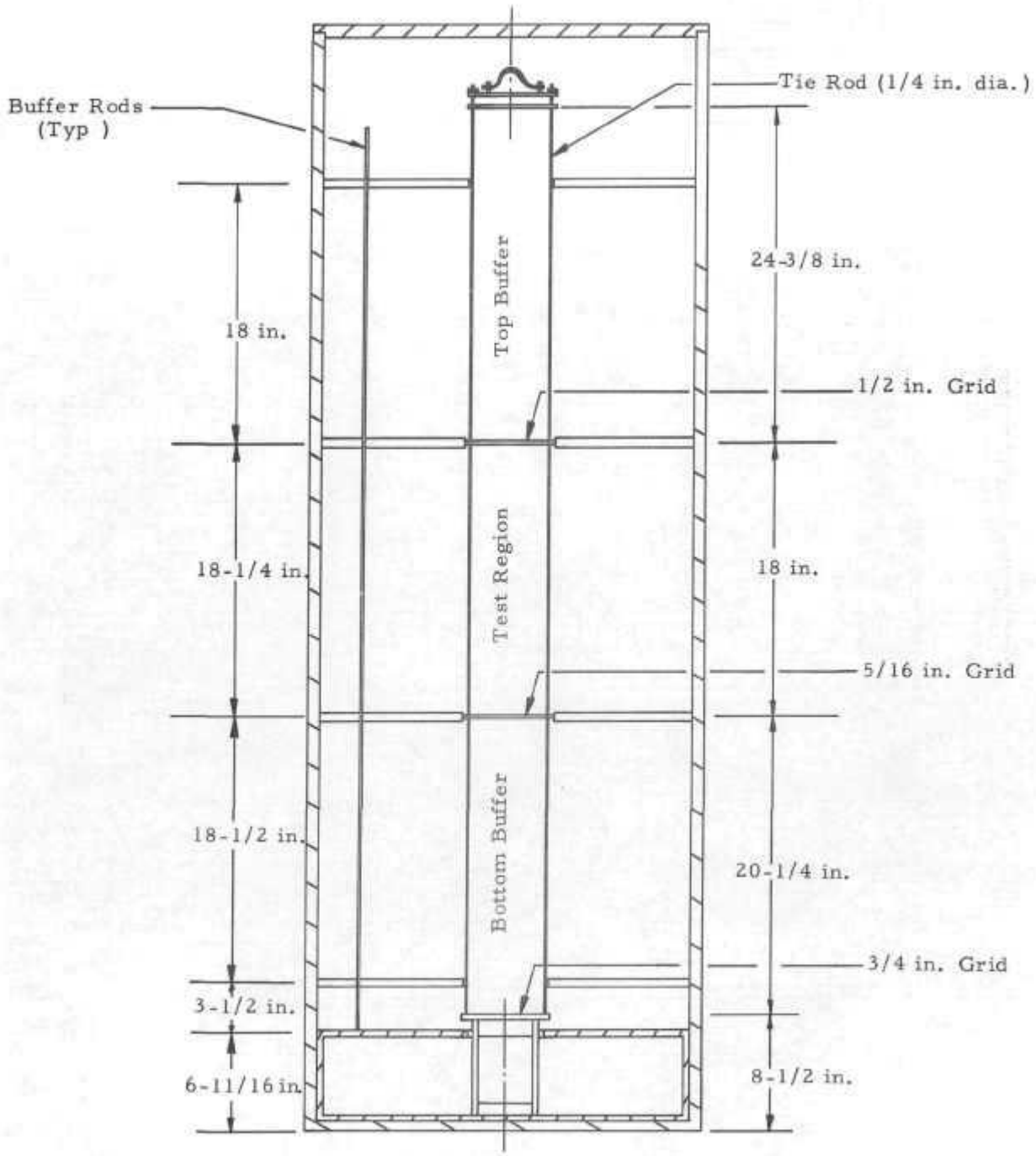

Figure 3-7. Test Insert (4.02%-Enriched UO_2 Experiments)

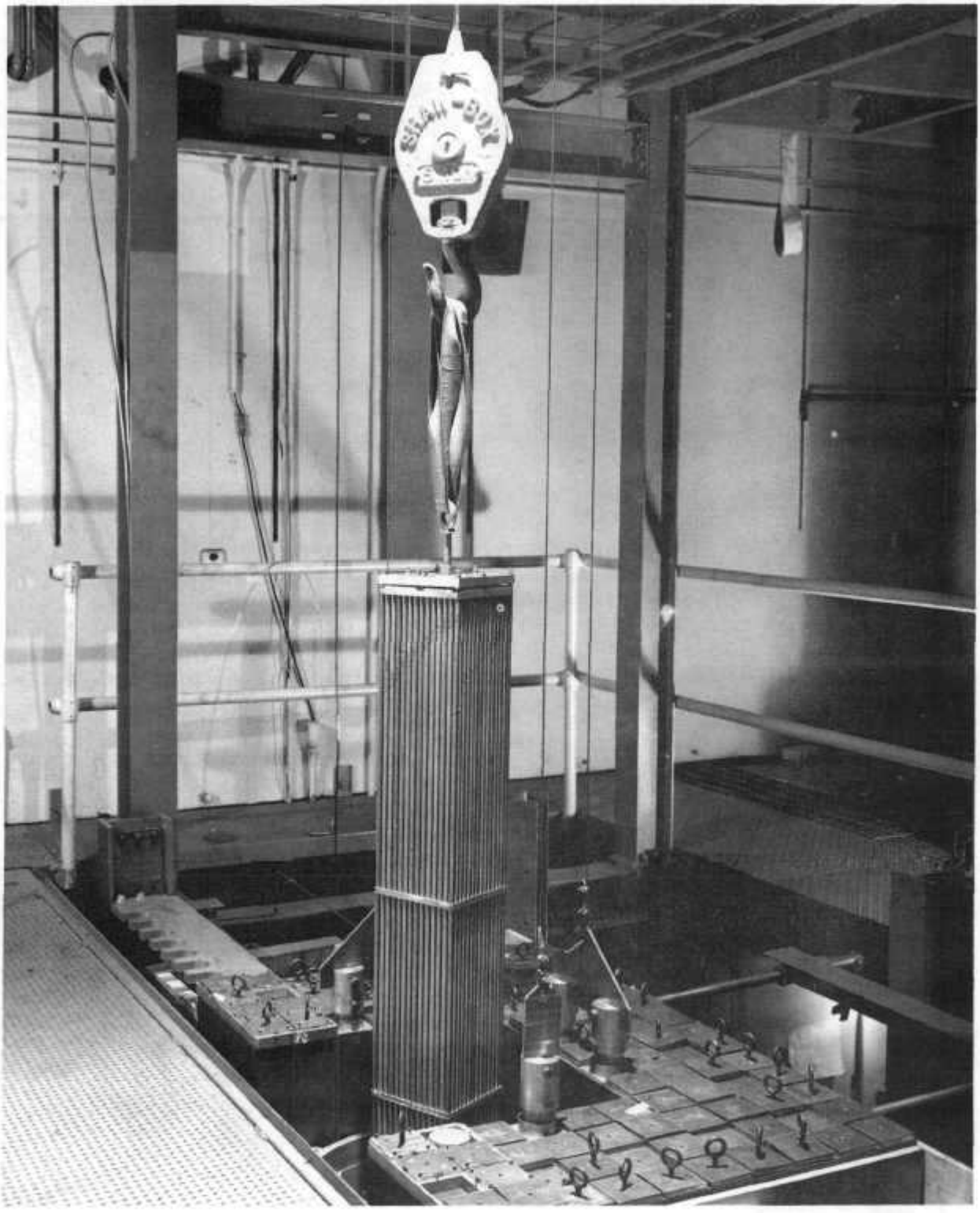

Figure 3-8. Unloaded Test Region (4.02%-Enriched UO_2 Experiments)

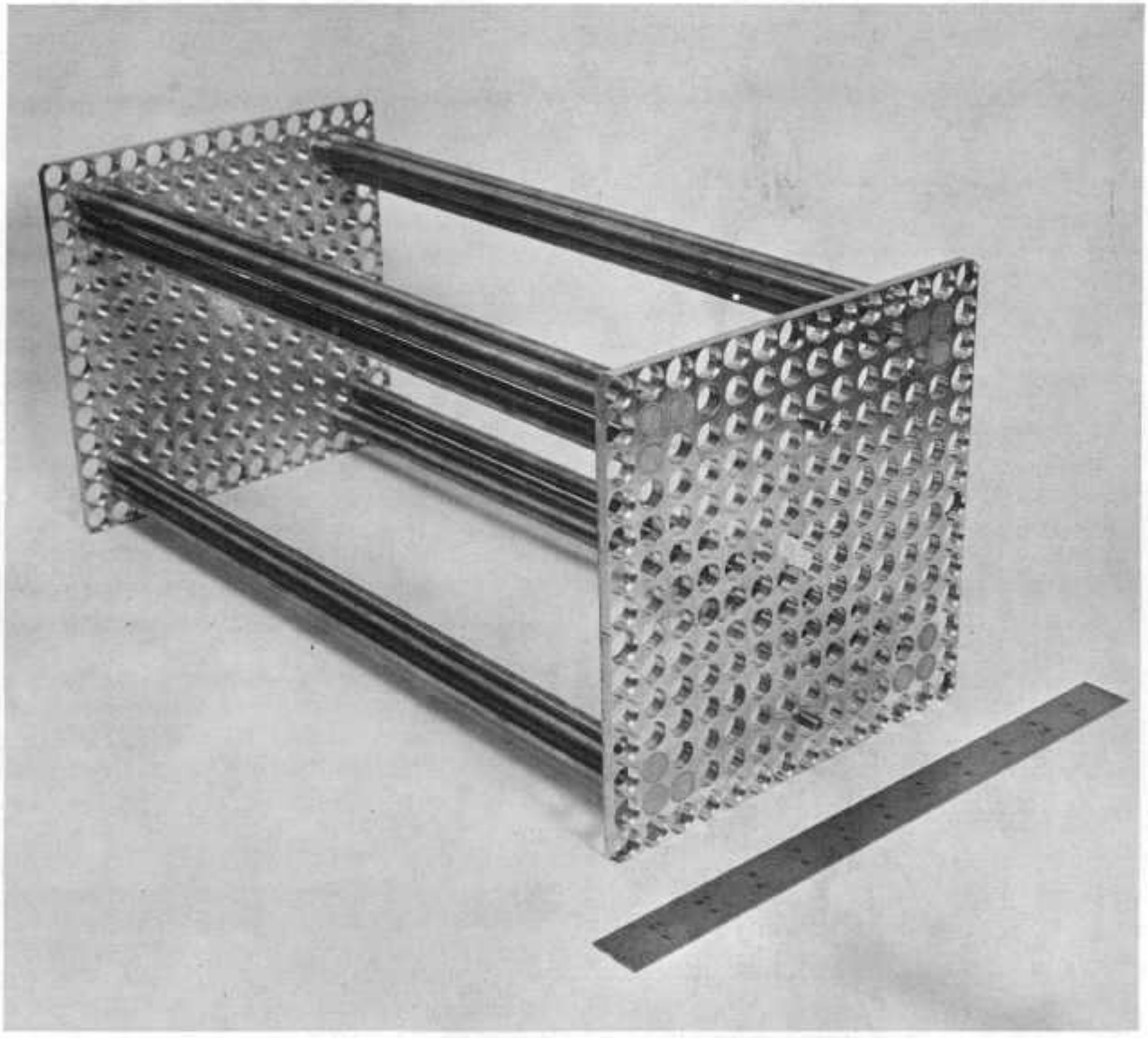

Figure 3-9. Void Can (4.02%-Enriched UO_2 Experiments)

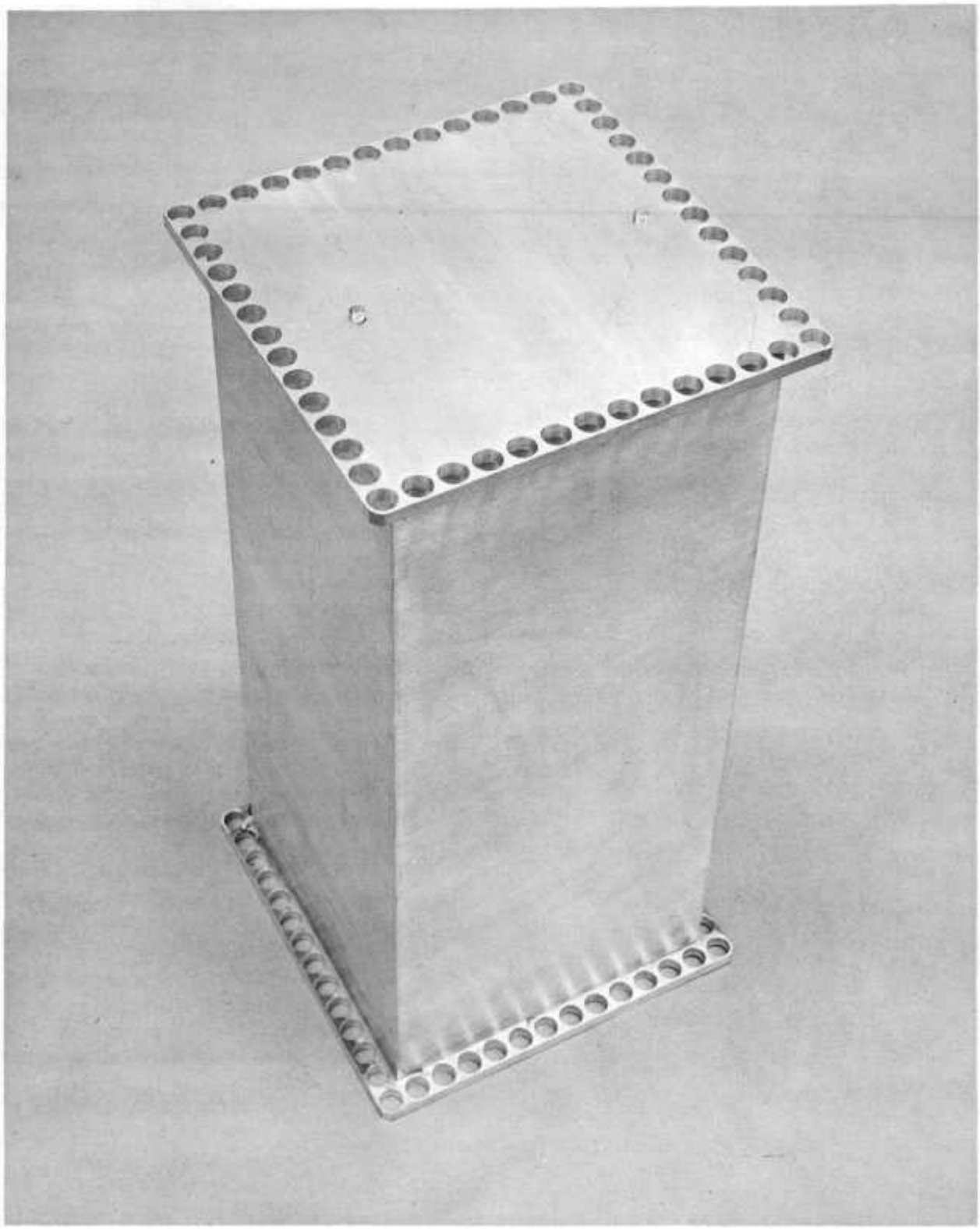

Figure 3-10. Test Insert Assembled With Test Region and Void Can (4.02%-Enriched UO_2 Experiments)

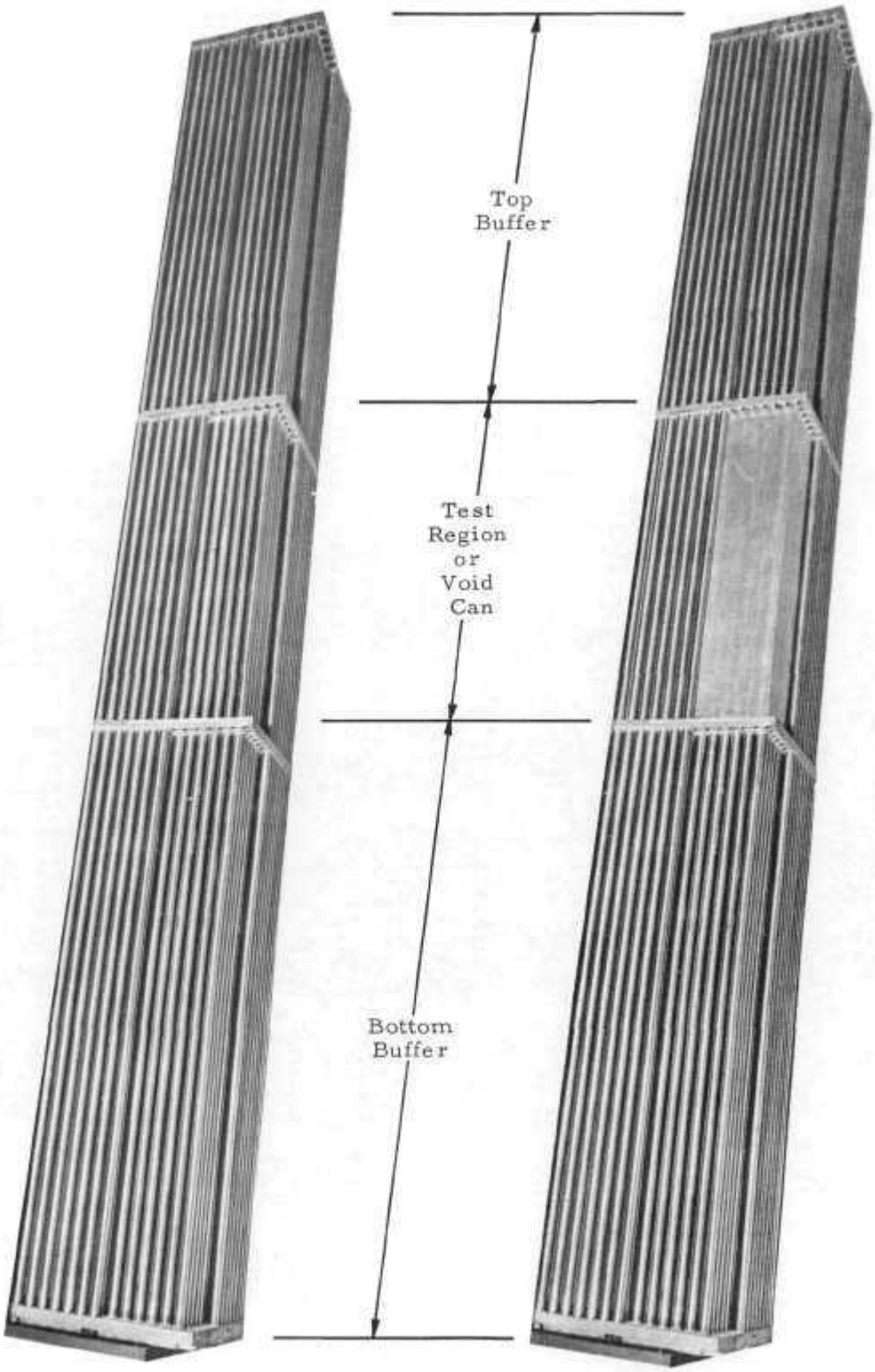

4. EXPERIMENTS WITH 4.02%-ENRICHED UO_2 FUEL (69.7% D_2O)

4.1. Preliminary Experiments

The reactivity worth of the control rods, measured by standard rod-drop and rod-bump-period methods, was found to depend slightly on the loading of U-235 in the driver. The minimum worth (unfueled driver) was approximately $2.40 for each pair of safety rods and approximately $1.80 for the single regulating rod (Rod No. 2).

The accuracy of the measurement of k_∞ depends on the consistency and reproducibility of the variables that affect null-reactivity measurements. The maximum effects of these variables are shown in Table 4-1. The overall reproducibility also includes the effects of structural changes caused by reassembling the test insert. Although the reproducibility could have been improved substantially, the sensitivity of the experiment was sufficiently large, due to the size of the test region, that the error in k_∞ was only ±0.1%.

Table 4-1. Reproducibility of Null-Reactivity Measurements

Variable	Differential worth	Reproducibility	Error, cents
Control rod position	0.5¢/cm	0.05 cm	0.03
Moderator level	2.60¢/cm	0.05 cm	0.13
Table gap	0.06¢/mil	1 mil	0.06
Temperature	−(1±1)¢/C	<0.5 C	<0.5
Moderator degradation	0.05%/3 mo.	- -	0.06
Overall	- -	- -	≈0.5

4.2. Unpoisoned Test, Unpoisoned Buffer

4.2.1. Loading Configuration

Criticality was first achieved on September 28, 1962. After a number of preliminary experiments the moderator was changed to its final concentration (69.7 mole % D_2O), and criticality was reached with six driver channels in the first row fueled with 0.48 kg of U-235. All the remaining channels in the 144-channel driver were filled with graphite. The excess reactivity of this loading was approximately 25 cents, and the worth of a fueled channel, compared to an unfueled one (graphite only), varied from 8 to 14 cents.

4.2.2. Flux Distributions

Radial and axial flux traverses were made with bare and cadmium-covered 1/4-inch-diameter by 0.005-inch-thick gold foils and with bare 1/4-inch-diameter by 0.007-inch-thick Dy-Al (≈5 wt % Dy) foils. The foils were mounted on 1/2-inch-wide by 0.005-inch-thick spring-steel tapes. After being irradiated for 20 minutes at a power level of a few hundred watts, the foils were beta counted once on each side in each of three end-window, gas-flow proportional counters. Bare and cadmium-covered runs were normalized by two gold monitor foils.

The results are shown in Figures 4-1 and 4-2. The cadmium-covered gold traverse gives the shape of the epithermal flux distribution. The thermal flux distribution was obtained by two methods: from the bare dysprosium traverses, since dysprosium has a high cadmium ratio in this lattice and is primarily responsive to thermal neutrons; and from the difference between the normalized bare and cadmium-covered gold distributions. The results are in good agreement, although the latter measurement has a much larger uncertainty since the gold cadmium ratio is close to unity. The large peaks in the axial distributions at the top and bottom of the test region are caused by the absence of fuel at the end caps of the cut fuel rods. The lower curves show the extent of the asymptotic region. The ratio of thermal-to-epithermal activity is given by the cadmium ratio of gold minus one and also, on an unnormalized scale, by the ratio of dysprosium to cadmium-covered gold activity. As predicted by calculations, the asymptotic region extends well into the inner buffer.

Although comparisons of thermal and cadmium-covered gold activities prove that the neutron spectrum is asymptotic to at least 5 ev, it is important to know whether the spectrum is also asymptotic at higher energies. The radial distribution of higher energy neutrons was mapped with 0.005-inch-thick thorium foils, covered with thorium and cadmium. The purpose of the thorium covers was to screen neutrons at the principal thorium resonances of 22, 24, and possibly 70 ev, so that the thorium foil within responded primarily to neutrons above 30 ev. After irradiation the Th-233 activity was beta counted in end-window, gas-flow proportional counters; background corrections were made by counting the foils the same way prior to irradiation.

The radial flux shapes for cadmium-covered gold and cadmium- and thorium-covered thorium are shown in Figure 4-3, where the thermal distribution obtained from the Dy-Al foil traverse is repeated for comparison. The unnormalized ratios of thermal-to-epithermal activity, obtained by dividing the Dy-Al data by the epithermal gold or epithermal thorium data, show that the neutron spectrum is asymptotic into the inner buffer even at energies well above 5-ev gold resonance.

4.2.3. Thermal Disadvantage Factor

The thermal disadvantage factor $\overline{\phi}_m/\overline{\phi}_f$, defined as the ratio of the average thermal neutron flux in the moderator to that in the fuel, was measured in a central cell of the test region. This lattice parameter is used to calculate the thermal utilization of the unpoisoned test region, which enters in the derivation of k_∞.

The measurements were made by standard techniques used earlier in the SSCR critical experiment program.[3] As shown in Figure 4-4, the flux in the fuel and moderator was sampled with 0.007-inch-thick Dy-Al (5 wt % Dy) sector foils using a 0.444-inch-diameter round (R) foil in the fuel and a scalloped (S) foil, 0.595 inch across flats, in the moderator. Measurements were made in two loadings, designated I and II. Three R-foils and three S-foils were irradiated simultaneously in each run. After a 20-minute irradiation the foils were counted five times in a 4π proportional counter. The foils were calibrated for variations in dysprosium content by irradiating them on a wheel rotating in a region of relatively constant flux and counting them in the same 4π

geometry. Very small corrections for the differences in axial flux at the foil positions were also applied.

A small correction to the bare foil activity ratio $\bar{A}_m/\bar{A}_f$ was made to account for the slight difference in epithermal activity between the fuel and moderator. This correction was obtained by measuring the cadmium ratio of R-foils in the fuel (C_f) and in the moderator (C_m). Thus, the thermal disadvantage factor was determined by the following equation:

$$\frac{\bar{\phi}_m}{\bar{\phi}_f} = \frac{\bar{A}_m}{\bar{A}_f}\left(\frac{C_m - 1}{C_m}\right)\left(\frac{C_f}{C_f - 1}\right).$$

Table 4-2 summarizes the results obtained from Loading I. No significant difference between the three fuel rods was observed. However, two measurements by exactly the same technique in Loading II using another fuel rod (designated Rod a) gave a value about 2% higher ($\bar{A}_m/\bar{A}_f = 1.148 \pm 0.005$). Essentially the same result (1.146 ± 0.008) was obtained from three measurements on the same Rod a in an equivalent critical experiment. Thus, the discrepancy may be attributed to differences in the fuel rods, rather than to a lack of equivalent asymptotic conditions in the two types of experiments. The same difference was observed in C_{25} measurements, discussed in the next section. Although the value obtained from Loading I is probably the proper one to use in the analysis, k_∞ is so insensitive to $\bar{\phi}_m/\bar{\phi}_f$ that the difference is insignificant.

Table 4-2. $\bar{\phi}_m/\bar{\phi}_f$ in Unpoisoned Test Region

	$\bar{A}_m/\bar{A}_f$			
Run no.	Rod 1	Rod 2	Rod 3	Average
97	1.110	1.136	1.118	1.121
100	1.107	1.123	1.107	1.112
122	1.138	1.159	1.142	1.146
128	1.145	1.120	1.122	1.129
129	1.125	1.114	1.124	1.121
130	1.146	1.113	1.126	1.128
Average	1.129	1.128	1.123	1.127 ± 0.012

$$\left(\frac{C_m - 1}{C_m}\right)\left(\frac{C_f}{C_f - 1}\right) = 1.010 \pm 0.005$$

$$\bar{\phi}_m/\bar{\phi}_f = 1.138 \pm 0.013$$

4.2.4. Cadmium Ratio of U-235

The cadmium ratio of U-235 for fissions, C_{25}, is used for the derivation of k_∞. It is also a basic lattice parameter, so it is important to show that the value obtained in the SLE is the same as that measured in the center of an equivalent critical experiment. Agreement would support the assumption that the neutron spectrum in the center of the two types of experiments is the same.

Using standard techniques developed earlier in the SSCR critical experiment program[3], C_{25} measurements were made along the radius of the test region in Loading I, as shown in Figure 4-5, and were repeated in the central cell using Loading II with two different fuel rods. The data foils were 93%-enriched U-Al alloy (18 wt % U), 0.010 inch thick by 0.444 inch in diameter, having the same diameter as the fuel in the swaged fuel rods. In the bare runs the data foils were sandwiched between carefully cut and sealed ends of fuel rods, and accurate alignment was achieved by joining the cut ends with a 1/4-inch-long thin-walled stainless-steel sleeve. In the cadmium-covered runs each U-Al foil was covered with two 0.444-inch-diameter by 0.020-inch-thick

cadmium discs, and the stainless-steel sleeve was replaced by a 0.020-inch-wall cadmium sleeve.

The foils were irradiated for 20 minutes and were gamma counted five times in a sodium iodide scintillation spectrometer that was biased to count photons above 200 kev. Bare and cadmium-covered runs were normalized by simultaneously irradiating two or three U-Al monitor foils and counting them in the same sequence. The same data foils, corrected for background, were used in comparable bare and cadmium-covered runs to eliminate foil calibration errors.

The measurements in Loading I, summarized in Table 4-3, show no significant difference between the three fuel rods. The values in Loading II were, however, 2.440 ± 0.006 for Rod a and 2.495 ± 0.006 for Rod b. Identical measurements in the equivalent critical experiment gave 2.434 ± 0.012 for Rod a and 2.475 ± 0.006 for Rod b. Several conclusions can be drawn from these results. First, the same asymptotic spectrum exists in the SLE and the equivalent critical assembly, since the cadmium ratios from Rods a and b agree. This conclusion is further strengthened by the agreement between the two measurements of the U-238 cadmium ratio reported in the next section. Second, the difference between Rod a and the three rods in Loading I is 2%, the same difference observed in the disadvantage factor measurements. Since Rod b agrees fairly well with the three rods in Loading I, it may be assumed that the thermal component of the activation of Rod a is consistently 2% too small, both in the $\overline{\phi}_m / \overline{\phi}_f$ and the C_{25} measurements. Although careful examination of the cut ends of the fuel rods (by X-ray) and remeasurements of the outer diameter and lattice spacing revealed no significant differences, local variations in inner diameter and fuel density can account for the discrepancy.

Table 4-3. C_{25} Measurements in Unpoisoned Test Region

Run no.	Rod 1	Rod 2	Rod 3	Average
88/95	2.517	2.529	2.517	2.521
96/89	2.513	2.498	2.459	2.490
98/90	2.480	2.434	2.453	2.456
99/91	2.434	2.468	2.511	2.471
125/120	2.505	2.469	2.482	2.482
Average	2.489	2.480	2.484	2.484 ± 0.014

4.2.5. Cadmium Ratio of U-238

Although C_{28}, the cadmium ratio of U-238, is not required for the determination of k_∞, its importance as a basic lattice parameter warrants comparative measurements in the SLE and in the equivalent critical assembly. The measurements were made by the thermal activation technique, a method used extensively in the SSCR critical experiment program.[12] This technique has the dual advantages of eliminating perturbations by the cadmium and of measuring $C_{28} - 1$ directly.

The working equation is as follows:

$$\frac{C_{28} - 1}{C_{28}} = \left(\frac{A_D^B}{A_U^B}\right)_R \left(\frac{C_D - 1}{C_D}\right)_R \left(\frac{A_U'^B - A_U'^C}{A_D'^B}\right)_\phi \left(\frac{C_D}{C_D - 1}\right)_\phi K$$

where A is the weight-normalized saturated activity, C is the cadmium ratio, R designates irradiations in the SLE lattice, and ϕ designates irradiations in a well-thermalized flux. K is a small calculated correction for the non-1/v behavior of dysprosium. The superscripts B and C refer to bare and cadmium covered, and the subscripts U and D refer to uranium and dysprosium.

Figure 4-6 shows the loading arrangement in the test region. In the bare run A_U^B was obtained by dissolving the 0.5-inch-long irradiated fuel slug, removing fission product and other contaminating activity by solvent extraction, and beta counting the U-239 activity. The 0.444-inch-diameter Dy-Al reference foils above and below the fuel slug were beta counted to give A_D^B. In the cadmium-covered run, the Dy-Al foils were counted to obtain C_D. The uranium and Dy-Al samples were weight-calibrated by irradiating them on a wheel in a region of relatively constant flux. Details on the measurement of the ϕ-parameters are given in Reference 12.

The results are summarized in Table 4-4. The internal consistency of the data is very good, and the average value agrees well with that measured in the equivalent critical experiment (C_{28} = 1.087 ± 0.004).

Table 4-4. C_{28} Measurements in Unpoisoned Test Region

Parameter	Run 102	Run 103	Run 104	Run 106	Average
$(A_U^B)_R \times 10^5$	2.759	2.909	2.866	- -	2.845 ± 0.045
$(A_D^B)_R \times 10^5$	6.484	6.502	6.513	- -	6.500 ± 0.013
$(A_D^B)_R/(A_0^B)_R$	0.426	0.448	0.440	- -	0.438 ± 0.007
$(A_D^C)_R \times 10^5$	- -	- -	- -	0.934	0.934 ± 0.013
$(C_0)_R$	- -	- -	- -	- -	6.962 ± 0.098
$\left[(C_0 - 1)/C_0\right]_R$	- -	- -	- -	- -	0.856 ± 0.002
$\left(\frac{A_U'^B - A_U'^C}{A_0'^B}\right)_\phi \left(\frac{C_0}{C_0 - 1}\right)_\phi$	- -	- -	- -	- -	0.0379 ± 0.0004
K	- -	- -	- -	- -	1.067 ± 0.013
C_{28}	1.0887	1.0840	1.0855	- -	1.086 ± 0.002

4.3. Poisoned Test, Unpoisoned Buffer

4.3.1. Loading Configuration

On completion of the measurements in the unpoisoned test region (buffer unpoisoned), the test region was poisoned incrementally with Binal foils, and the reactivity difference between the poisoned test region and the void can was measured. During this sequence of experiments the buffer region (both radial and axial) was not poisoned. To measure the reactivity differences by movement of a calibrated regulating rod, the driver was shimmed to have about 48 cents excess reactivity when the void can was substituted for the test region. In this configuration 16 of the driver channels were fueled with 1.3 kg of U-235, and the remaining channels were filled with graphite. The moderator composition remained at 69.7 mole % D_2O.

4.3.2. Null-Reactivity Measurements

Although the most valid null-reactivity measurements were made with the flux flattened by poisoning the buffer region as well as the test region, measurements were also made with the buffer region unpoisoned to evaluate the error in the determination of k_∞ due to lack of flux flatness. The critical regulating rod position was measured when the test insert contained the void can. The test insert was then removed; the void can was replaced by the unpoisoned test region; the test insert was reloaded into the buffer lattice; and the new critical rod position was measured. This procedure was repeated, as additional Binal foils were loaded in the test region, until the null-reactivity point was reached.

The data in Figure 4-7 show the reactivity difference between the poisoned test region and the void can as a function of the total mass of Binal (and the number of equivalent whole Binal foils). The Binal foils in this experiment were 3.02 inches wide by 17.4 inches long. The uncertainty in $\Delta\rho$ due to errors in rod calibration approaches zero as the null-point is reached. However, the reproducibility is somewhat poorer than that achieved during the more careful measurements with the poisoned buffer. The uncorrected mass of Binal for null-reactivity is

$$M_p = 584 \pm 8 \text{ gm (unpoisoned buffer)}.$$

4.3.3. Flux Distributions

Radial and axial flux distributions were measured by the same techniques described above for the case of 26 Binal foils in the test region. As shown in Figures 4-8 and 4-9, the poison strongly depresses the thermal flux in the test region and has very little effect on the epithermal flux. The flux shapes in the outer buffer differ slightly from the case of the unpoisoned test region because the loading of the driver was changed.

4.4. Poisoned Test, Poisoned Buffer

4.4.1. Loading Configuration

The final measurements were made with the buffer and the test region poisoned to flatten the radial and axial flux shapes. The radial buffer was poisoned with two silver wires attached to each fuel rod in the two inner rows of buffer rods outside the test insert, as shown in Figure 4-10. To reduce the peaks in the axial flux curves, four layers of Binal foils were placed between the pairs of grid plates above and below the test region. Binal foils were also placed horizontally in the end buffers to flatten the axial flux shape. The number of Binal foils in each 3-inch vertical section is shown in the axial flux distribution (see Figure 4-12). Under these conditions the assembly was critical ($\rho_{ex} \approx 13¢$) with the driver loaded as shown earlier in Figure 3-2 (44 channels fueled with 3.5 kg of U-235). The moderator composition remained at 69.7 mole % D_2O.

4.4.2. Flux Distributions

Flux distributions for the final loading of buffer poison are shown in Figures 4-11 and 4-12. The large dip in the epithermal traverse near the silver wires in the buffer is probably caused primarily by interference between the gold and silver resonances; so the other epithermal groups are likely to be flatter. The spectrum appears to be asymptotic over most of the test region. The 2% increase in the thermal-to-epithermal flux ratio at the edge of the test region does not introduce an appreciable error in the measurement of k_∞, as will be shown later.

Information on the thermal flux shape at the edges and corners of the test region was also obtained. Figure 4-13 shows the

ratio of the activity of Dy-Al foils along one edge of the test region to that at the center. One traverse was located at the elevation of the test region midplane and the other at the top of the test region. These data demonstrated the flatness of the flux to within 5% over the entire volume of the test region. Other traverses taken when the poisoned test region was replaced by the void can showed less than a 5% change in the thermal flux distribution over the surface of the void can.

4.4.3. Cell Flux Ratios

The ratio of the average thermal flux in the poison (Binal foil) to the average thermal flux in the fuel, $\bar{\phi}_p / \bar{\phi}_f$, is needed to calculate the thermal utilization in the poisoned test region. This ratio was obtained by measuring the individual ratios in the equation:

$$\frac{\bar{\phi}_p}{\bar{\phi}_f} = \left(\frac{\bar{A}_p}{A_p^s}\right)\left(\frac{A_p^s}{A_f^s}\right)\left(\frac{A_f^s}{\bar{A}_f}\right)\left(\frac{C_m - 1}{C_m}\right)\left(\frac{C_f}{C_f - 1}\right)\left(\frac{\int A_p(w)\, dw}{\int dw}\right)$$

The first term, the ratio of the average thermal flux through the Binal foil to that at its surface, was obtained by extrapolating measurements of bare dysprosium foil activities at the surface and at the center of stacks of two and four Binal foils. Since the ratio was close to unity, the average activity through the Binal foil was assumed to be equal to the average of the inside and surface activities. The ratio of the flux at the surface of the Binal foil to that at the surface of a fuel rod depends on the position of the Binal foil in the cell. Since the Binal foils were positioned randomly, this ratio was measured as a function of the spacing between a Binal foil and an adjacent fuel rod. The experiment was performed by mounting 1/4-inch-diameter Dy-Al foils along the 17.4-inch length of a Binal foil and opposite a similar set of foils on an adjacent fuel rod. The foils were then exposed with the Binal foil tilted so that it rested against one fuel rod at the bottom and against an adjacent fuel rod at the top. The results, given in Figure 4-14, show an average ratio of 0.998 and a maximum possible variation of ±0.007 in this ratio.

The ratio of thermal flux at the surface of the fuel rod to that inside the fuel rod was measured with 0.444-inch-diameter Dy-Al foils at the surface and between cut fuel rods using the geometry for C_{25}

measurements (Loading I). The ratio of Dy-Al cadmium ratios in the moderator C_m and in the fuel C_f is a small correction for the change in the fraction of epicadmium activation in the Dy-Al foils between the fuel and moderator. These parameters were taken from the $\bar{\phi}_m/\bar{\phi}_f$ measurements reported previously. The integrals in the equation, used to calculate the average flux along the width of the Binal foil, were obtained by activating appropriately spaced Dy-Al foils on a Binal foil. The results of all the measurements are summarized in Table 4-5.

Table 4-5. Flux Ratios in Poisoned Cell

Flux ratio	Symbol	Value
Average thermal flux through Binal to thermal flux at surface of Binal	$\bar{A}_p/A_p^s$	0.993 ± 0.004
Activity at surface of Binal to that at surface of fuel rod	A_p^s/A_f^s	0.998 ± 0.007
Activity at surface of fuel rod to average activity in fuel rod	$A_f^s/\bar{A}_f$	1.06 ± 0.01
Fraction thermal activity of Dy-Al in moderator to that in fuel rod	$\left(\frac{C_m - 1}{C_m}\right)\left(\frac{C_f}{C_f - 1}\right)$	1.010 ± 0.005
Cell average flux along Binal	$\int A_p(w)\, dw / \int dw$	1.04 ± 0.01
Average thermal flux in Binal to average thermal flux in fuel	$\bar{\phi}_p/\bar{\phi}_f$	1.10 ± 0.02

4.4.4. Null-Reactivity Measurements

The final null-reactivity measurements made after the buffer region was poisoned are shown in Figure 4-15. As predicted by calculations, the curve is not exactly linear over the entire range, but it is sufficiently linear near the null-point for accurate interpolation. The locations of the Binal foils in the test region for those loadings near the null-point are shown in Figure 4-16. Since each of the 144 cells in the test region could not be poisoned identically because of the heterogeneity of the poison, the importance of a single Binal foil was

measured at two dissimilar locations, designated Loadings 25A and 25B. The results confirm predictions that the heterogeneity of the poison loading has a negligible effect on the null-point. The mass of Binal at the null-point, uncorrected for void can effects, is

$$M_p = 592 \pm 5 \text{ gm (poisoned buffer)}.$$

The uncertainty is based on a precision $\Delta\rho$ near the null-point of approximately ±0.5 cents. Higher precision could have been obtained but was unnecessary for these experiments.

4.4.5. Corrected Null-Point

The small correction to the mass of poison for null-reactivity is required for the aluminum in the void can. The reactivity worth of aluminum was estimated by measuring the reactivity coefficients of 0.080-inch-thick plates of aluminum (Type 6061) and magnesium (AZ-31B, QQM-44A) placed around the periphery of the poisoned test region. The reactivity coefficients, including the displacement of moderator, were approximately 0.349¢/in.^{3} for aluminum and 0.346¢/in.^{3} for magnesium. To separate the very large moderator coefficient, the assumption was made that the reactivity coefficients of aluminum and magnesium were proportional to their thermal absorption cross sections, 0.23 b and 0.063 b, respectively. Solving a set of three simultaneous equations, the following reactivity coefficients were obtained:

$$\alpha_{Mod} = (3.4 \pm 0.3) \times 10^{-1} \text{ ¢/in.}^3$$

$$\alpha_{Al} = (5.4 \pm 3.7) \times 10^{-3} \text{ ¢/in.}^3$$

$$\alpha_{Mg} = (1.5 \pm 1.0) \times 10^{-3} \text{ ¢/in.}^3$$

Using this α_{Al} for the 79.4 in.^{3} of aluminum in the walls and the 27.2 in.^{3} of aluminum in the dividers of the void can, the total correction is $-(0.6 \pm 0.4)$ cents, or $-(5 \pm 3)$ gm Binal. This value is somewhat less than the calculated correction of $-(15 \pm 5)$ gm Binal given in Appendix B. Since the assumption that the reactivity coefficients of aluminum and magnesium are proportional to their thermal absorption cross sections is probably an oversimplification, because the resonance integral of magnesium is appreciable (≈0.9 b for Mg vs ≈0.2 b for Al), the calculated value is preferred. The correction is

sufficiently small, however, that little error is introduced by this choice. A very small correction of +(1.0 ± 0.6) gm Binal is also applied for slight dimensional differences between the test region and the void can. Thus, the corrected mass of poison for null-reactivity is:

$$M_p = 578 \pm 7 \text{ gm Binal}$$

Although not used as a correction, the reactivity effect due to the displacement of moderator by the Binal foils was measured by adding additional pure aluminum foils to the poisoned test region. The reactivity worth for 15.6 $in.^3$ of displacement was (0.24 ± 0.05) ¢/ $in.^3$, which is in reasonably good agreement with the above value when differences in reactivity importance are taken into account.

4.4.6. Cadmium Ratio of U-235

The fission cadmium ratio of U-235 was measured in the poisoned test region using Loading I (see Figure 4-5) and identical experimental techniques. The results of the C_{25} measurements are summarized in Table 4-6. The values for the central fuel rod (Rod 1) varied substantially from run to run and in all cases were much larger than the Rod 2 values. This behavior is attributed to Binal foil misalignment, which caused the cell in which Rod 1 was located to be slightly underpoisoned. Therefore, the value for Rod 2 represents C_{25} in the central part of the poisoned test region. C_{25} is higher in Rod 3 for two reasons. First, the spectrum departs slightly from its asymptotic value at the edge of the test region, as was seen in Figure 4-11. Second, the 26 equivalent Binal foils could not be arranged to poison each cell in the test region identically. Therefore, the Binal foils were deliberately arranged in a symmetrical configuration for these measurements so that 120 of the 144 cells were "fully" poisoned, 20 were "half" poisoned, and 4 were "unpoisoned". Rod 3 was located in one of the "unpoisoned" cells.

Table 4-6 C_{25} Measurements in Poisoned Test Region

Run no.	Rod 2	Rod 3
67/63	2.159	2.337
64/60	2.166	2.333
66/61	2.150	2.299
68/65	2.155	2.308
Average	2.157 ± 0.007	2.319 ± 0.019

A limit to the effective U-235 cadmium ratio for the poisoned test region can be obtained by weighting the Rod 2 value by 120, the Rod 3 value by 4, and the average of Rods 2 and 3 by 20. This result (C_{25} = 2.173) is an upper limit, since it includes not only the effects of Binal foil heterogeneity and nonuniform distribution, which should be corrected, but also the nonasymptotic condition at the edge of the test region, which should be considered as a spectral mismatch error rather than as a correction. Fortunately, the difference between the upper and lower limits is only 0.7%, so the best value for C_{25} in the poisoned test region (26 Binal foils) can be taken as 2.165 ± 0.010, where the uncertainty is sufficiently large to cover both extremes.

Since C_{25} was measured in a test region containing 617 gm Binal and since the corrected null-point actually corresponded to 578 gm Binal, an additional small correction is required. On the assumption that $(1 + \delta_{25})$ is linearly proportional to M_p, the corrected value of C_{25} at the null-point is C_{25} = 2.182 ± 0.011.

Since the interpolation is small, the linear assumption should not increase the error in C_{25} appreciably. An alternate approach in which an apparent value of k_∞ is derived from data of the 617 gm Binal case and this value is corrected to the true null-point on the assumption that $(k_\infty)_p$ is linearly proportional to M_p gives the same final result.

4.5. Derivation of k_∞

The infinite medium multiplication factor was derived by the procedure described in Section 2 using the experimental data listed in Table 4-7. The concentration of D_2O in the moderator was measured

by a density technique described in Reference 3. No degradation beyond the limits quoted was observed between the first- and last-day samples.

The final results are summarized in Table 4-8, which compares the values of k_∞ obtained by the two methods described in Section 2. The results are discussed in more detail in Section 7.

Table 4-7. Summary of Data for k_∞ Derivation

D_2O concentration, mole %	69.7 ± 0.1
Fuel material	4.02%-enriched UO_2
Rod outer diameter, inch	0.4755
Lattice pitch, inch	0.595
M/W ratio	1.006
Volume of test region, cm^3	1.4619×10^4

	Unpoisoned	Poisoned
Mass of Binal, gm	0	578 ± 7
N_B, atoms B/cm^3 test region	0	$(5.570 \pm 0.044) \times 10^{19}$
Volume displaced by Binal, cm^3	0	220
$\bar{\phi}_m/\bar{\phi}_f$	1.138 ± 0.013	1.138
$\bar{\phi}_c/\bar{\phi}_f$	1.07 ± 0.02	1.06 ± 0.01
$\bar{\phi}_p/\bar{\phi}_f$	0	1.10 ± 0.02
C_{25}	2.484 ± 0.014	2.182 ± 0.011
$1 + \delta_{25}$	1.674 ± 0.006	1.846 ± 0.007

Table 4-8. Derivation of k_∞

Parameter	Unpoisoned	Poisoned	Ratio
f	0.8445	0.7304	1.156 ± 0.004
ϵ	1.0854	1.0978	0.989 ± 0.002
p	0.3386	0.3107	1.090 ± 0.004
$l + \delta_{25}$	1.674	1.846	0.907 ± 0.005
L	- -	- -	0.995 ± 0.003
$l - \Gamma$	- -	- -	0.971 ± 0.002
k_∞ (Equation 2-6)			1 125 ± 0.009
k_∞ (Equation 2-8)			1.122 ± 0.005

Figure 4-1. Radial Flux Distribution (Unpoisoned Test and Buffer)

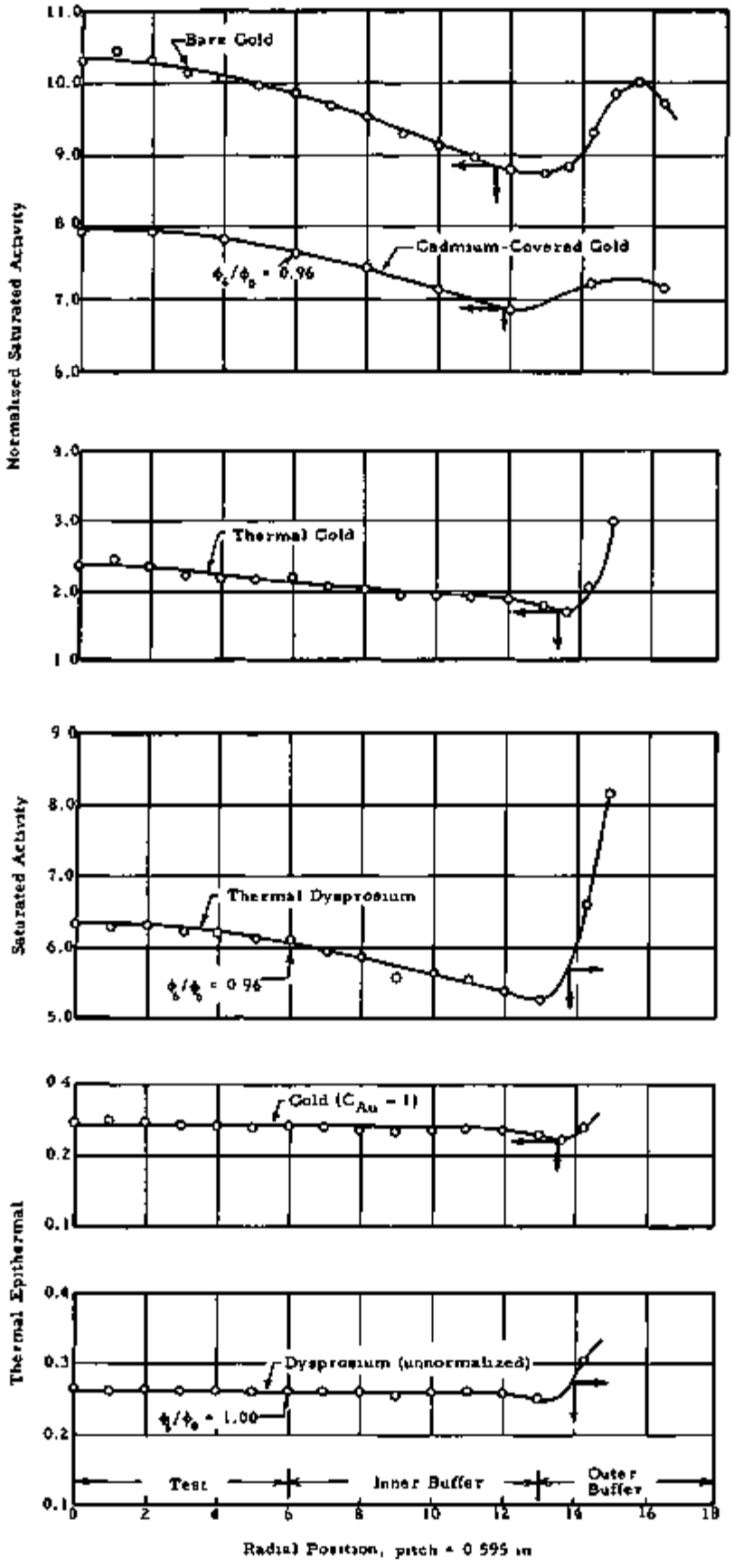

Figure 4-2. Axial Flux Distribution (Unpoisoned Test and Buffer)

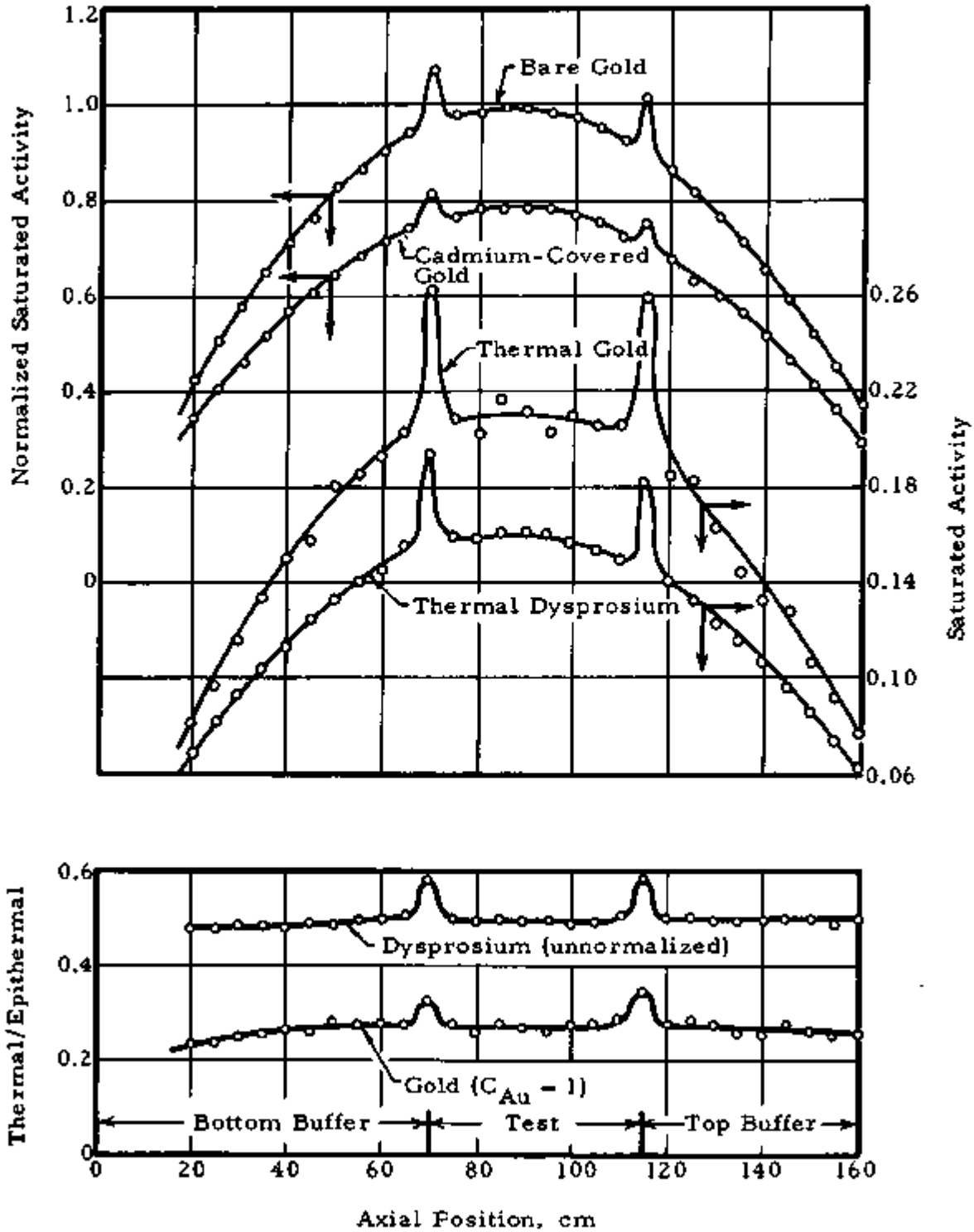

Figure 4-3. Epithermal Flux Distribution (Unpoisoned Test and Buffer)

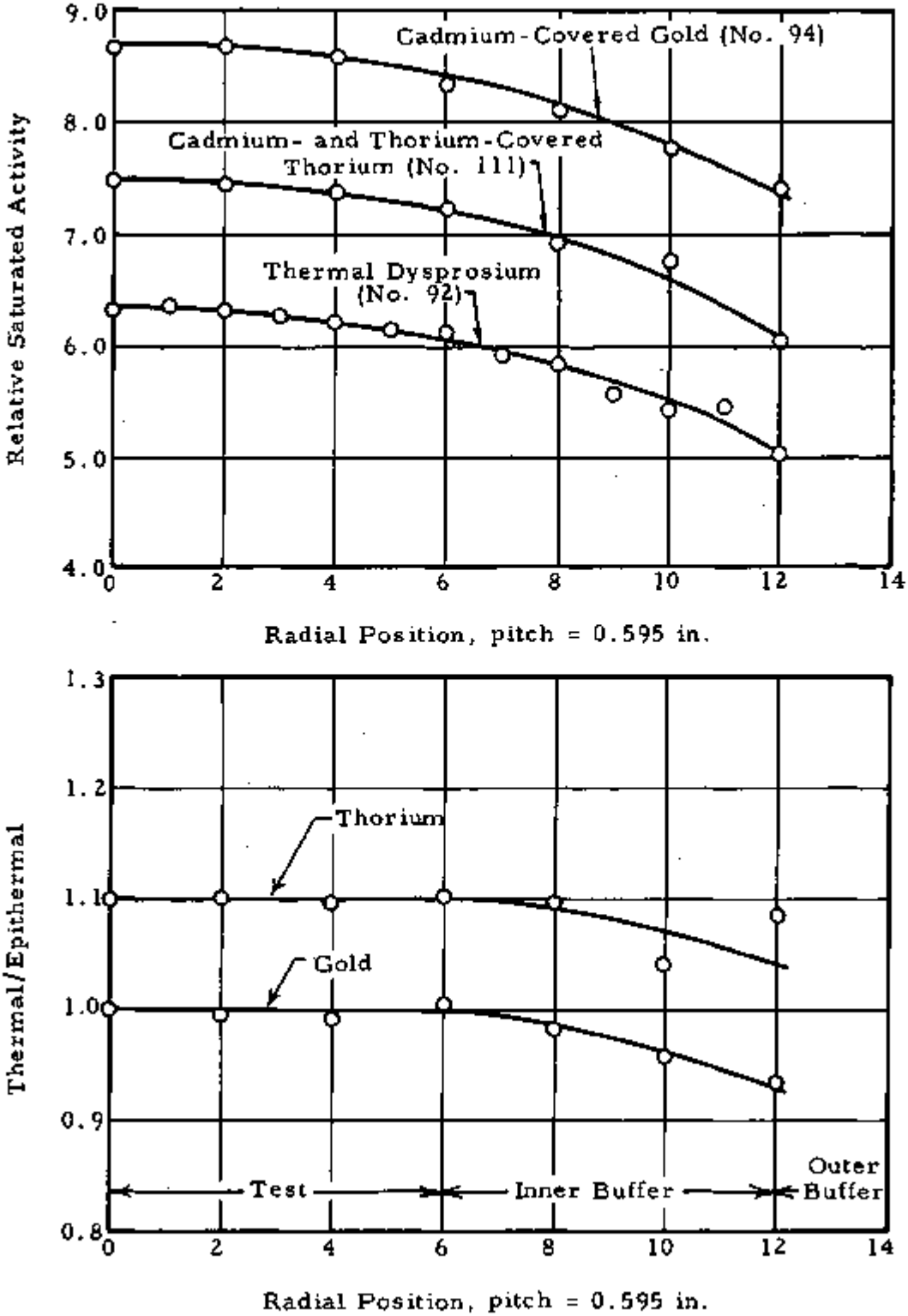

Figure 4-4. Sector Foils in $\overline{\phi}_m / \overline{\phi}_f$ Measurement

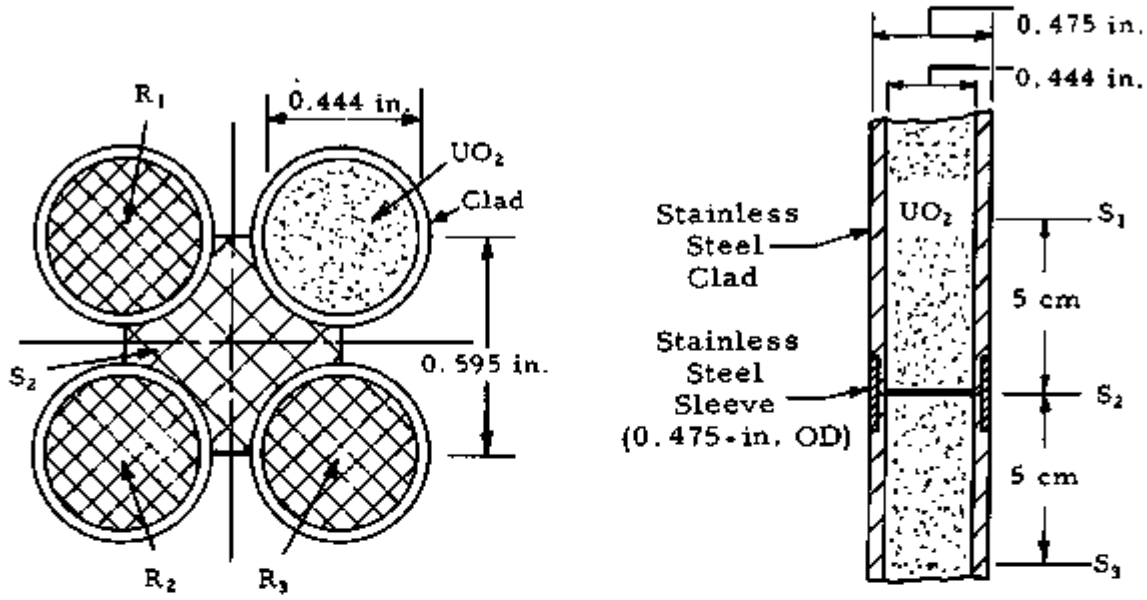

Loading I

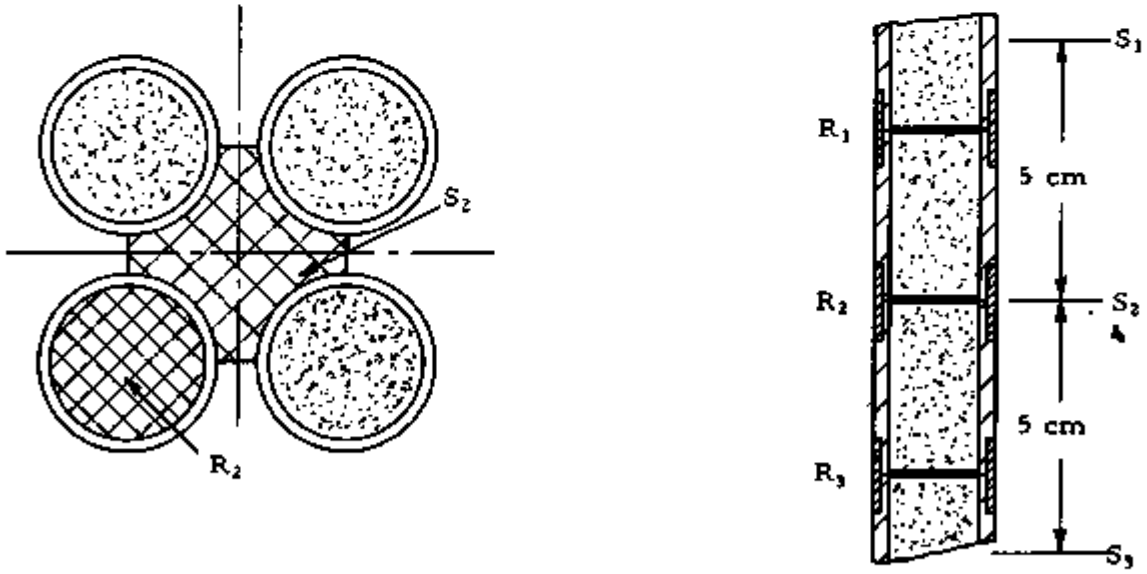

Loading II

Figure 4-5. U-Al Foils in C_{25} Measurement

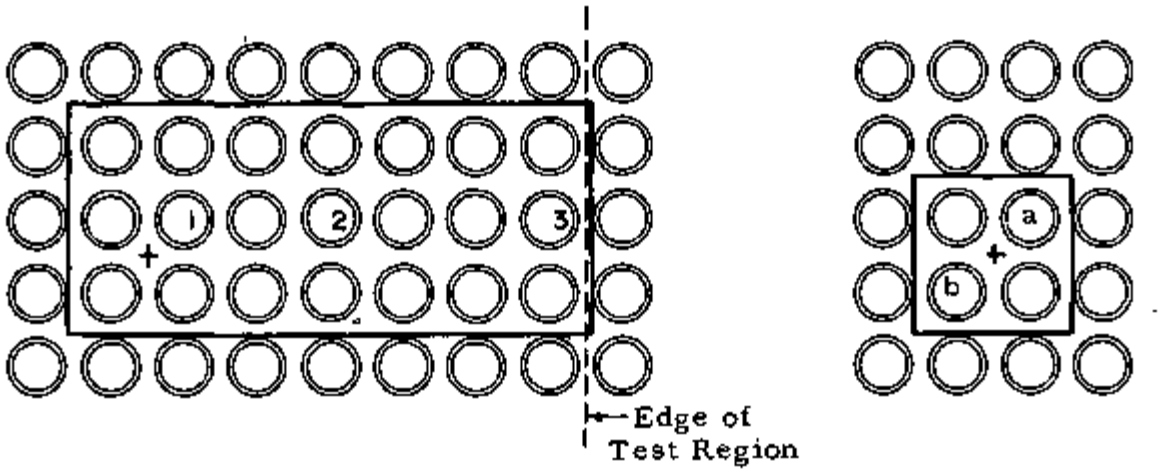

Loading I

Loading II

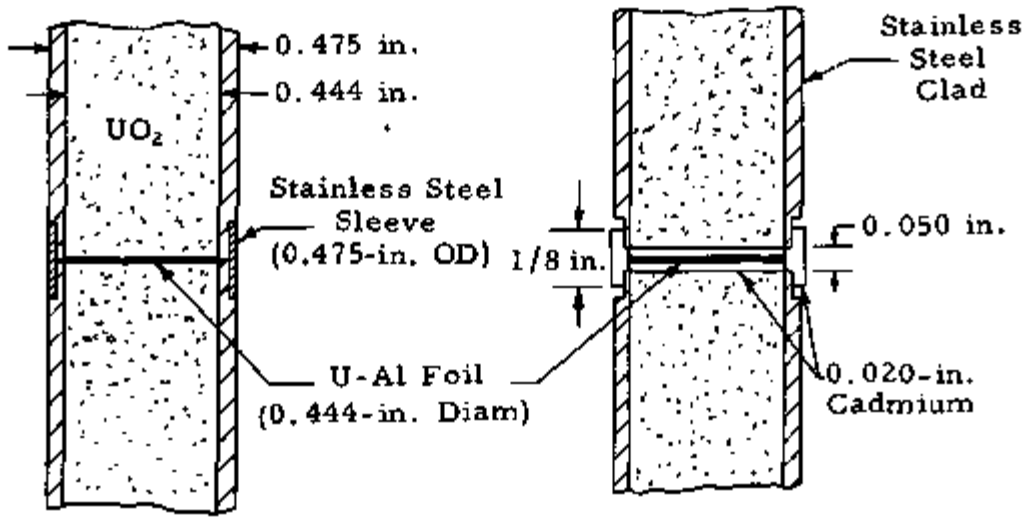

Bare

Cadmium-Covered

Figure 4-6. Loading Arrangement for C_{28} Measurement

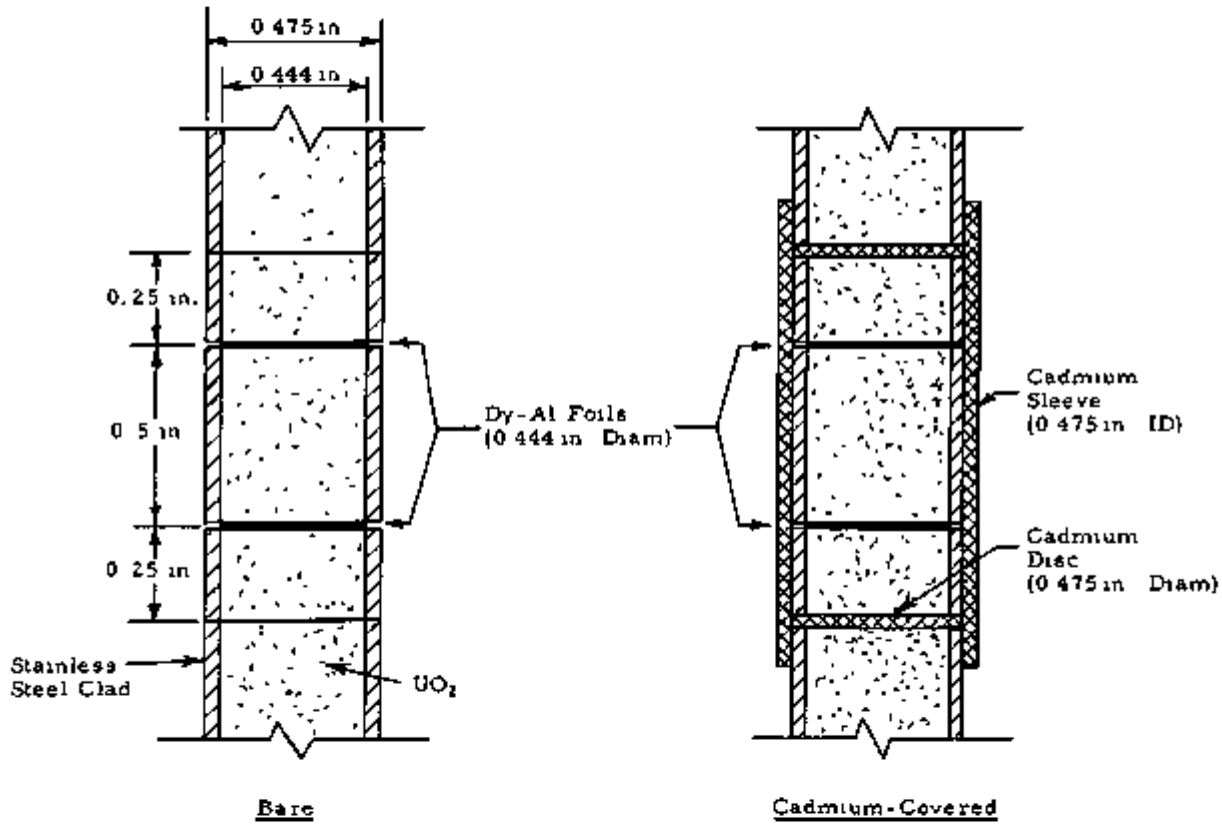

Figure 4-7. Δρ Vs Mass of Poison (Unpoisoned Buffer)

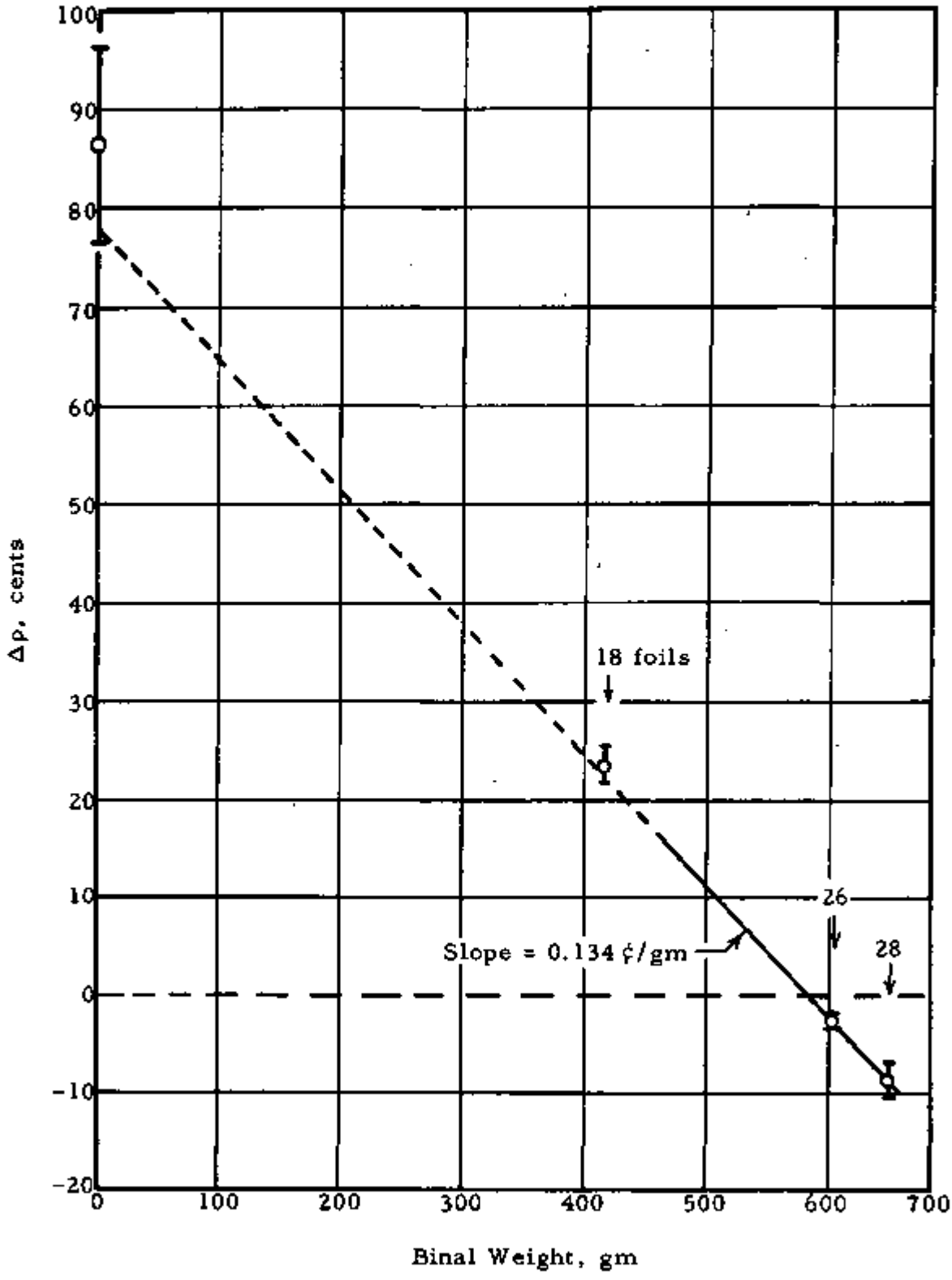

Figure 4-8. Radial Flux Distribution (Poisoned Test, Unpoisoned Buffer)

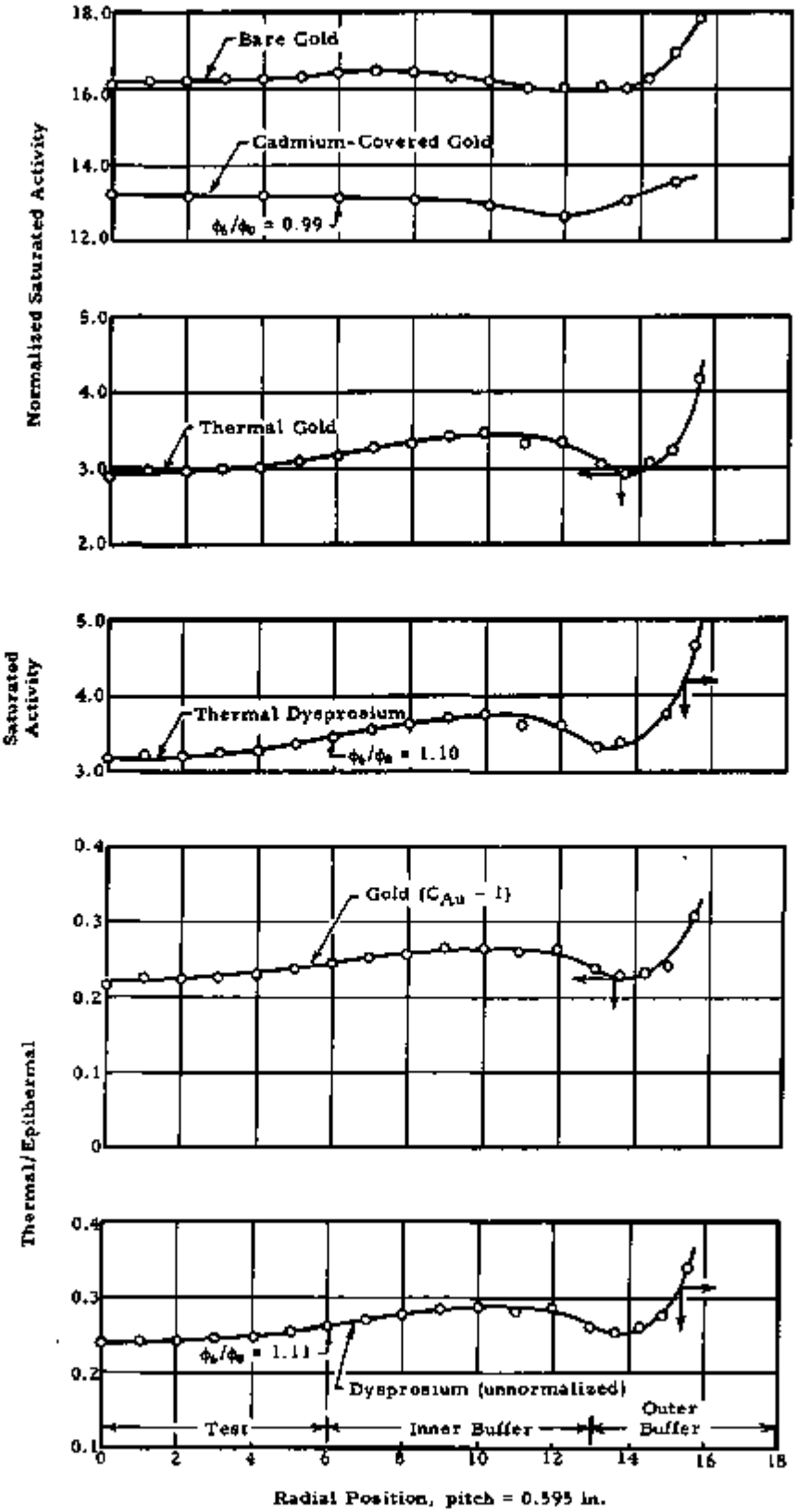

Figure 4-9. Axial Flux Distribution (Poisoned Test, Unpoisoned Buffer)

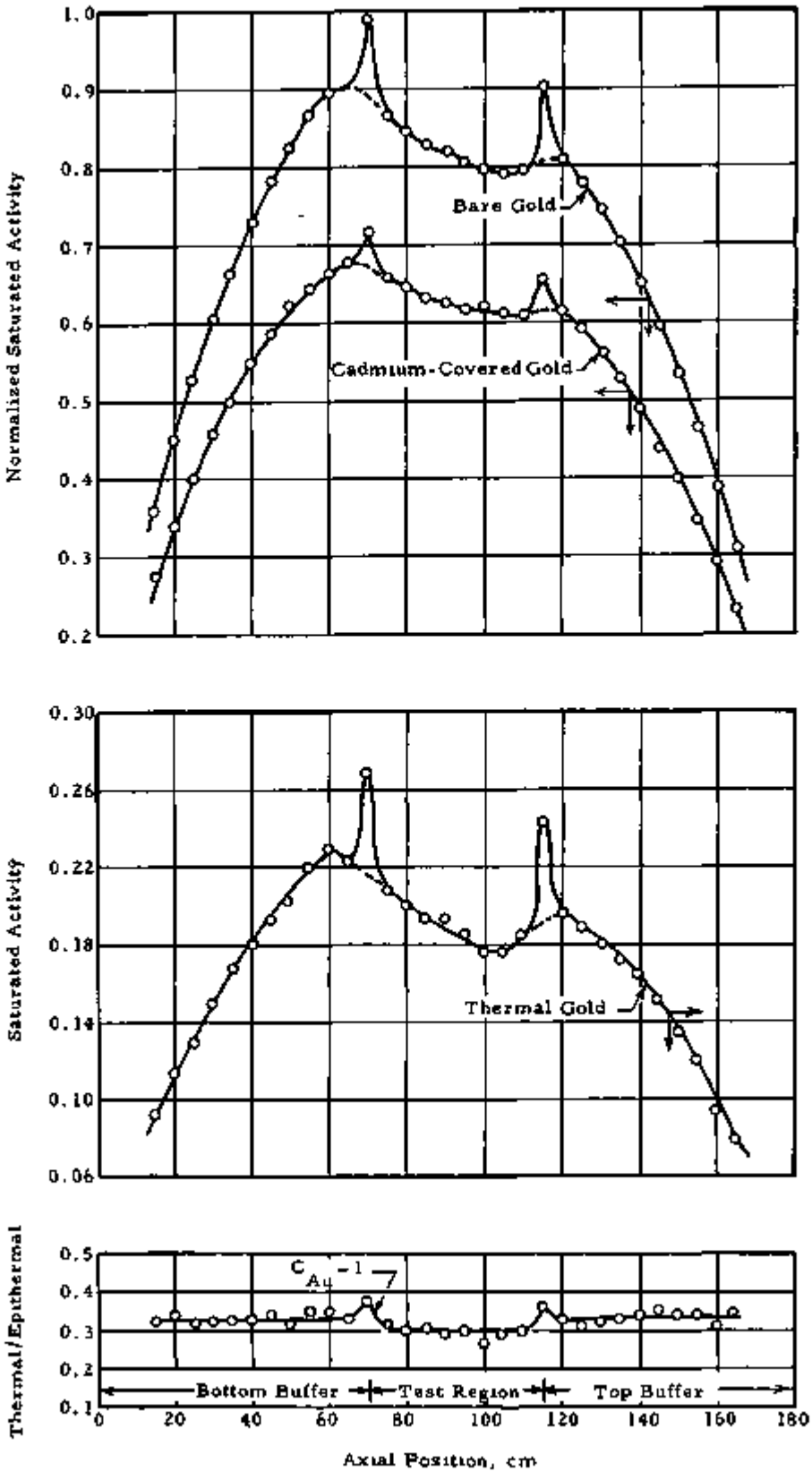

Figure 4-10. Location of Poison Wires in Buffer

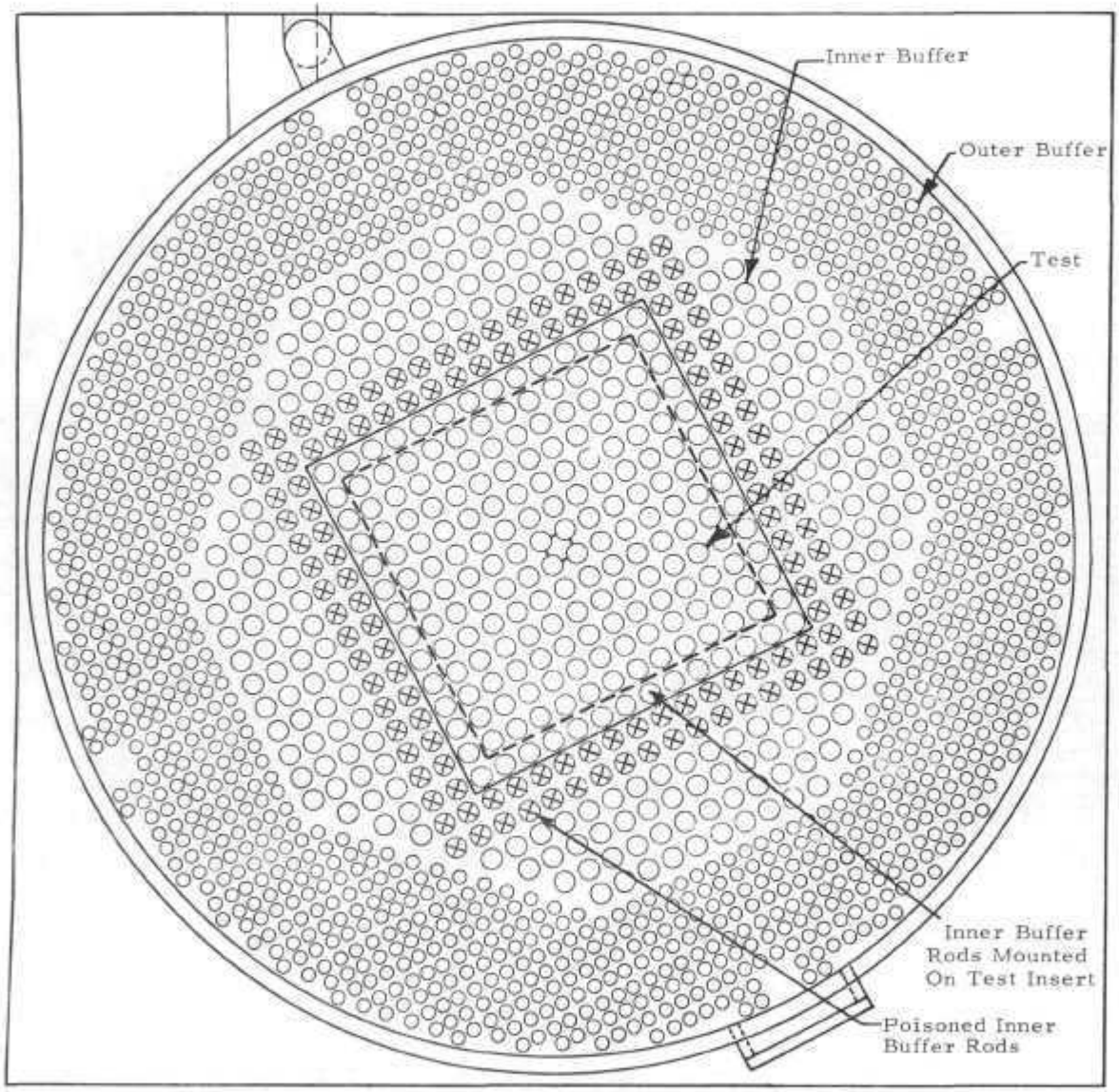

Figure 4-11. Radial Flux Distribution (Poisoned Test and Buffer)

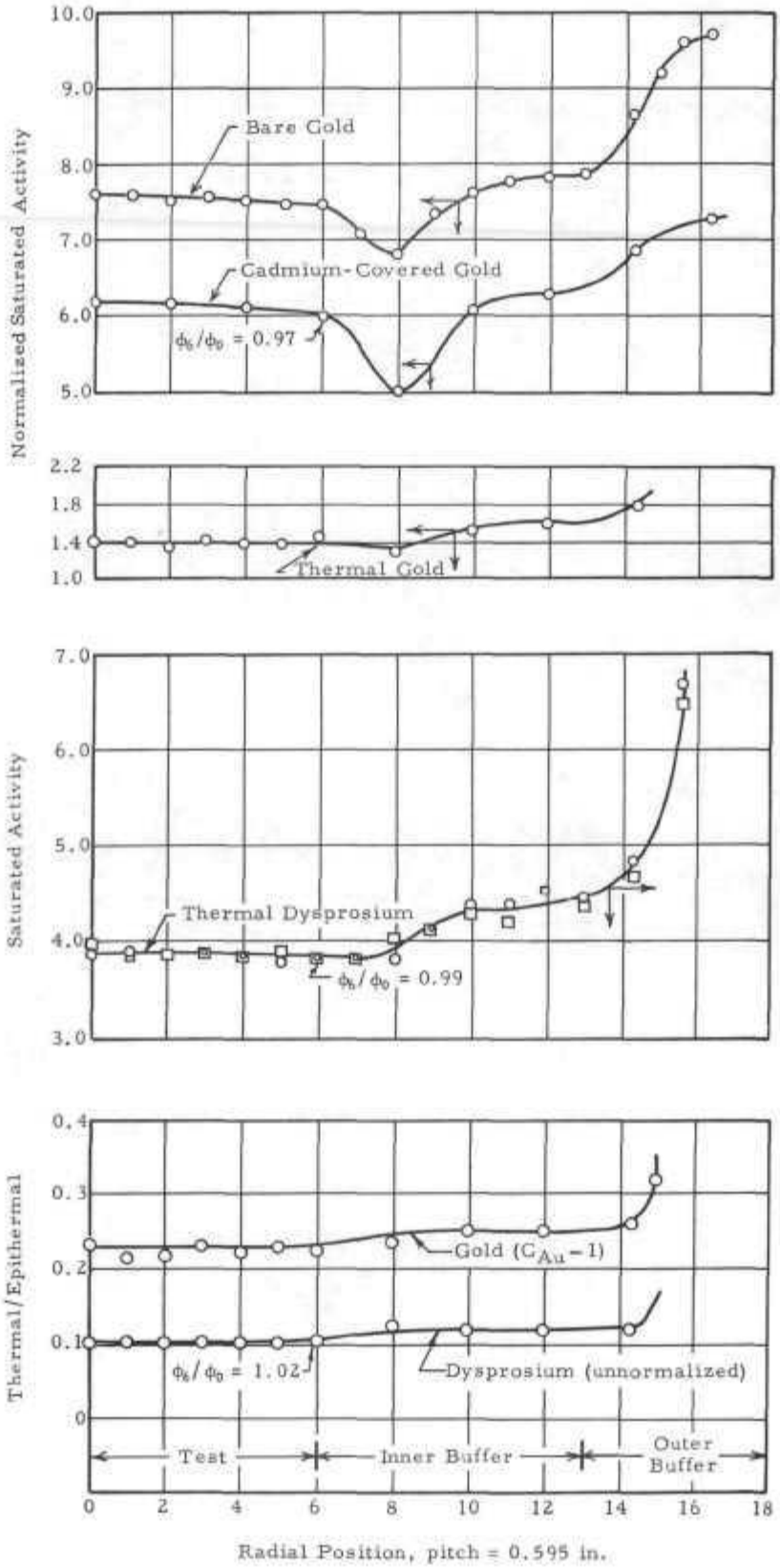

Figure 4-12. Axial Flux Distribution (Poisoned Test and Buffer)

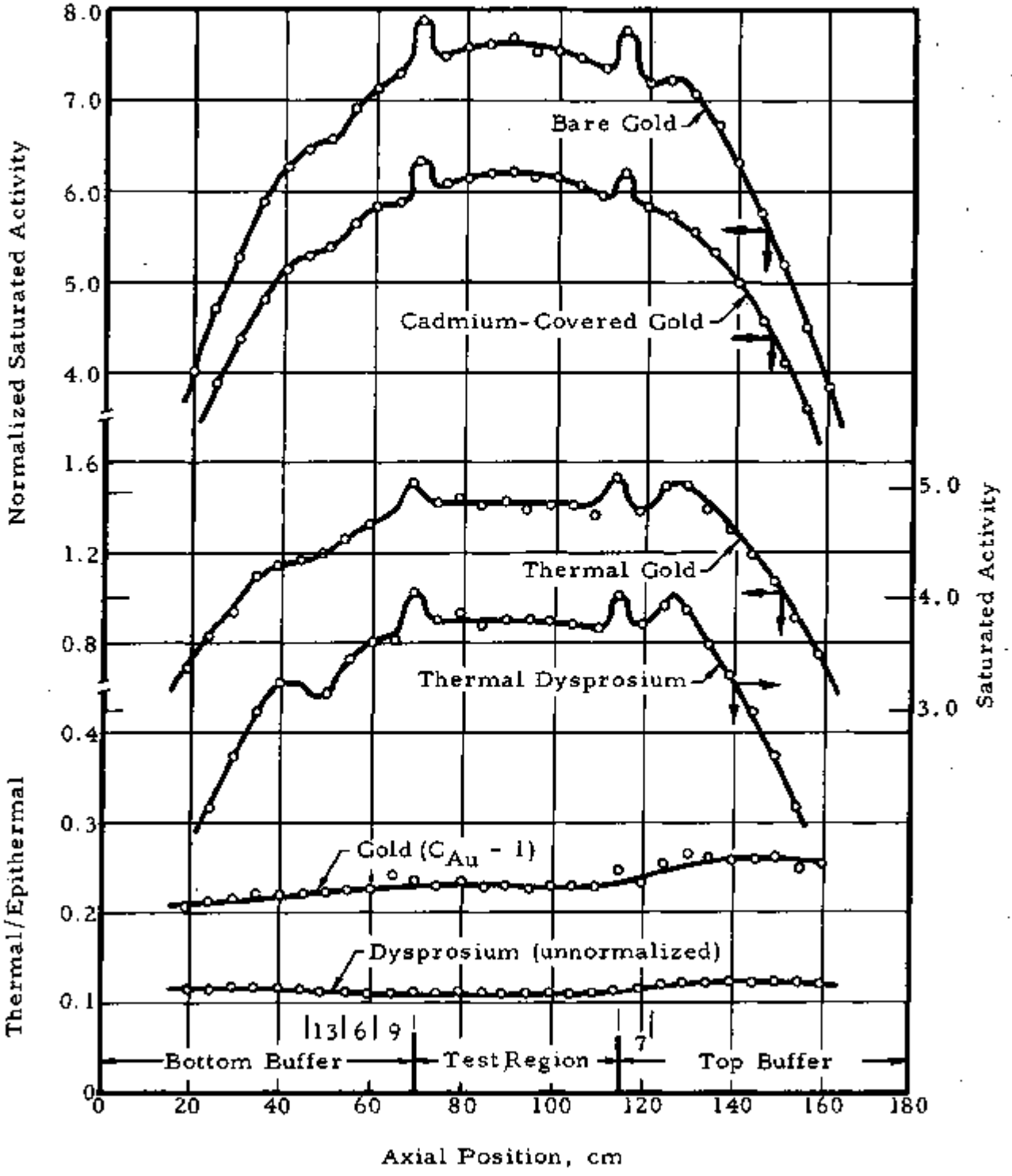

Figure 4-13. X-Y Flux Distribution (Poisoned Test and Buffer)

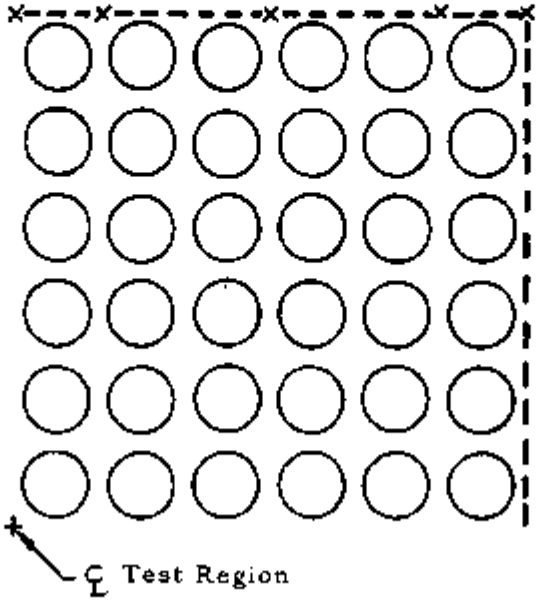

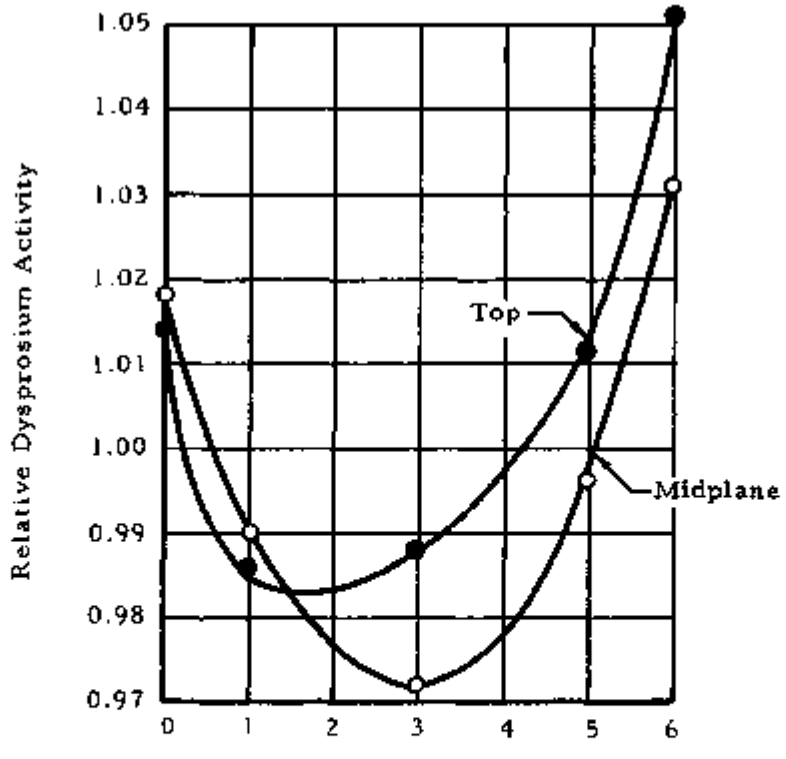

Figure 4-14. Ratio of Flux at Surface of Binal to Flux at Surface of Fuel Rod

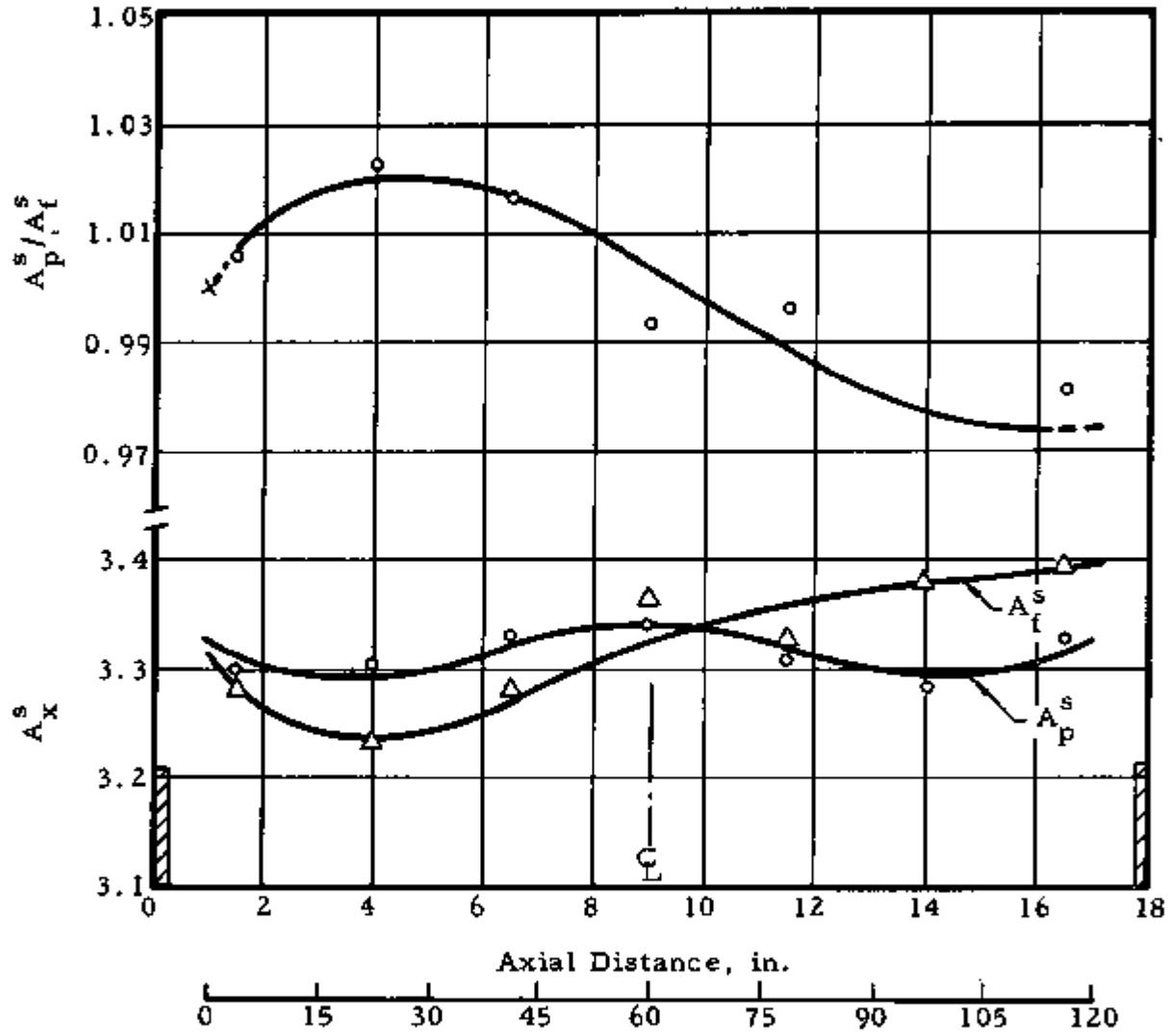

Figure 4-15. $\Delta\rho$ Vs Mass of Poison (Poisoned Buffer)

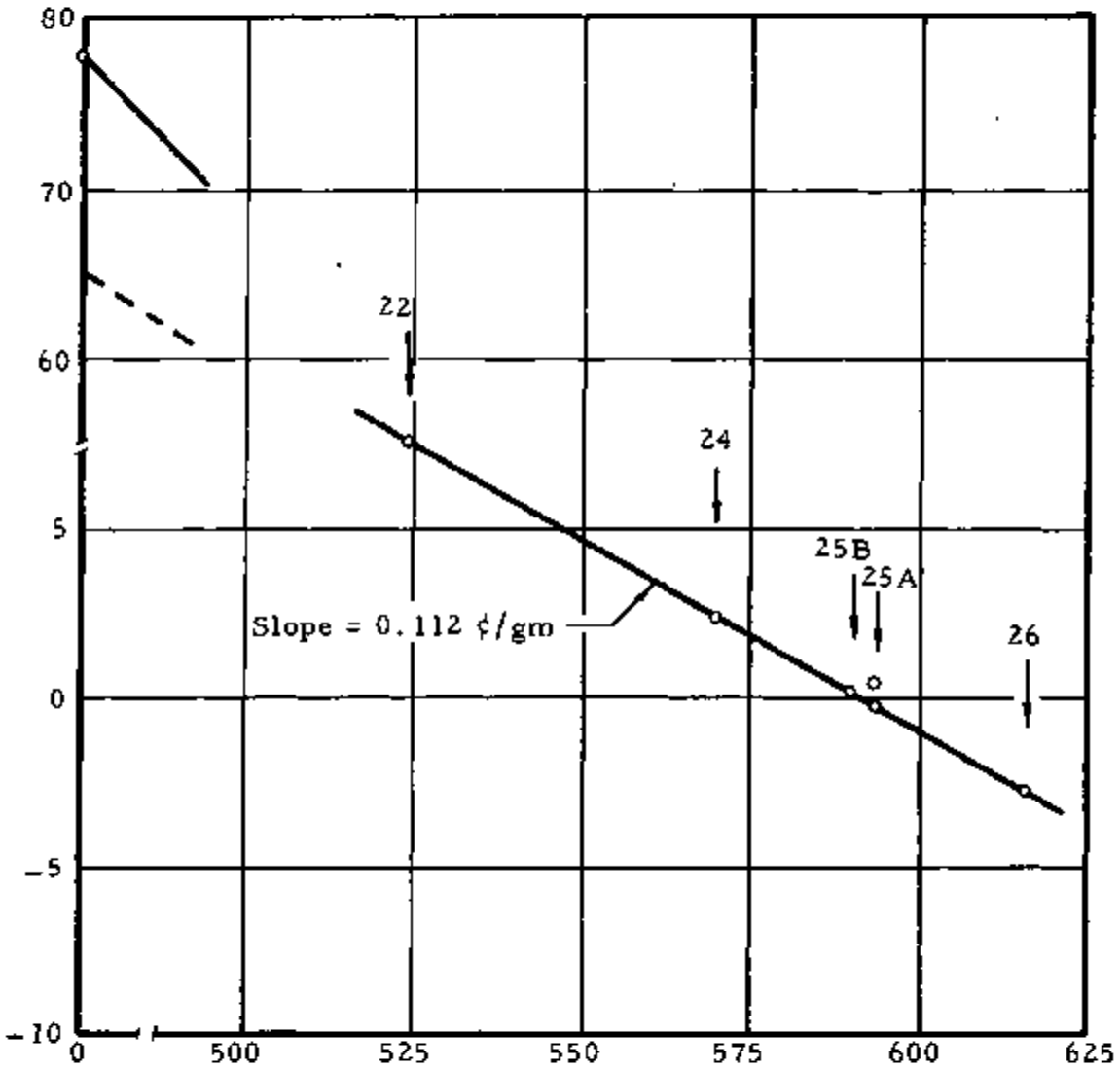

Figure 4-16. Loading Pattern of Binal Foils in Test Region

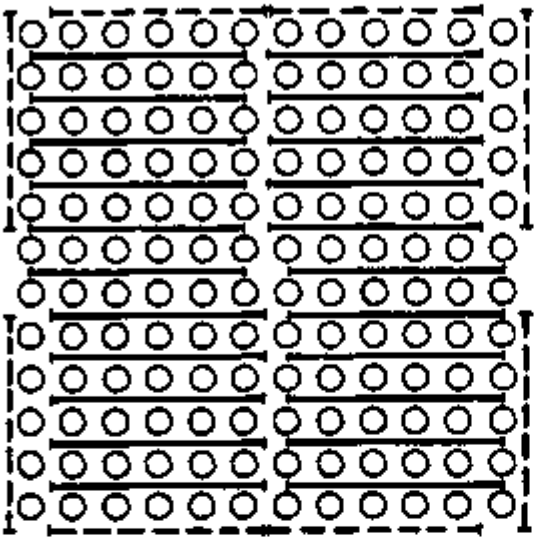

26 Equivalent Foils

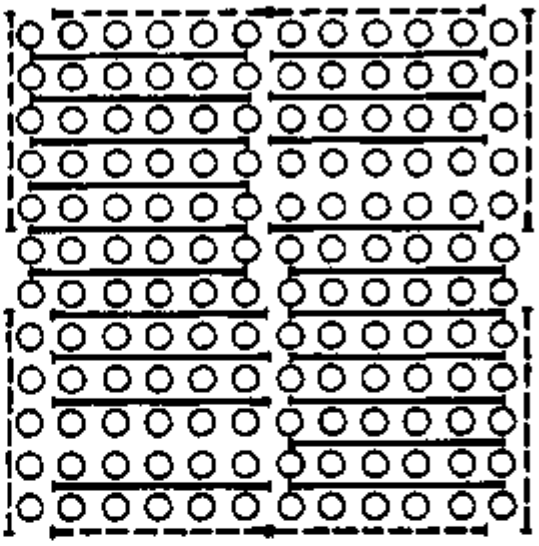

24 Equivalent Foils

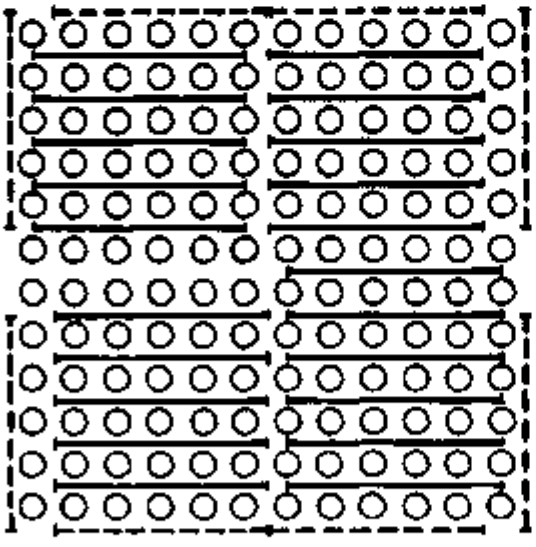

25 Equivalent Foils (A)

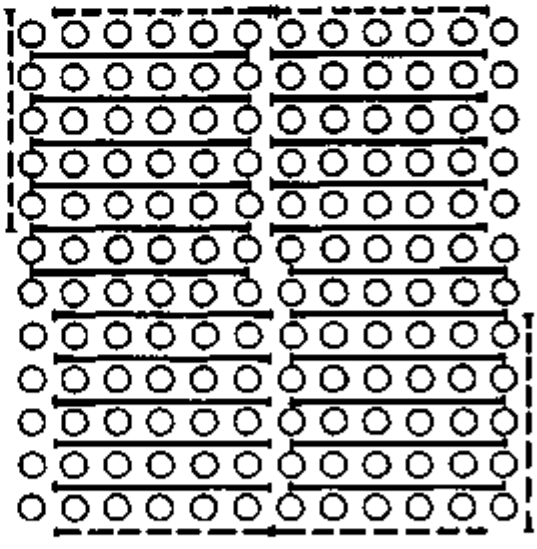

25 Equivalent Foils (B)

Whole Foils
Perforated Foils

5. EXPERIMENTS WITH UO_2-ThO_2 FUEL (70.4% D_2O)

5.1. Preliminary Experiments

The reactivity worth of the control rods was measured to be approximately \$1.70 for each of the three pairs of safety rods and approximately \$0.65 for the single regulating rod. These values are somewhat lower than in the preceding experiments because the driver was less heavily loaded. The uncertainty in reactivity measurements due to variations in the moderator level was reduced by raising the overflow about 2 inches above the level used in the preceding experiments and obtaining a value for $\partial\rho/\partial h$ of about 2¢/cm. The effect of moderator degradation was measured to be about 70 cents per percent change in D_2O concentration. The net reproducibility for null-reactivity measurements remained at about ± 0.5 cents.

5.2. Unpoisoned Test, Unpoisoned Buffer

5.2.1. Loading Configuration

The buffer and test regions contained a total of 2543 UO_2-ThO_2 fuel rods on a uniform lattice pitch of 0.387 inch. Therefore, the effective radius of the buffer region was 11.01 inches. The moderator composition was 70.4 ± 0.1 mole % D_2O. Criticality was achieved with 68 driver channels filled with graphite. Figure 5-1 is a plan view of the buffer and test regions; it also shows where the poison was added to the buffer region for later experiments (see Section 5.4).

5.2.2. Flux Distributions

Radial and axial flux distributions were measured with bare and cadmium-covered gold and Dy-Al foils by the same techniques described in Section 4. The radial traverses are shown in Figure 5-2, where the thermal flux obtained from the gold and Dy-Al data have been normalized on the same scale. The ratio of thermal-to-epithermal activity is equal to the cadmium ratio of gold minus one; the normalized

ratio of Dy-Al to cadmium-covered gold activity is also shown for comparison. As expected, the spectrum is asymptotic well into the buffer region. The ratio of the flux at the edge of the test region to that at its center is 0.97 for both the thermal and epithermal fluxes.

5.2.3. Thermal Disadvantage Factor

The thermal disadvantage factor $\bar{\phi}_m/\bar{\phi}_f$ was measured in the central fuel rod by the same techniques described in Section 4.2.3. Three 0.260-inch-diameter Dy-Al foils were loaded in the fuel rod, separated by single fuel pellets (≈0.4 inch long). In the cadmium-covered runs, the aluminum cladding was replaced by a 2.0-inch-long by 0.016-inch-wall cadmium sleeve having the same outer diameter as the aluminum cladding and closed at the ends by 0.020-inch-thick cadmium discs. The results of the measurements are given in Table 5-1. Each value is the average of three separate determinations.

Table 5-1. $\bar{\phi}_m/\bar{\phi}_f$ in Unpoisoned Test Region

Run no.	Average $\bar{A}_m/\bar{A}_f$	$\left(\frac{C_m - 1}{C_m}\right)\left(\frac{C_f}{C_f - 1}\right)$	$\bar{\phi}_m/\bar{\phi}_f$
190	1.14	--	1.19
193	1.11	--	1.16
195	1.12	--	1.17
197	1.12	--	1.17
Average	1.12 ± 0.01	1.045 ± 0.002	1.17 ± 0.01

5.2.4. Cadmium Ratio of U-235

C_{25}, the cadmium ratio of U-235 for fissions, was measured by the same technique used in the previous experiments (Loading I), except that the U-Al foils were 0.260 inch in diameter to match the diameter of the fuel pellets. The measurements were made along the radius of the test region in every other fuel rod. Rod 1 was at the center of the test region, and Rod 4 was in the outer row of fuel rods (see Figure 5-5).

The results are summarized in Table 5-2. The difference between fuel rods does not appear to be statistically significant, particularly if the low point for Rod 4 (215/221) is ignored. Therefore, C_{25} is essentially constant over the test region, in agreement with the gold cadmium ratio data, and the neutron spectrum should be asymptotic. One of the monitor foils in Runs 214/220 was suspect. If the values from these runs are weighted only half as strongly, C_{25} decreases to 2.240, and, if the suspicious low point is eliminated, C_{25} increases to 2.247. Both values are, however, within the standard deviation quoted.

Table 5-2. C_{25} in Unpoisoned Test Region

Run no.	Rod 1	Rod 2	Rod 3	Rod 4	Average
212/219	2.248	2.225	2.201	2.244	2.230 ± 0.015
214/220	2.275	2.241	2.275	2.278	2.267 ± 0.012
215/221	2.239	2.261	2.262	2.181	2.236 ± 0.028
Average	2.254 ±0.019	2.242 ±0.018	2.246 ±0.042	2.234 ±0.049	2.244 ± 0.010

5.2.5. Cadmium Ratio of Th-232

C_{02}, the cadmium ratio of Th-232, is not required for the derivation of k_∞ but was included in the program because of its importance as a lattice parameter. The measurements were made in the central fuel rod using the same loading arrangement as for the $\overline{\phi}_m/\overline{\phi}_f$ measurements. The thorium metal foils were 0.260 inch in diameter (diameter of fuel pellet) and 0.010 inch thick. After irradiation, the Th-233 activity was beta counted in proportional counters. The same foils were used in the same positions in comparable bare and cadmium-covered irradiations, and the foils were counted in the same sequence and at the same counting times. Background corrections were applied by counting the foils prior to irradiation. The runs were normalized by three bare gold monitor foils. The results are summarized in Table 5-3.

Table 5-3. Cadmium Ratio of Th-232

Run no.	Foil 2	Foil 3	Foil 4	Average
192/194	1.29	1.29	1.30	1.29 ± 0.01
196/198	1.24	1.25	1.26	1.25 ± 0.01
Average	--	--	--	1.27 ± 0.02

5.3. Poisoned Test, Unpoisoned Buffer

5.3.1. Loading Configuration

On completion of the measurements in the unpoisoned test region, the test region was poisoned incrementally with Binal foils until the null-point was reached. The moderator composition was unchanged, and the buffer was unpoisoned. Criticality was reached with 80 driver channels filled with graphite.

5.3.2. Null-Reactivity Measurements

Although the most valid null-reactivity measurements were made with the flux flattened by poisoning the buffer, measurements were also made with the buffer unpoisoned to evaluate the error in k_∞ due to lack of flux flatness. The uncorrected (for void can) mass of Binal for null-reactivity was

$$M_p = 568 \pm 5 \text{ gm (unpoisoned buffer)}$$

More details on these measurements are given in Section 5.4.

5.3.3. Flux Distribution

Radial and axial flux distributions were mapped with bare Dy-Al foils by the same techniques described above. As shown in Figure 5-3, the ratio of the flux at the edge of the test region to that at its center was 1.17 radially and about 1.3 axially.

5.4. Poisoned Test, Poisoned Buffer

5.4.1. Loading Configuration

With the test and buffer regions poisoned in their final configuration (described in Section 5.4.4), criticality was reached by

filling all except 12 (3 at each corner) of the driver channels with graphite and adding fuel to six of the channels in the first row. Each of the fueled channels contained 72 U-Al foils distributed over a length of 6 feet. The total mass of U-235 was approximately 0.7 kg.

5.4.2. Flux Distribution

In an attempt to flatten the flux across the poisoned test region, poison was added to the buffer region in a number of different configurations. It proved to be impossible to satisfy both requirements simultaneously, i.e., constant thermal flux and constant cadmium ratio, although either one could be achieved separately. However, a reasonable compromise was reached with the buffer and test region loadings described in Section 5.4.4. Figure 5-4 shows the radial and axial flux distributions. The ratios of the flux at the edge of the test region to that at its center are approximately 0.94 and 0.96, respectively, for the thermal and epithermal components, and the ratio of the thermal-to-epithermal components is constant to within about one cell of the edge of the test region, where it appears to rise about 2%. The accuracy of these data is limited by the low cadmium ratio of gold in these lattices.

The peaks in the axial flux distribution at the ends of the test region, due to the absence of fuel in the end caps, are highly localized. Distributions measured with Dy-Al foils mounted directly on the Binal poison foils (open squares) represent a more realistic picture of the axial flux shape in the active part of the test region. The ratio of the thermal flux at the end of the test region to that at its center is about 1.03 ± 0.02. Other data showed that the thermal flux was within about 5% of its central value at all points at the edges and corners of the test region.

5.4.3. Flux Ratios

The ratio of the average thermal flux in the poison (Binal) to that in the fuel $\overline{\phi}_p/\overline{\phi}_f$ was measured by the same procedure described for the first experiment (Section 4.4.3). In that terminology,

$$\frac{\bar{\phi}_p}{\bar{\phi}_f} = \left(\frac{\bar{A}_p}{A_p^s}\right)\left(\frac{A_p^s}{\bar{A}_f}\right)\left(\frac{C_m - 1}{C_m}\right)\left(\frac{C_f}{C_f - 1}\right)\left(\frac{\int A_p(w)\, dw}{\int dw}\right)$$

where the second and third terms have been combined to simplify the measurement. Table 5-4 summarizes the results, where $\bar{A}_p/A_p^s$ was taken from Section 4.4.3, since it should be relatively independent of the lattice spectrum and geometry, and the cadmium ratios were taken from the disadvantage factor measurement (Table 5-1).

Table 5-4. $\bar{\phi}_p/\bar{\phi}_f$ in Poisoned Test Region

Symbol	Value
$\bar{A}_p/A_p^s$	0.993 ± 0.004
$A_p^s/\bar{A}_f$	1.079 ± 0.019
$\left(\frac{C_m - 1}{C_m}\right)\left(\frac{C_f}{C_f - 1}\right)$	1.045 ± 0.002
$\int A_p(w)\, dw/\int dw$	1.03 ± 0.01
$\bar{\phi}_p/\bar{\phi}_f$	1.15 ± 0.02

5.4.4. Null-Reactivity Measurements

The final null-reactivity measurements were made with the buffer region poisoned to approximate flat-flux conditions. As shown in Figure 5-1, the two rows of buffer fuel rods surrounding the test insert were poisoned with silver wires. In addition, Binal foils were placed in that part of the buffer region included in the test insert itself as follows: one thickness of Binal on the outer row of buffer fuel rods in the test insert, three thicknesses between the two rows of buffer fuel rods, and no Binal between the outer row of fuel rods in the test

region and the inner row of buffer fuel rods. In the axial direction, two thicknesses of Binal foils were placed between the pair of grid plates above the test region and three were placed below the test region to reduce the flux peak at the grid plate locations. Binal foils were also distributed in the top and bottom buffers to improve axial flux flatness.

The distribution of Binal foils in the test region is shown in Figure 5-5, where the case labeled "unpoisoned buffer" shows the poison configuration referred to in Section 5.3.2. The dashed lines represent perforated Binal foils, which weigh approximately half as much as the regular foils. Three configurations of poison were considered in these measurements with the poisoned buffer. As shown in the lower curve of Figure 5-6 (the upper curve presents the data referred to in Section 5.3.2 for the unpoisoned buffer), the 545.8 gm case is slightly underpoisoned, and the 568.5 gm case is slightly overpoisoned. The mass of Binal at the null-point, uncorrected for void can effects, is

$$M_p = 560 \pm 7 \text{ gm (poisoned buffer)}$$

These and other supplementary measurements also show that the mass of poison for null-reactivity is quite insensitive to the physical distribution of the Binal foils. Note also the small difference in M_p from that obtained with the unpoisoned buffer. The last case shown in Figure 5-5 (544.5 gm) represents a more uniform poison distribution, which was used for the flux measurements.

5.4.5. Corrected Null-Point

Two small corrections to the mass of Binal for null-reactivity are required, as described in Section 6.4.5. The correction for the aluminum in the void can is $-(10 \pm 5)$ gm Binal, and the correction for the aluminum posts is $+(17 \pm 5)$ gm Binal. Thus, the corrected mass of poison for null-reactivity is

$$M_p = 567 \pm 10 \text{ gm Binal}$$

5.4.6. Cadmium Ratio of U-235

C_{25} was measured in the poisoned test region using the same techniques used in the unpoisoned measurements (see Section 5.2.4). In this case, however, some difficulty was experienced in

achieving asymptotic conditions throughout the test region. The data listed at the top of Table 5-5 were obtained with the buffer slightly underpoisoned, and the cadmium ratio was observed to increase radially. When the poison loading in the buffer was increased, the lower set of data was obtained, and an opposite trend was found. Although the two sets of data should bracket the proper value of C_{25}, the extreme sensitivity of C_{25} to slight changes in the buffer poisoning decreased the precision with which C_{25} could be determined. The best value of C_{25} consistent with all data is 1.88 ± 0.03. Since the measurements were made in the test region containing 545 gm Binal and since the null-point was at 567 gm Binal, the corrected value of C_{25} at the null-point is

$$C_{25} = 1.86 \pm 0.03$$

Table 5-5. C_{25} in Poisoned Test Region

Run no.	Rod 1	Rod 2	Rod 3	Rod 4
237/243	--	1.843	1.864	1.880
238/244	--	1.844	--	1.871
239/245	--	1.831	1.869	1.870
Average	--	1.84	1.87	1.87
257/261	1.948	1.911	1.935	1.892
258/262	1.952	1.884	1.918	1.892
259/263	1.899	1.918	1.885	1.851
Average	1.93	1.90	1.91	1.88

5.5. Derivation of k_∞

The experimental data used to derive k_∞ are summarized in Table 5-6, and the results are given in Table 5-7. The accuracy of the measurement of k_∞ by Equation 2-6 is appreciably lower than the accuracy by Equation 2-8 because of the difficulty with the measurement of C_{25} in the poisoned test region. The results are discussed in more detail in Section 7.

Table 5-6. Summary of Data for k_∞ Derivation

D_2O concentration, mole %	70.4 ± 0.1	
Fuel composition	UO_2 - ThO_2	
Rod outer diameter, inch	0.308	
Lattice pitch, inch	0.387	
M/W ratio	0.990	
Volume test region, cm^3	7128.9	
	Unpoisoned	Poisoned
Mass Binal, gm	0	567 ± 10
N_B, atoms B/cm^3 test region	0	1.120×10^{20}
Volume displaced by Binal, cm^3	0	212
$\overline{\phi}_m/\overline{\phi}_f$	1.17 ± 0.01	1.17
$\overline{\phi}_p/\overline{\phi}_f$	--	1.15 ± 0.02
C_{25}	2.244 ± 0.010	1.86 ± 0.03
$1 + \delta_{25}$	1.804 ± 0.006	2.163 ± 0.041

Table 5-7. Derivation of k_∞

Parameter	Unpoisoned	Poisoned	Ratio
f	0.8409	0.6498	1.294 ± 0.008
ϵ	1.0124	1.0157	0.997 ± 0.001
p	0.4010	0.3433	1.168 ± 0.011
$1 + \delta_{25}$	1.804	2.163	0.83 ± 0.016
L	--	--	0.995 ± 0.003
$1-\Gamma$	--	--	0.959 ± 0.003
k_∞ (Equation 2-6)			1.24 ± 0.02
k_∞ (Equation 2-8)			1.241 ± 0.008

Figure 5-1. Arrangement of Buffer and Test Regions

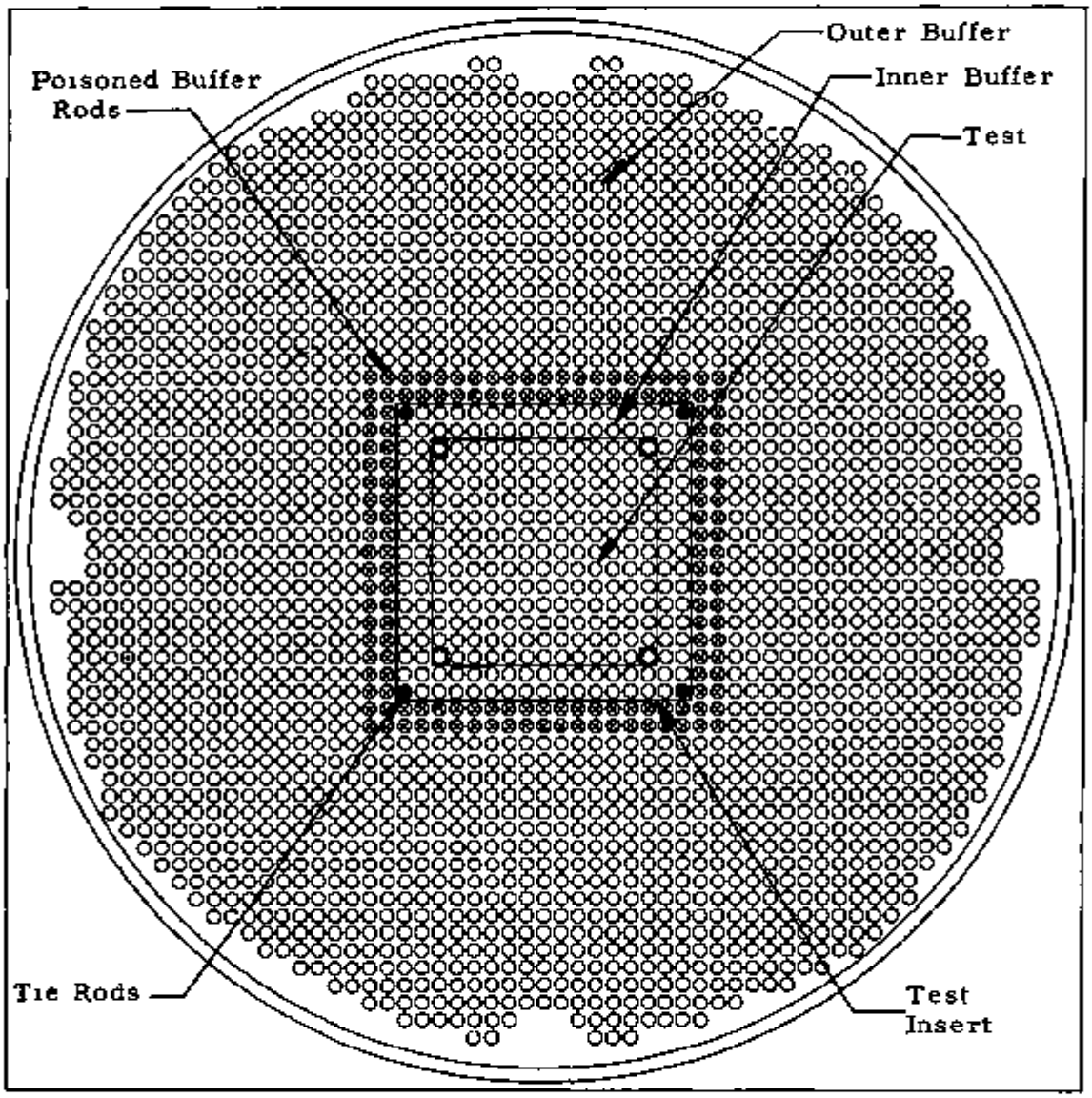

Figure 5-2. Flux Distribution (Unpoisoned Test and Buffer)

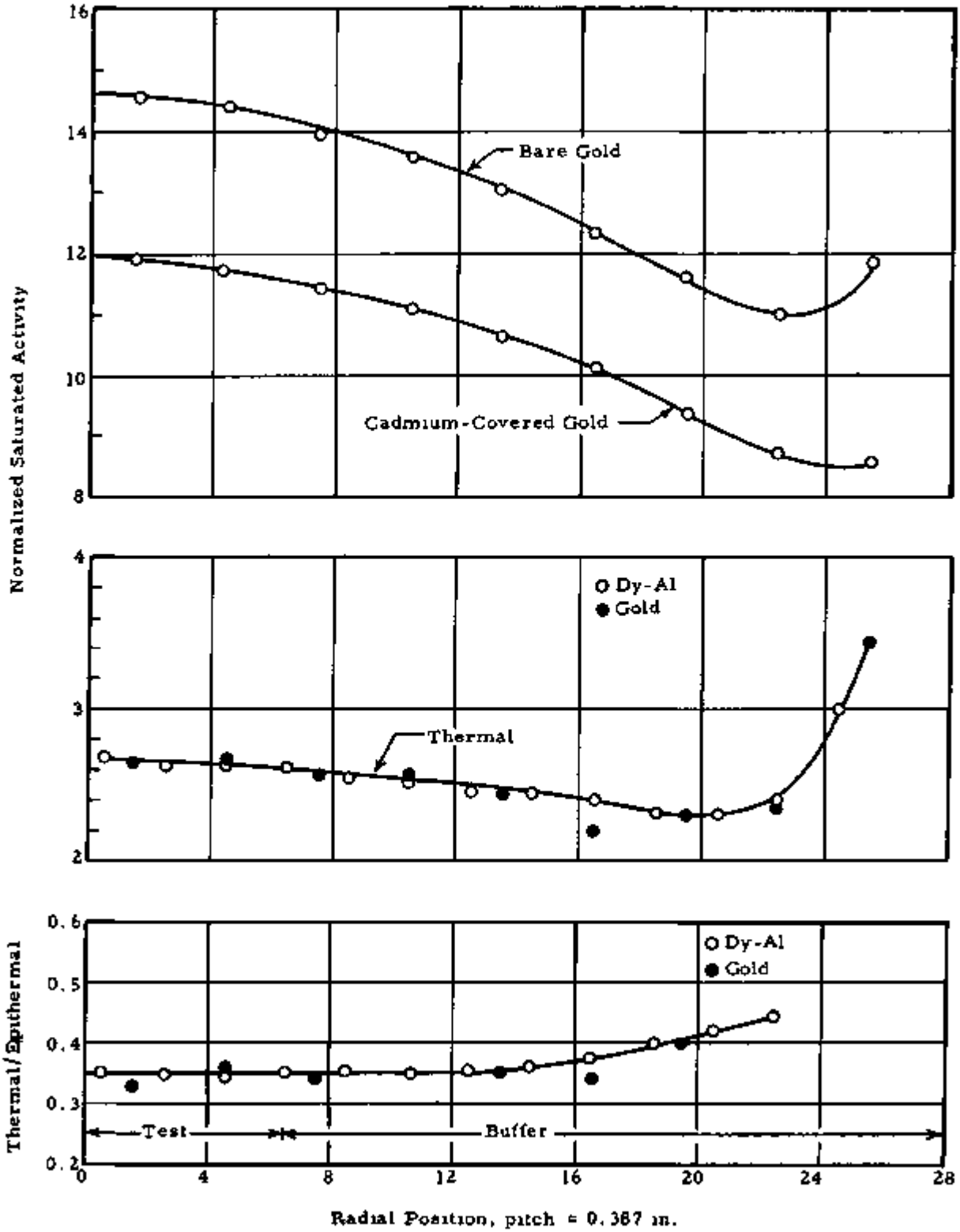

Figure 5-3. Flux Distribution (Poisoned Test, Unpoisoned Buffer)

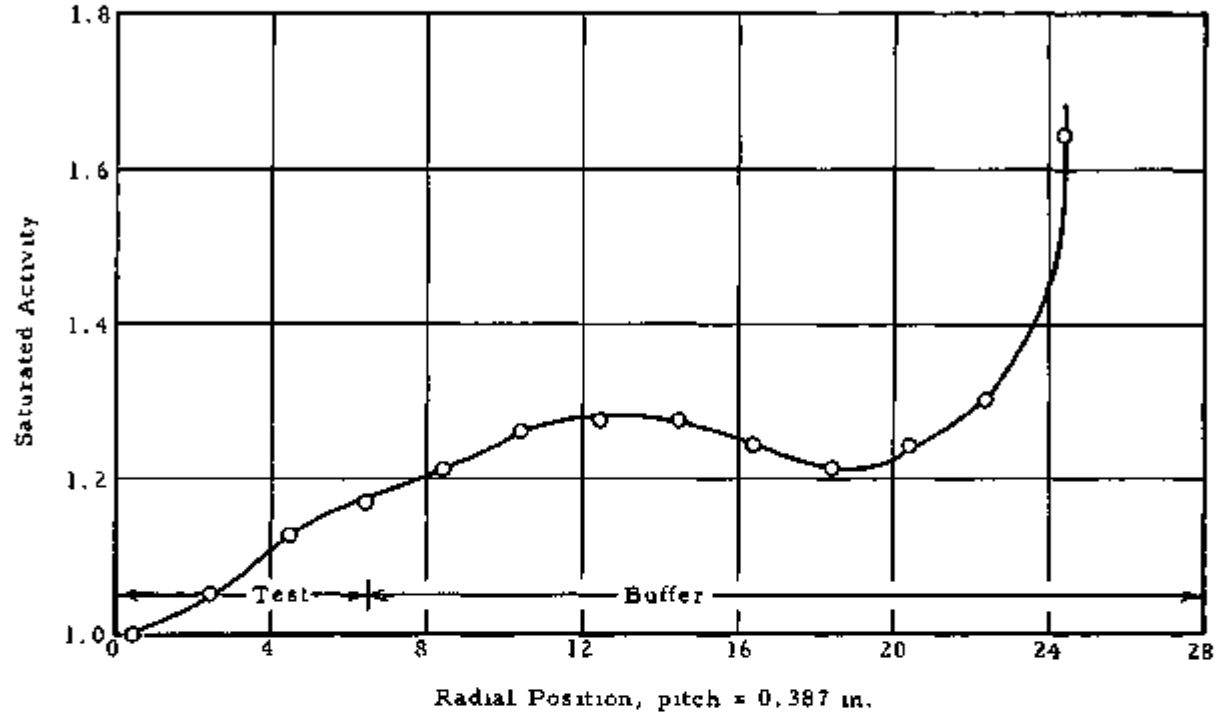

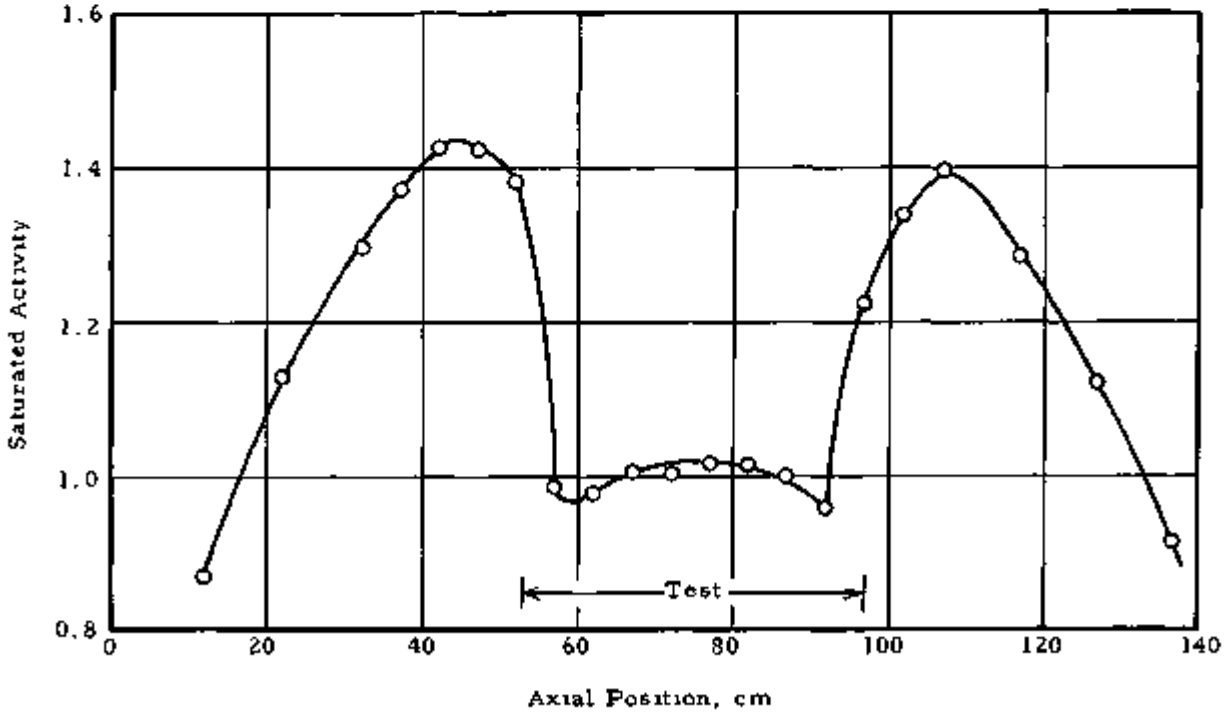

Figure 5-4. Flux Distribution (Poisoned Test and Buffer)

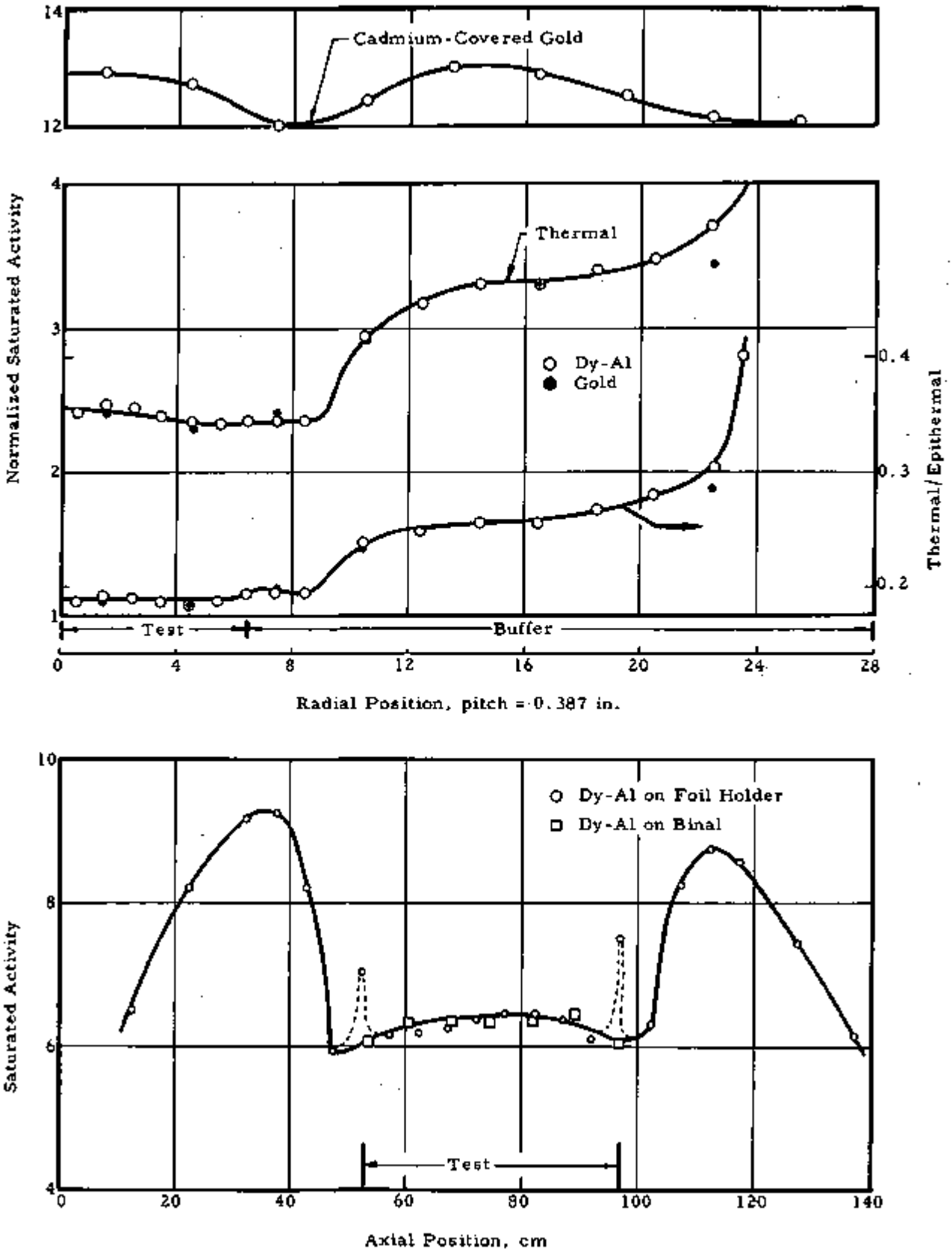

Figure 5-5. Loading Arrangement of Binal Foils

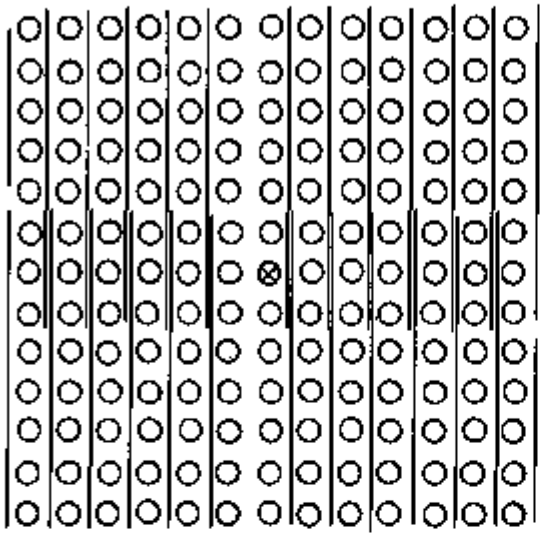

Unpoisoned Buffer
568.5 gm

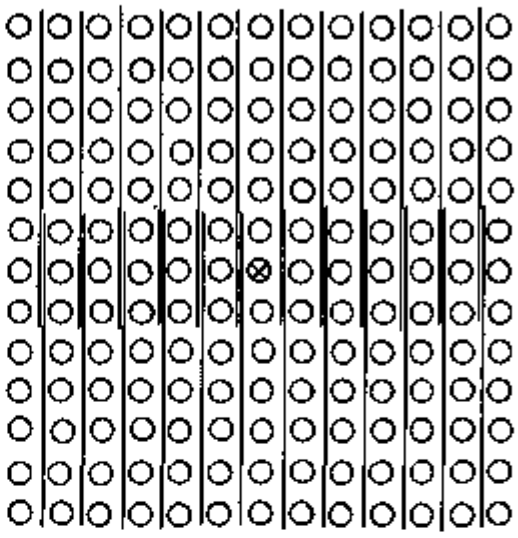

Poisoned Buffer
545.8 gm

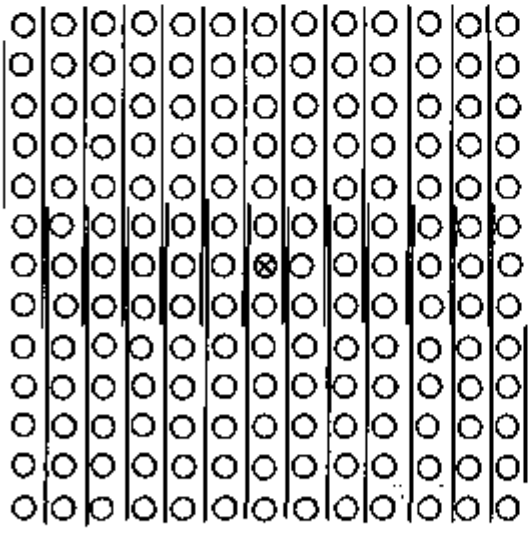

Poisoned Buffer
568.5 gm

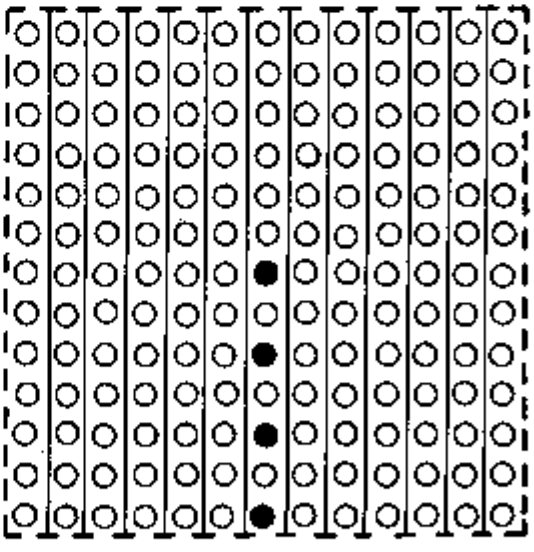

Poisoned Buffer
544.5 gm

Figure 5-6. $\Delta\rho$ Vs Mass of Poison

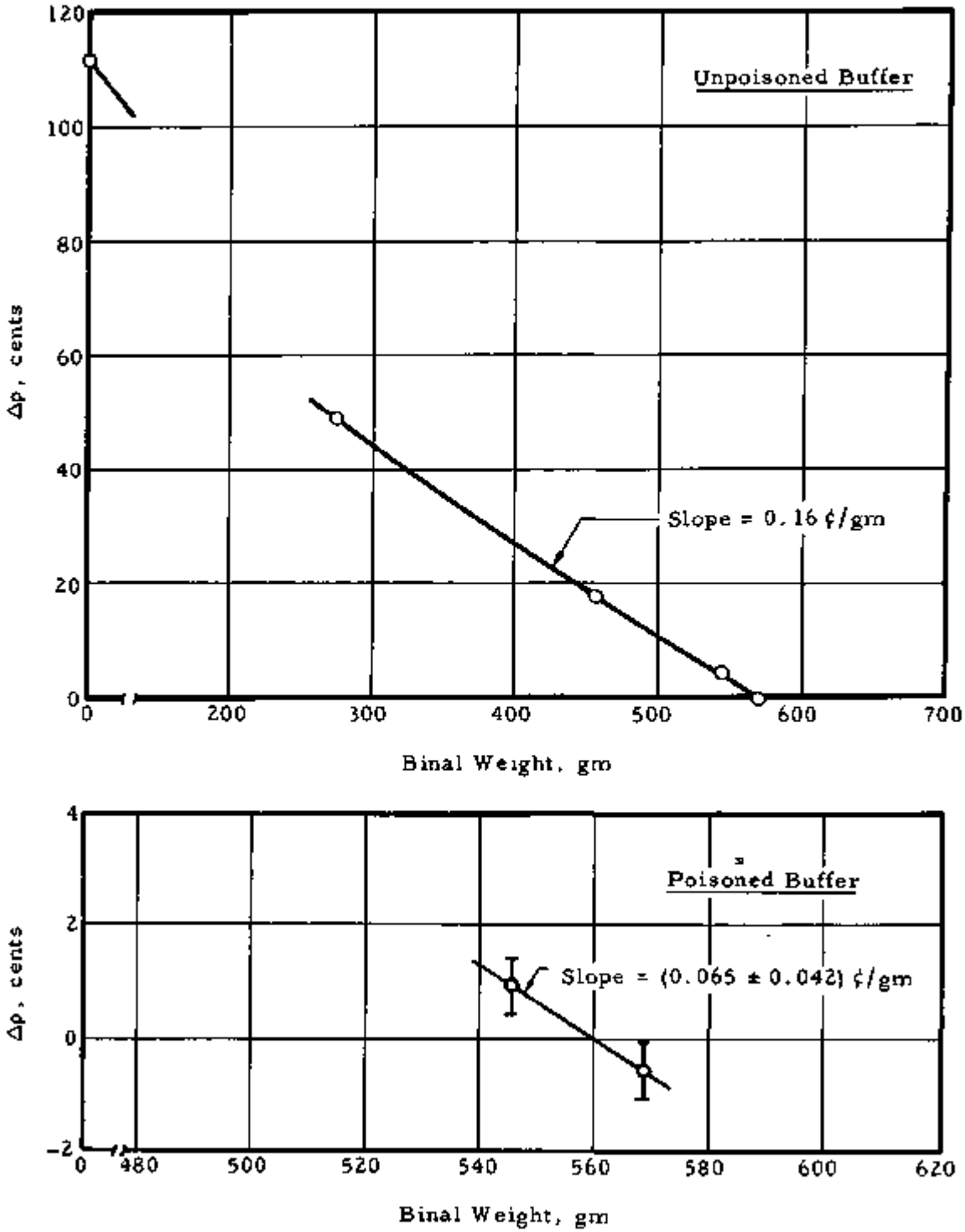

6. EXPERIMENTS WITH UO_2 - ThO_2 FUEL (80.4% D_2O)

6.1. Preliminary Experiments

The reactivity worth of the control rods was measured to be approximately \$2.50 for each of the three pairs of safety rods and approximately \$1.15 for the single regulating rod. The effect of table separation on reactivity was remeasured, and the value of 0.06¢/mil reported in Section 4.1 was confirmed. The moderator (D_2O-H_2O) temperature coefficient was measured to be about - 0.12¢/C.

6.2. Unpoisoned Test, Unpoisoned Buffer

6.2.1. Loading Configuration

The buffer and test regions in these experiments were identical to the preceding ones, except that the D_2O concentration in the moderator was changed to 80.4 ± 0.1 mole %. Criticality was achieved with 24 inner driver channels fueled with approximately 2 kg of U-235 and 116 outer channels filled with graphite only.

6.2.2. Flux Distributions

The flux distributions are shown in Figure 6-1. The asymptotic region extends well into the buffer, and the ratio of the flux at the edge of the test region to that at its center is 0.98 for both the thermal and epithermal components.

6.2.3. Thermal Disadvantage Factor

The thermal disadvantage factor $\overline{\phi}_m/\overline{\phi}_f$ was measured by the technique described in Section 5.2.3, and the results are summarized in Table 6-1. Each value is the average of three separate determinations.

Table 6-1. $\bar{\phi}_m/\bar{\phi}_f$ in Unpoisoned Test Region

Run no.	Average $\bar{A}_m/\bar{A}_f$	$\left(\frac{C_m - 1}{C_m}\right)\left(\frac{C_f}{C_f - 1}\right)$	$\bar{\phi}_m/\bar{\phi}_f$
168	1.09	--	1.14
170	1.09	--	1.14
174	1.11	--	1.16
Average	1.10 ± 0.01	1.045 ± 0.005	1.15 ± 0.01

6.2.4. Cadmium Ratio of U-235

The U-235 cadmium ratio was measured in the test region by the same technique used in the preceding experiment at 70.4% D_2O (see Section 5.2.4). The results are summarized in Table 6-2. Rod 1 was at the center of the test region; Rods 2, 3, and 4 were located at every other lattice position (Rod 4 at outer edge of test region). C_{25} is constant across the test region within the precision of the data, in agreement with the results of the flux measurements.

Table 6-2. C_{25} in Unpoisoned Test Region

Run no.	Rod 1	Rod 2	Rod 3	Rod 4	Average
292/298	1.958	1.941	1.932	1.937	1.942 ± 0.011
293/299	1.974	1.958	1.958	1.950	1.960 ± 0.010
304/307	1.952	1.940	1.926	1.946	1.941 ± 0.011
305/308	1.961	1.945	1.936	1.954	1.949 ± 0.011
Average	1.961 ±0.009	1.946 ±0.008	1.938 ±0.014	1.947 ±0.007	1.948 ± 0.005

6.2.5. Cadmium Ratio of Th-232

C_{02}, the cadmium ratio of Th-232, was measured in the central fuel rod by the same techniques employed in the previous experiment (see Section 5.2.5). The results are summarized in Table 6-3.

Table 6-3. Cadmium Ratio of Th-232

Run no.	Foil 2	Foil 3	Foil 4	Average
169/171	1.18	1.22	1.17	1.19 ± 0.02
169/175	1.19	1.22	1.22	1.21 ± 0.02
Average	--	--	--	1.20 ± 0.02

6.3. Poisoned Test, Unpoisoned Buffer

Although the best null-reactivity measurements were made with the flux flattened by poisoning the buffer, measurements were also made with the buffer unpoisoned to investigate the influence of the flux shape on the null-point. The uncorrected mass of Binal for null-reactivity is

$$M_p = 443 \pm 6 \text{ gm (unpoisoned buffer)}$$

Additional details on these measurements are given in Section 6.4.

6.4. Poisoned Test, Poisoned Buffer

6.4.1. Loading Configuration

With the test and buffer regions poisoned in their final configuration to be described in Section 6.4.4, criticality was reached by filling all except 12 (3 at each corner) of the driver channels with graphite and adding fuel to 48 of the inner channels. The total mass of U-235 was about 3.8 kg.

6.4.2. Flux Distribution

Approximately flat flux and asymptotic conditions were achieved by poisoning the buffer region as described in Section 6.4.4. Figure 6-2 shows the resulting flux distributions. The ratios of the flux at the edge of the test region to that at its center are approximately 1.00 and 0.98, respectively for the thermal and epithermal components. The ratio of the thermal-to-epithermal components appears to be constant to within about one cell of the test region boundary, where it increases 2%. As in the preceding experiments, more precise data were not possible because of the low cadmium ratio of gold in these

lattices. Neglecting the localized peaks at the grid plate positions in the axial distribution, the ratio of the thermal flux at the ends of the test region to that at its center is approximately 0.98.

6.4.3. Flux Ratios

The ratio of the average thermal flux in the poison (Binal) to that in the fuel $\overline{\phi}_p/\overline{\phi}_f$ was measured as described in Section 5.4.3. Table 6-4 summarizes the results.

Table 6-4. $\overline{\phi}_p/\overline{\phi}_f$ in Poisoned Test Region

Symbol	Value
$\overline{A}_p/A_p^s$	0.993 ± 0.004
$A_p^s/\overline{A}_f$	1.075 ± 0.027
$\left(\frac{C_m - 1}{C_m}\right)\left(\frac{C_f}{C_f - 1}\right)$	1.045 ± 0.005
$\int A_p(w)\,dw/\int dw$	1.02 ± 0.01
$\overline{\phi}_p/\overline{\phi}_f$	1.14 ± 0.03

6.4.4. Null-Reactivity Measurements

The final null-reactivity measurements were made by poisoning the buffer region to approximate flat flux conditions. The two rows of buffer fuel rods surrounding the test insert were poisoned with silver wires, and Binal foils were placed in that part of the buffer region included in the test insert itself as follows: no foils between the outer row of fuel rods in test region and the first row of inner buffer rods, two thicknesses of Binal between the two rows of buffer rods in the test insert, and no foils between the outer row of buffer rods in the test insert and the first row of buffer rods outside the test insert. In the axial direction, two thicknesses of Binal foils were placed between the pair of grid plates above the test region and three were placed below

the test region. Binal foils were also distributed in the top and bottom buffers to improve axial flux flatness.

The distribution of the Binal foils in the test region is shown in Figure 6-3, where the cases labeled "unpoisoned buffer" refer to the measurements reported in Section 6.3. The dashed lines represent perforated foils, which contain approximately half as much Binal as regular foils. As shown in Figure 6-4, the 441.4 gm loading is slightly underpoisoned, and the 468.2 gm loading is overpoisoned. The mass of Binal at the null-point, uncorrected for void can effects, is

$$M_p = 456 \pm 6 \text{ gm (poisoned buffer)}$$

These and other supplementary measurements show that the mass of poison for null-reactivity is quite insensitive to the physical distribution of the Binal foils. Note also the small difference in the null-point from that obtained with an unpoisoned buffer. The symmetrical loading designated 458.6 gm was also used for the flux traverses and cadmium ratio measurements with the poisoned buffer.

6.4.5. Corrected Null-Point

Two small corrections to the mass of Binal for null-reactivity are required. The correction for the aluminum in the void can was measured by determining the reactivity difference between the void can and a solid block of aluminum having the same external dimensions. The reactivity coefficient of aluminum (no moderator displacement) was found to be $-0.021¢/in.^3$ Therefore, the correction for the 56.1 $in.^3$ of aluminum in the void can, using the slope of Figure 6-4, is approximately -12 gm Binal. The correction was also computed using the model described for the 4.02%-enriched UO_2 experiments, in cylindrical geometry (see Appendix B). On this basis the correction varied between -5 and -15 gm Binal, depending on the assumptions used. Since the measured value has an appreciable uncertainty due to cumulative errors in the measurement of small reactivity differences and to flux depression in the solid aluminum block, a value of $-(10 \pm 5)$ gm Binal consistent with all information is used for the void can correction. This correction is sufficiently small that its relatively large uncertainty produces a negligible error in k_∞.

The second correction arises from the fact that the four corner fuel rod positions in the test region were replaced by solid 0.387-inch-square aluminum posts to provide structural support. Thus the test region actually contained 165 rather than 169 lattice cells, and the mass of poison should be increased by the ratio of 169/165 to apply to a 169-cell-test region. Making a further small correction for neutron absorptions in the aluminum, the mass of poison should be increased by a total of 3%, or + (15 ± 4) gm Binal. Therefore, the corrected mass of poison for null-reactivity is

$$M_p = 460 \pm 9 \text{ gm Binal}$$

6.4.6. Cadmium Ratio of U-235

C_{25} was measured in the poisoned test region using techniques identical to those for the unpoisoned measurement (see Section 6.2.4). The results are given in Table 6-5. Neglecting the Rod 4 value, which is affected by a slight degree of spectral mismatch at the surface of the test region, C_{25} appears to be asymptotic across most of the test region and has the value:

$$C_{25} = 1.672 \pm 0.005$$

Since the mass of Binal (458.6 gm) in the test region during these measurements was so close to the null-point, no correction to this value of C_{25} is required.

Table 6-5. C_{25} in Poisoned Test Region

Run no.	Rod 1	Rod 2	Rod 3	Rod 4	Average
272/275	1.675	1.672	1.648	1.710	1.676
273/276	1.669	1.675	1.688	1.692	1.681
274/277	1.658	1.684	1.682	1.708	1.683
Average	1.667 ±0.005	1.677 ±0.004	1.673 ±0.013	1.703 ±0.006	1.680

6.5. Derivation of k_∞

The experimental data used to derive k_∞ are summarized in Table 6-6, and the results are given in Table 6-7 for the two methods described in Section 2. The results are discussed in more detail in Section 7.

Table 6-6. Summary of Data for k_∞ Determination

D_2O concentration, mole %	80.4 ± 0.1	
Fuel composition	UO_2- ThO_2	
Rod outer diameter, inch	0.308	
Lattice pitch, inch	0.387	
M/W ratio	0.990	
Volume test region, cm^3	7128.9	
	Unpoisoned	Poisoned
Mass Binal, gm	0	460 ± 9
N_B atoms B/cm^3 test region	0	9.087×10^{19}
Volume displaced by Binal, cm^3	0	174
$\bar{\phi}_m/\bar{\phi}_f$	1.15 ± 0.01	1.15
$\bar{\phi}_p/\bar{\phi}_f$	--	1.14 ± 0.03
C_{25}	1.948 ± 0.005	1.672 ± 0.005
$1 + \delta_{25}$	2.055 ± 0.006	2.488 ± 0.011

Table 6-7. Derivation of k_∞

Parameter	Unpoisoned	Poisoned	Ratio
f	0.8444	0.6822	1.238 ± 0.008
ϵ	1.0132	1.0159	0.997 ± 0.001
p	0.3241	0.2778	1.167 ± 0.011
$1 + \delta_{25}$	2.055	2.488	0.826 ± 0.004
L	--	--	0.995 ± 0.003
$1 - \Gamma$	--	--	0.956 ± 0.003
k_∞ (Equation 2-6)			1.184 ± 0.014
k_∞ (Equation 2-8)			1.184 ± 0.008

Figure 6-1. Flux Distribution (Unpoisoned Test and Buffer)

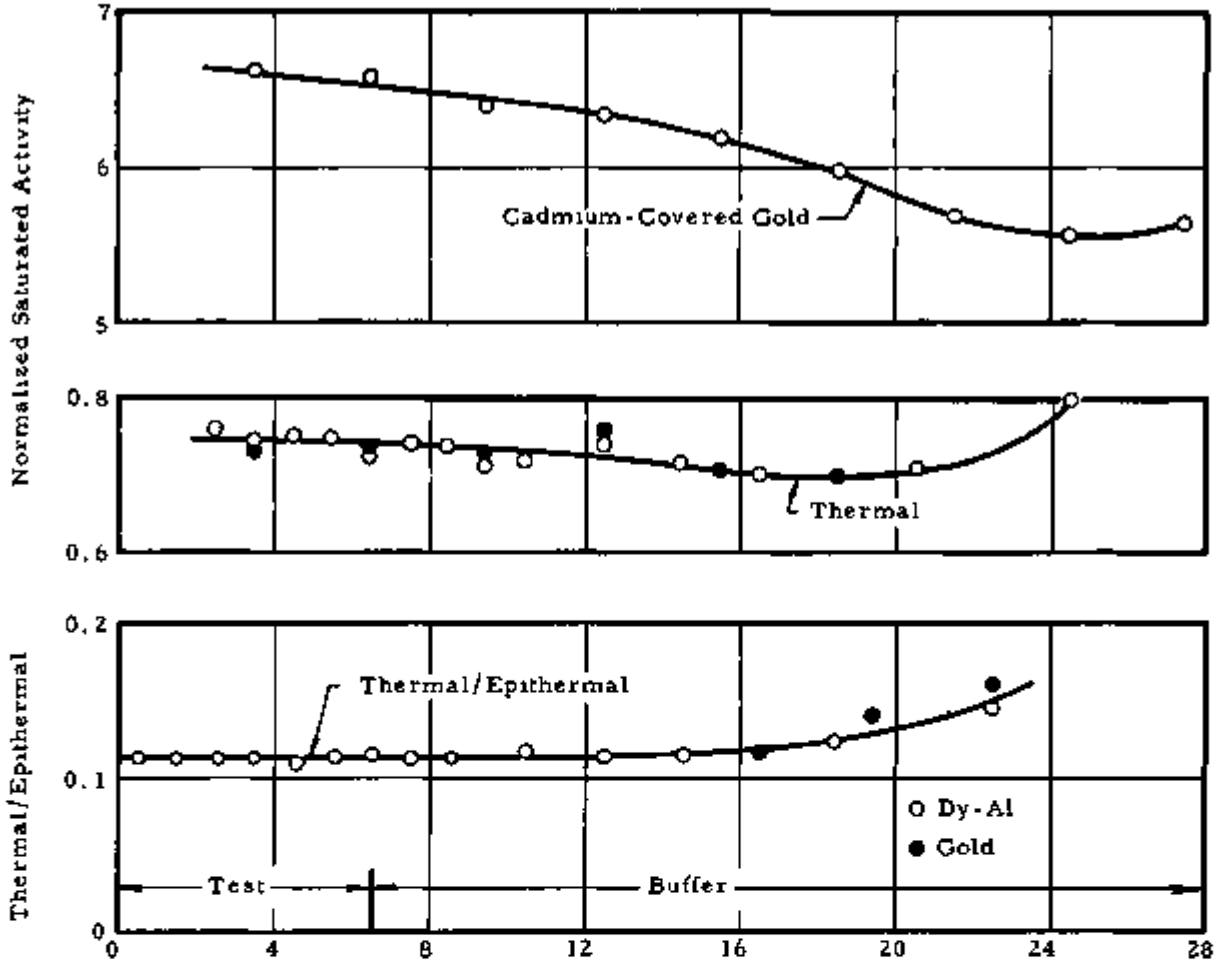

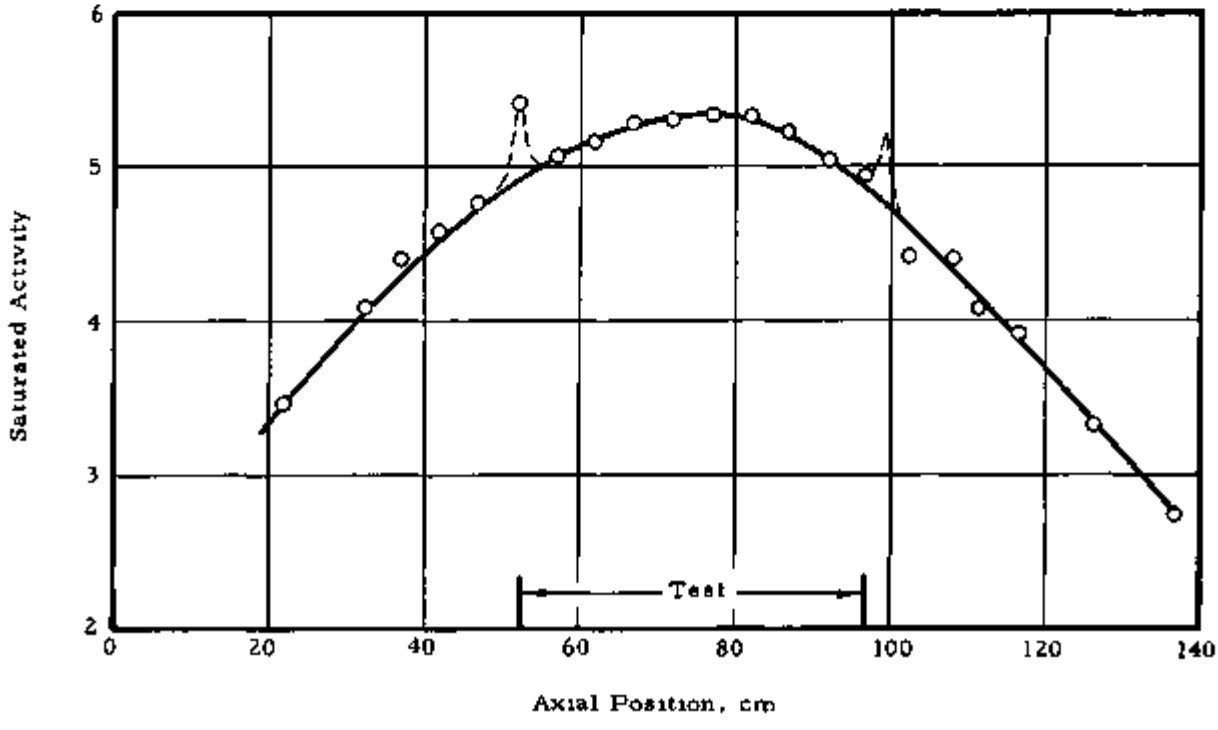

Figure 6-2. Flux Distribution (Poisoned Test and Buffer)

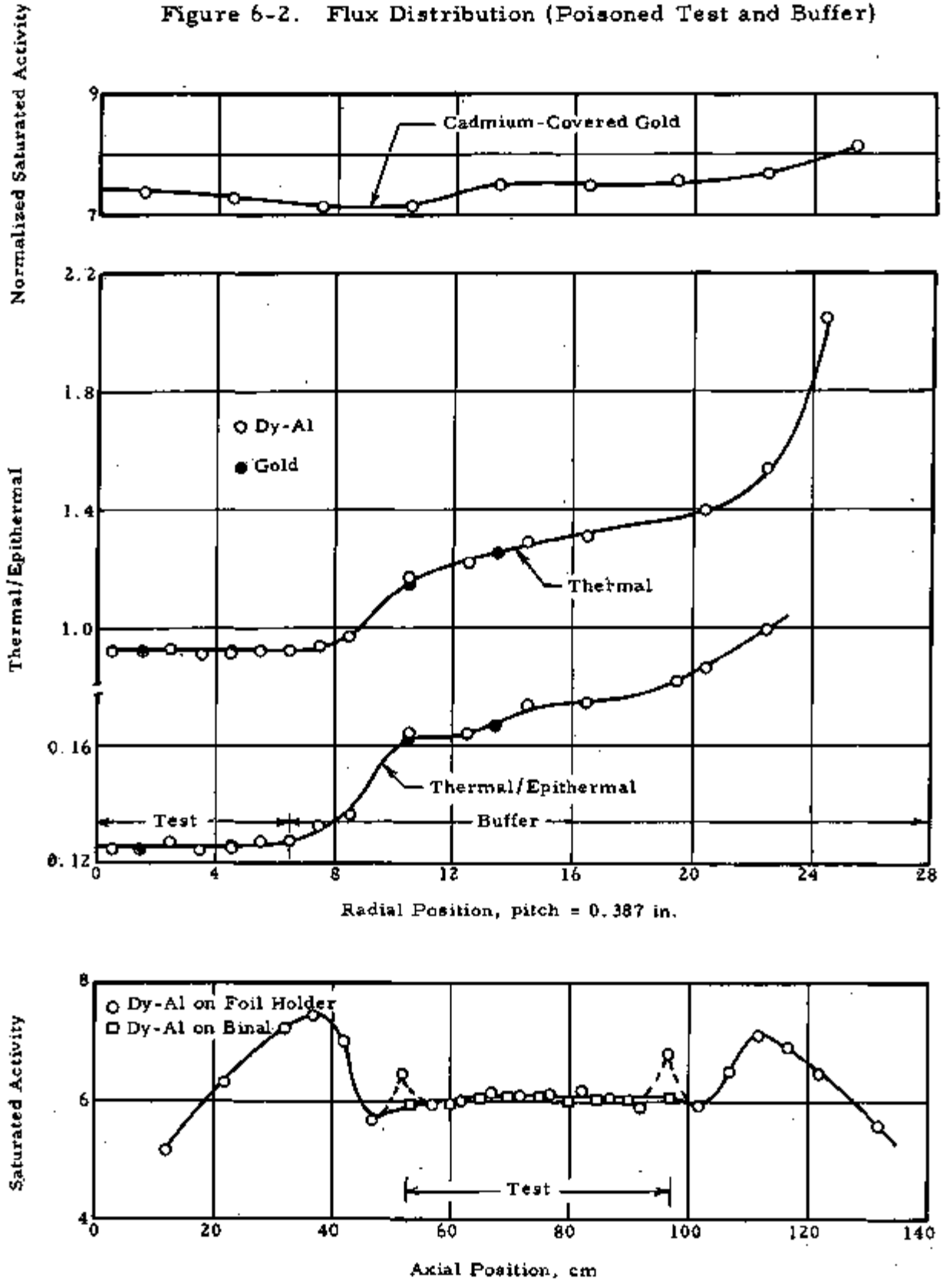

Figure 6-3. Loading Arrangement of Binal Foils

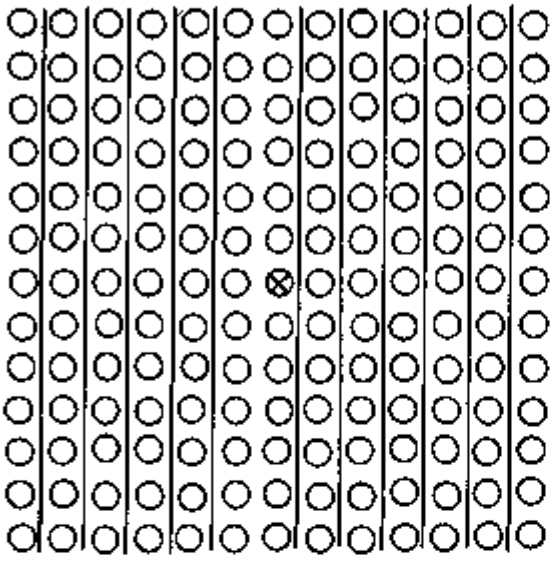

Unpoisoned Buffer
419.5 gm

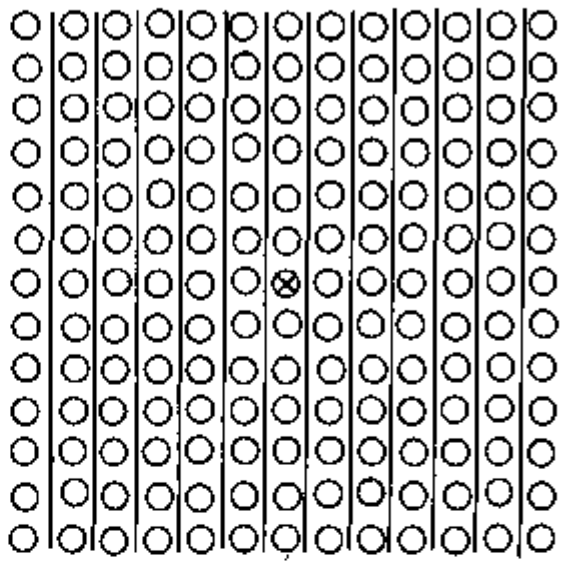

Unpoisoned Buffer
458.6 gm

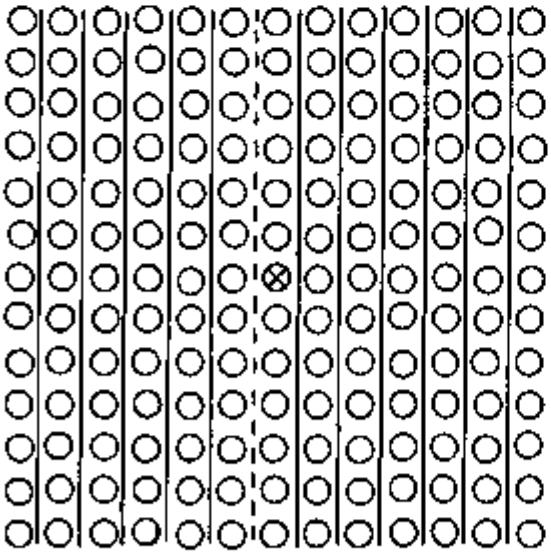

Poisoned Buffer
441.4 gm

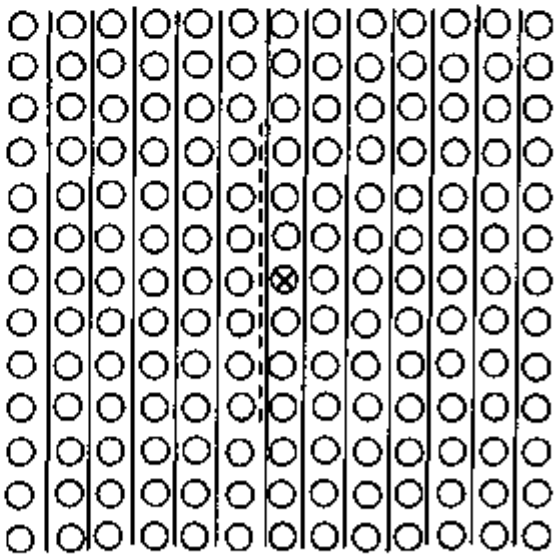

Poisoned Buffer
468.2 gm

Figure 6-4. Δρ Vs Mass of Poison

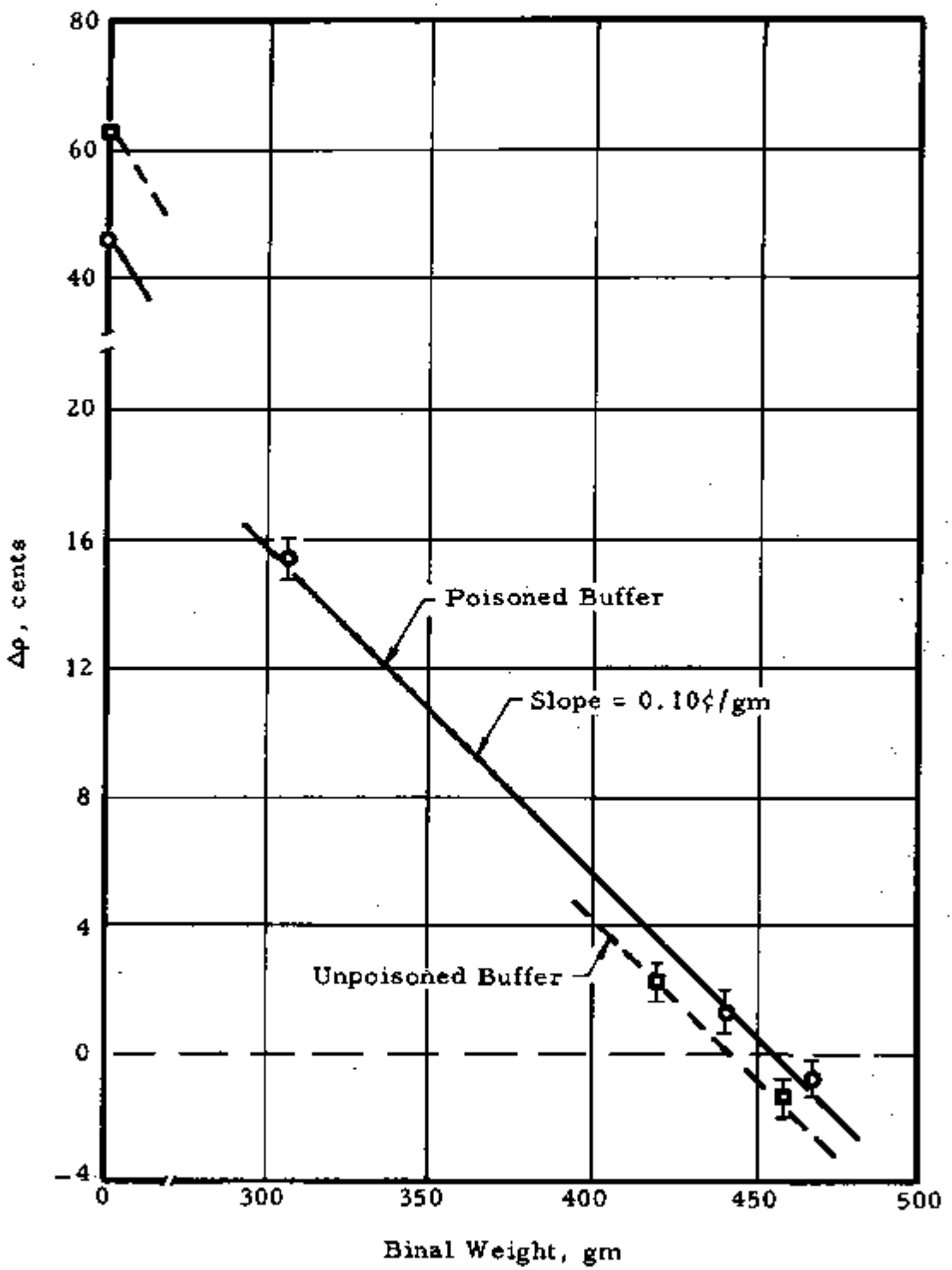

7. DISCUSSION OF RESULTS

7.1. Comparison With Critical Experiment

The best test of the validity of the Small Lattice Experiment (SLE) technique for epithermal lattice studies is to compare the results of SLE measurements with those in an equivalent critical assembly. This comparison was made for the 4.02%-enriched UO_2 lattice. Table 7-1 summarizes the results of the SLE measurements in Section 4 and equivalent critical experiment data given in Appendix C. The SLE value of k_∞ is taken from Equation 2-8, which, as discussed in Section 7.3, appears to give somewhat more accurate results than Equation 2-6. The lattice parameters in both types of experiments were measured in the same fuel rod to facilitate the comparison.

Table 7-1. Comparison of Small Lattice and Critical Experiment Results (4.02%-Enriched UO_2)

Parameter	Small lattice experiment	Critical experiment
k_∞	1.122 ± 0.005	1.126 ± 0.005
$\bar{\phi}_m/\bar{\phi}_f$	1.159 ± 0.007	1.157 ± 0.009
C_{25}	2.440 ± 0.006	2.434 ± 0.012
C_{28}	1.086 ± 0.002	1.087 ± 0.004

It is apparent that the lattice parameters ($\bar{\phi}_m/\bar{\phi}_f$, C_{25}, and C_{28}) measured in the two types of experiments are essentially identical. This equivalence proves that the neutron spectrum in the central cell of the SLE is sufficiently asymptotic for valid measurements.

The measurement of k_∞ requires the establishment of asymptotic conditions over a much larger volume. However, the agreement between SLE and critical experiment values of k_∞ shows that asymptotic conditions extend over a sufficiently large part of the test region and that small departures from the asymptotic state at the edge of the test region are of minor importance. This conclusion is strengthened by the analysis of spectral mismatch error in Appendix A. In this SLE the spectral mismatch error is $\leq 0.1\%$ in k_∞, which is negligible in comparison with other sources of error.

7.2. Summary of UO_2-ThO_2 Experiments

The results of the measurements in the two UO_2-ThO_2 lattices described in Sections 5 and 6 are summarized in Table 7-2. The value of k_∞ is taken from Equation 2-8. Although no equivalent critical experiments are available for comparison, the results appear to be consistent and are in reasonably good agreement with theoretical predictions.

Table 7-2. Results of UO_2-ThO_2 Experiments

Parameter	70.4% D_2O	80.4% D_2O
k_∞	1.241 ± 0.008	1.184 ± 0.008
$\overline{\phi}_m/\overline{\phi}_f$	1.17 ± 0.01	1.15 ± 0.01
C_{25}	2.244 ± 0.010	1.948 ± 0.005
C_{02}	1.27 ± 0.02	1.20 ± 0.02

7.3. Alternate Equations for k_∞

The two expressions for k_∞ developed in Section 2 differ primarily in that p/p_p is calculated and $(1 + \delta_{25})/(1 + \delta_{25})_p$ is measured in Equation 2-6, whereas the product $(1 - \Gamma)$ is calculated in Equation 2-8. The difference between the two approaches can be represented by $k_\infty/(f/f_p)$. As shown in Table 7-3, the error using Equation 2-6 is always larger than that using Equation 2-8. Although the major

APPENDIX A

Mismatch Error Analysis

contributor to the error is the measurement of the U-235 cadmium ratio, particularly for the second lattice, the uncertainty in the calculation of p/p_p is also appreciable. In the UO_2-ThO_2 cases, the change in p due to poison addition is of the order of 17%, which is considerably more than occurs in the 4.02%-enriched UO_2 lattice. Furthermore, only about half of this change is caused by boron absorptions. Thus the application of Equation 2-6 becomes less favorable as p/p_p increases, i.e., as the epithermality and k_∞ of the lattice increase.

Table 7-3. Comparison of $k_\infty/(f/f_p)$

Method	4.02%-enriched UO_2	UO_2-ThO_2, 70.4% D_2O	UO_2-ThO_2, 80.4% D_2O
Equation 2-6	0.973 ± 0.007	0.958 ± 0.20	0.956 ± 0.012
Equation 2-8	0.971 ± 0.002	0.959 ± 0.003	0.956 ± 0.003

The use of Equation 2-8 avoids the experimental errors inherent in the U-235 cadmium ratio measurements and, if the error analysis in Section 2 is correct, also eliminates an appreciable part of the calculational error in p/p_p by combining this calculation with the calculation of $(1 + \delta_{25}^{\infty})/(1 + \delta_{25}^{\infty})_p$. Additional study is required to establish more general criteria for the degree of error cancellation in the computation of $1 - \Gamma$. However, for the three lattices investigated in this program, the error analysis in Section 2 and the agreement between the two methods (Table 7-3) furnish strong evidence for the validity of this approach.

7.4. Conclusions

The small lattice experiment appears to be a useful technique for measuring the infinite medium properties of epithermal lattices where fuel cost or availability is an important consideration. The basic theory of the technique has been confirmed by comparative measurements in an equivalent critical assembly, and additional confidence in its validity has been gained through the results and analysis of higher k_∞ UO_2-ThO_2 lattices. In addition, analytical procedures for the design

of new experiments have been developed and tested (see Appendix B). These procedures can be used to predict the minimum quantity of test fuel required, consistent with a given allowable error in k_∞.

In comparison with critical experiments, small lattice experiments can be performed with less than 1% of the test fuel, and the lattice parameters can be measured with comparable accuracy. Although small lattice experiments are more time consuming, k_∞ can be measured to a higher degree of accuracy than is possible in critical experiments. For the types of lattices studied here, k_∞ can be measured to an accuracy of 0.5 to 1% for values of k_∞ up to at least 1.24. An upper limit has not been established, although the error of k_∞ should increase roughly in proportion to $k_\infty - 1$. Experimental data on k_∞ accurate to approximately 1% are sufficiently good, particularly when supplemented by lattice parameter data, such as δ_{25} and ρ_{28}, to provide a useful test of theoretical methods for the analysis of new lattices.

For future applications, several modifications to the experimental procedures should be considered. First, the size of the test region can be substantially reduced without increasing the error in k_∞. This will decrease the total inventory of test fuel if the required thickness of the inner buffer region in new experiments does not change. Second, the use of soluble rather than solid heterogeneous materials to poison the test region has obvious advantages in that the measurements of $\bar{\phi}_p/\bar{\phi}_f$ and C_{25} would be simplified and more precise shimming to the null-point would be possible. These improvements must be weighed against the mechanical complications that a soluble poison would entail.

APPENDIX A
Mismatch Error Analysis

1. Introduction

The infinite medium multiplication factor of the clean test lattice in the SLE for constant ν_{25} is given by:

$$k_\infty = \left(\frac{\epsilon}{\epsilon_p}\right)\left(\frac{f}{f_p}\right)\left(\frac{p}{p_p}\right)\frac{(1 + \delta_{25}^{\infty})}{(1 + \delta_{25}^{\infty})_p} \qquad \text{(A-1)}$$

where the subscripted parameters are determined for the poisoned test lattice that balances a void in the test cavity. Under this condition it is assumed that k_∞ of the poisoned test lattice is unity, i.e., no distortion of the spectrum or spatial distribution of the flux in the test region occurs when the void is replaced by the poisoned test lattice. The severity of the distortion that may occur in the substitution experiment determines the magnitude of the mismatch error introduced in k_∞ as given by Equation A-1.

The null-reactivity condition states only that the perturbation in the absorption and leakage properties of the test region upon insertion of the poisoned lattice has no net effect on the reactivity of the reactor assembly. In modified two-group notation this condition may be expressed as follows, where the integrals are over the test region:

$$-\int \phi_1^\dagger\, \delta(W_1)\phi_1\, dV + \int \phi_1^\dagger\, \delta(f_1)\phi_1\, dV + \int \phi_1^\dagger\, \delta(f_2)\phi_2\, dV + \int \phi_2^\dagger\, \delta(\beta_1)\phi_1\, dV$$
$$- \int \phi_2^\dagger\, \delta(W_2)\phi_2\, dV - \int \nabla\phi_1^\dagger\, \delta(D_1)\, \nabla\phi_1\, dV$$
$$- \int \nabla\phi_2^\dagger\, \delta(D_2)\, \nabla\phi_2\, dV = 0 \qquad \text{(A-2)}$$

In this equation,

$W_1 = \sum_1^R + \beta_1$ = removal cross section for the fast group

$\beta_1 = q(U_{th})/\phi_1$ = fast to thermal scattering source

$q(U_{th})$ = slowing down density at thermal cutoff

$\phi_1 f_1$ = epithermal fission source

$\phi_2 f_2$ = thermal fission source

D_i = diffusion coefficient for group i

$\phi_i^\dagger$ = adjoint flux in group i

ϕ_i = neutron flux in group i

The neutron and adjoint fluxes in the test region are given by:

$$D_1\nabla^2\phi_1 - W_1\phi_1 + (f_1\phi_1 + f_2\phi_2) = 0 \qquad \text{(A-3)}$$

$$D_2\nabla^2\phi_2 - W_2\phi_2 + \beta_1\phi_1 = 0 \qquad \text{(A-4)}$$

$$D_1\nabla^2\phi_1^\dagger - W_1\phi_1^\dagger + (f_1\phi_1^\dagger + \beta_1\phi_2^\dagger) = 0 \qquad \text{(A-5)}$$

$$D_2\nabla^2\phi_2^\dagger - W_2\phi_2^\dagger + f_2\phi_1^\dagger = 0 \qquad \text{(A-6)}$$

In this notation k_∞ is given by

$$k_\infty = \frac{f_1 + f_2\phi_2/\phi_1}{(W_1 - \beta_1) + W_2\phi_2/\phi_1} \qquad \text{(A-7)}$$

where ϕ_2/ϕ_1 is the ratio of fast-to-thermal flux in the infinite medium. Note that, if the flux is flat in the poisoned lattice, i.e., if the gradient of the adjoint and neutron fluxes vanish, we obtain the following:

$$\frac{\phi_2}{\phi_1} = \frac{W_1 - f_1}{f_1} = \frac{W_2}{\beta_1} \qquad \text{(A-8)}$$

$$\frac{\phi_2^\dagger}{\phi_1^\dagger} = \frac{W_1 - f_1}{\beta_1} = \frac{W_2}{f_2} \qquad \text{(A-9)}$$

These ratios are identical to those existing in the infinite medium; hence, from Equation A-7, k_∞ is unity. In addition, for flat flux in the poisoned test lattice, Equation A-2 reduces to

$$-\phi_1^\dagger W_1\phi_1 + \phi_1^\dagger f_1\phi_1 + \phi_1^\dagger f_2\phi_2 + \phi_2^\dagger \beta_1\phi_1 - \phi_2^\dagger W_2\phi_2 = 0 \qquad \text{(A-10)}$$

since W_1, f_1, and β_1 are zero for the void and since the gradient of the adjoint and neutron fluxes vanishes. With ϕ_2/ϕ_1 and $\phi_2^\dagger/\phi_1^\dagger$ given by Equations A-8 and A-9, the left side of Equation A-10 is identically zero; hence the null-reactivity condition is satisfied for flat flux in the test region, and the ratios of the neutron and adjoint fluxes are equal to the corresponding ratios in an infinite medium of the same material.

In Equation A-2 the last two integrals represent the effect on the reactivity due to the change in leakage which results from the substitution. In principle, therefore, it would be possible to determine the magnitude of the spectral mismatch and nonflatness error by solving Equation A-2 iteratively for the poison concentration for null reactivity and comparing with the poison concentration required for a critical, infinite test lattice, which may be determined by a separate BPG calculation. A simpler method of estimating the combined spectral mismatch and nonflatness error is reported in the next section, where the experimental technique is approximated within the framework of first order transport and few-group diffusion theory.

2. Combined Spectral and Leakage Error

The error in k_∞ due to spectral mismatch and leakage was computed using BPG infinite medium and four-group calculations in a spherical model simulating the geometry of the experiment on the 4.02%-enriched UO_2 lattice (see Appendix C for geometry). Several degrees of buffer poisoning were assumed to bracket the experimental conditions. The following procedure was used. The void was placed in the test region, and the driver was adjusted to make k_{eff} unity ($k_{eff} = k_v$) in a multiregion four-group calculation. In a separate infinite-medium calculation, the concentration of boron that made $k_\infty = 1$ was determined. The void was then replaced by the test region containing that boron concentration, and the first calculation was repeated for exactly the same buffer and driver conditions ($k_{eff} = k_p$). The difference between k_v and k_p, therefore, is proportional to the error in the measurement. The proportionality was determined by making a small change in the boron concentration and calculating dk_{eff}/dk_∞.

The change in k_∞ necessary to balance the void is

$$\Delta k_\infty = \frac{k_v - k_p}{dk_{eff}/dk_\infty} \qquad \text{(A-11)}$$

and the infinite medium multiplication factor of the material that balances the void is

$$k'_\infty = 1 + \Delta k_\infty \qquad \text{(A-12)}$$

Therefore, the error in k_∞ is

$$k'_\infty - 1 = (k_\infty - 1) + \Delta k_\infty \qquad \text{(A-13)}$$

A division of the total error $(k'_\infty - 1)$ into the part due to noninfinite medium spectrum σ_1 and the part due to leakage σ_2 can be made as follows. The productions P in the test medium are given by

$$P = P_{NL}\ \eta^{th} f \epsilon' p' (1 + \delta'_{25}) \qquad \text{(A-14)}$$

where P_{NL} = nonleakage probability, and the primes denote finite medium values. The absorptions are given by $A = P_{NL}$; therefore:

$$P/A = \eta^{th} f \epsilon' p' (1 + \delta'_{25}) = k_\infty \left(\frac{\epsilon'}{\epsilon^\infty}\right)\left(\frac{p'}{p^\infty}\right)\left(\frac{1 + \delta'_{25}}{1 + \delta^\infty_{25}}\right) \qquad \text{(A-15)}$$

where the superscript ∞ denotes infinite medium values. σ_1 is obtained from

$$1 + \sigma_1 = \left(\frac{\epsilon^\infty}{\epsilon'}\right)\left(\frac{p^\infty}{p'}\right)\left(\frac{1 + \delta^\infty_{25}}{1 + \delta'_{25}}\right)$$

$$\sigma_1 = k_\infty / (P/A) - 1 \qquad \text{(A-16)}$$

In the test region $P/(A + L) = k_{eff}$, where L is the net leakage out of the test region, or $P/A = k_{eff}(1 + L/A)$. σ_2 is obtained from

$$1 + \sigma_2 = k_{eff}(1 + L/A)$$

$$\sigma_2 = (P/A) - 1 \qquad \text{(A-17)}$$

Equations A-16 and A-17 are combined to give the following result:

$$k_\infty = k_{eff}(1 + L/A)\left(\frac{\epsilon^\infty}{\epsilon'}\right)\left(\frac{p^\infty}{p'}\right)\left(\frac{1 + \delta^\infty_{25}}{1 + \delta'_{25}}\right) \qquad \text{(A-18)}$$

Therefore, provided $\sigma_1 \sigma_2 \ll (\sigma_1 + \sigma_2)$,

$$k'_\infty - 1 = \sigma_1 + \sigma_2 \qquad \text{(A-19)}$$

If conditions are perfect (L = 0), the finite parameters are equal to infinite medium parameters, and the medium that balances the void has $k_\infty = 1$. If the buffer is not perfect, $L \neq 0$ and the finite parameters differ from the infinite medium parameters. Calculations of P/A in the test medium that balances the void give σ_1 and σ_2.

In practice a number of BPG runs would be required to obtain the four-group coefficients for the exact value of k_∞ that balances the void. Therefore, σ_1 and σ_2 may be obtained by calculating σ_1 for a test material that nearly balances the void; σ_2 would then be obtained from

$$\sigma_2 = k'_\infty - 1 - \sigma_1$$

where k'_∞ is that calculated above to balance the void.

σ_1 and σ_2 were calculated for the three different buffer poisons. The values obtained are given in Table A-1 and plotted along with the total error from Equation A-13 in Figure A-1. The ratios of the four-group fluxes at the surface of the test region to the center values, $\phi_1(s)/\phi_1(0)$, are also shown in the table. It can be seen that the total error is very small because the errors due to nonasymptotic conditions and due to leakage tend to cancel.

Table A-1. Error in k_∞ Due to Spectral Mismatch

	Buffer poison		
Parameter	Zero	Same as test	1.76 × test
$\phi_1(s)/\phi_1(0)$	1.0005	1.0000	0.9925
$\phi_2(s)/\phi_2(0)$	0.9884	0.9999	1.0174
$\phi_3(s)/\phi_3(0)$	0.9826	0.9995	1.0232
$\phi_4(s)/\phi_4(0)$	1.1261	0.9994	0.9550
k_v	0.999221	1.0000025	0.999955
k_∞	0.99988	0.99988	0.99988
k_p	0.999146	1.0000144	0.999977
dk_{eff}/dk_∞	0.0605	0.0492	0.0415
Δk_∞	0.00124	-0.00024	-0.00053
k'_∞	1.00112	0.99964	0.99935
$k'_\infty - 1$, %	0.11	-0.036	-0.065
σ_1, %	-0.58	-0.042	0.19
σ_2, %	0.69	0.006	-0.25

During these calculations it became apparent that the computed errors were so small that severe requirements were placed on convergence and that consistent results were obtained only when the driver was adjusted to bring k_v very close to unity. This occurred because small changes in the driver loading caused appreciable changes in the importance functions over the test region.

As an additional check on the reliability of these results, the error analysis was repeated for the case of zero buffer poison. Using slightly different cross sections in the BPG code and infinite cylindrical geometry rather than spherical geometry to mock-up the experiment, particular care was taken to ensure convergence within 0.00003 of unity. In addition, the error was evaluated in terms of the difference between the poison concentration for $k_p = 1$ (when $k_v = 1$) and that for $k_\infty = 1$, rather than in terms of the difference between k_v (when $k_v = 1$) and k_p for a poison concentration that made $k_\infty = 1$. Although both approaches should be equivalent, the revised method simulates the experiment more directly. Finally, in view of the importance of the k_v calculation, exploratory studies were made to ensure the reliability of the model used for the void region.

The total error in k_∞ predicted by this calculation is +0.07%, which compares fairly well with the original calculation of +0.11% when the differences between the two approaches are taken into consideration. It may be concluded that convergence questions probably limit the range of applicability of this method of error analysis to errors of the order of 0.1% or larger on an absolute basis. However, calculations of relative errors or trends in the error such as are shown in Table A-1 are probably more reliable. The inapplicability of the method to mismatch errors less than 0.1% is not a serious limitation, since experimental errors are usually larger. From a practical standpoint, it is sufficient to show that the mismatch error is less than 0.1%; whereas, if it is larger than 0.1%, the method should be sufficiently sensitive to predict the correct value.

On the basis of this analysis, the mismatch error in these experiments should be less than 0.1% in k_∞. Evidence that the analytical method is reasonably valid can be obtained by comparing the null-reactivity measurements with the buffer both poisoned and unpoisoned. The poisoned buffer experiment corresponds to a case in which the buffer is poisoned

between 1 and 1.5 times the test region poisoning. Therefore, on the basis of Table A-1, the error analysis predicts that the difference between k_∞ measured with the poisoned buffer and that measured with the unpoisoned buffer should be (−0.05 − 0.11) or about −0.16%. The difference in the mass of poison for null-reactivity is (584 ± 8) − (592 ± 5), or −(8 ± 9) gm Binal, which corresponds to a difference in k_∞ of

$$\Delta k_\infty = \frac{-(8 \pm 9)}{592} \times 0.13 = -(0.2 \pm 0.2)\%$$

This value agrees very well with the prediction, although the experimental error is too large to consider this measurement as a conclusive test of the method of error analysis.

Figure A-1. Error in k_∞ Vs Buffer Poisoning

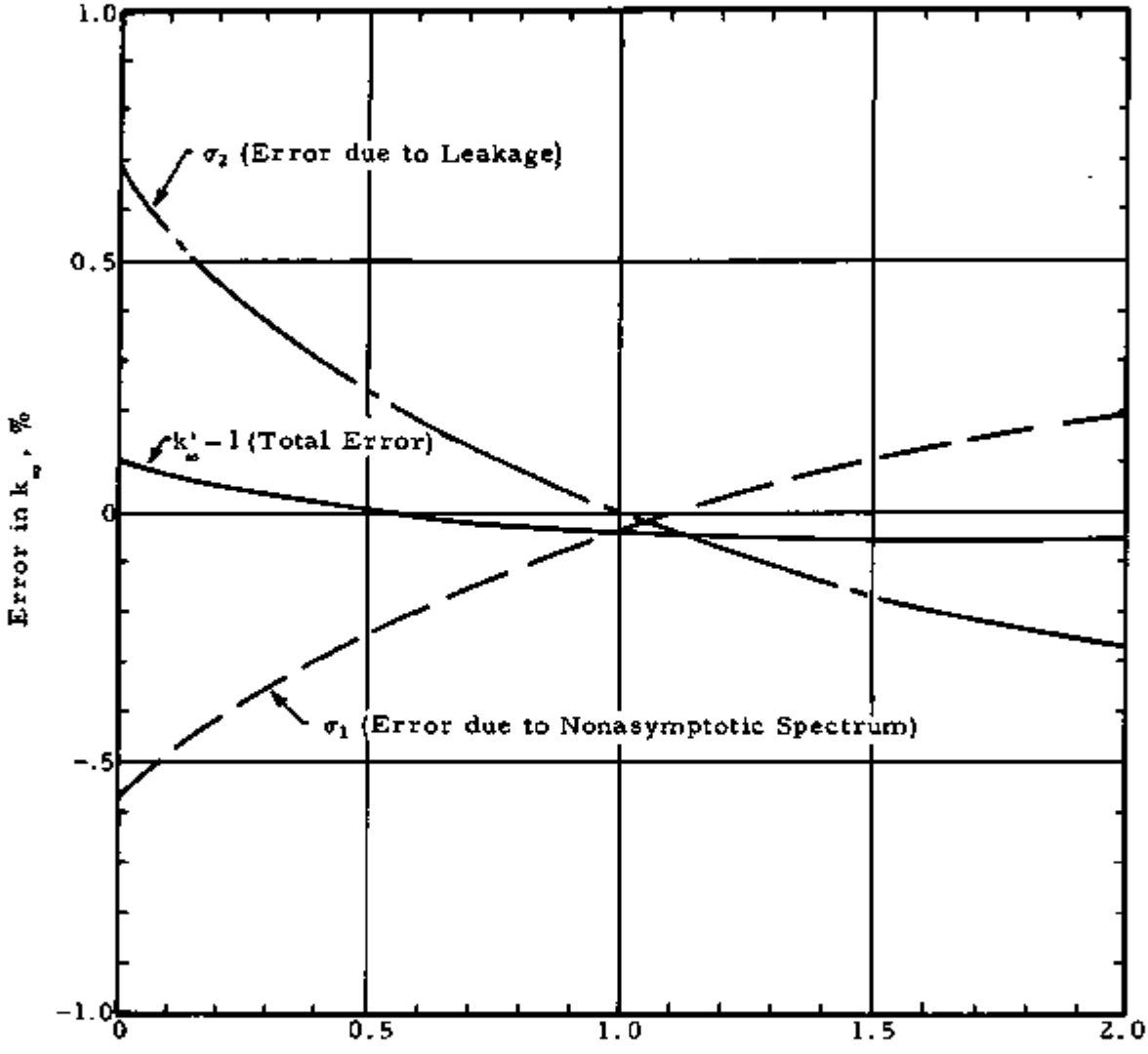

APPENDIX B

Validity of Analytical Model

APPENDIX B
Validity of Analytical Model

A secondary objective of this program was to develop and test an analytical method that can be used to optimize the design of future small lattice experiments. The primary design consideration is, of course, the error in the measured k_∞. One contributing factor is the size of the test region which dictates the sensitivity (reactivity difference between unpoisoned test region and void) of the experiment. Since the error in k_∞ due to a given error in the null-point measurement is inversely proportional to the sensitivity, the minimum test region volume can be determined if the sensitivity can be predicted. The size of the test region also influences the error due to flux mismatch, i.e., it is easier to establish flat and asymptotic fluxes across a small test region than a larger one, but the error in k_∞ due to a given mismatch is proportionally larger. The nuclear properties and dimensions of the buffer region also affect the degree of spectral mismatch and resulting error in k_∞ for the particular test and buffer combination under consideration. The analytical model should also permit fairly reliable estimates of the corrections, such as the aluminum in the void can and the displacement of moderator by the Binal poison foils, so that the experiment can be designed to minimize these corrections.

The validity of the analytical model used for the 4.02%-enriched UO_2 work was tested by comparing measurements and calculations wherever possible. As will be seen in the following sections, the agreement is satisfactory for a variety of quite different problems. Therefore, it is concluded that the model can be used with confidence to design future experiments.

1. Flux Shapes

Although three-dimensional analysis is needed for accurate calculations of the energy and spatial distribution of the flux because of the

geometrical complexity of the facility, satisfactory results were obtained by approximations in one or two dimensions. Calculations were performed using four-group coefficients derived from BPG calculations and the geometries shown in Figures B-1 through B-4. A standard four-group multiregion code was used for the one-dimensional spherical and cylindrical calculations based on equivalent volumes, and PDQ calculations were used for the two-dimensional X-Y and R-Z problems. The diffusion coefficient for the void region was computed by the method given in Reference 13. The group bounds were ϕ_4(0.4 ev), ϕ_3 (252 ev), ϕ_2 (9210 ev), and ϕ_1 (10 mev).

Figure B-5 compares the thermal flux distributions in the unpoisoned test region predicted by four methods, and Figure B-6 shows the four-group flux distributions for the same case computed in two-dimensional (X-Y) geometry. Figure B-7 is a one-dimensional cylindrical calculation from the poisoned test region. The buffer region was unpoisoned in all of these calculations.

The calculated and measured radial flux shapes are compared in Table B-1, using the Dy-Al data for ϕ_4 and the cadmium-covered gold data for ϕ_3, as reported in Section 4. The unpoisoned test region calculation was in two-dimensional X-Y geometry, and the poisoned test region calculation was in one-dimensional cylindrical geometry. The ratios of flux at the edge of the test region (six lattice pitches) to that at the center are in excellent agreement; the slight discrepancy for the poisoned case can be attributed to the difference between the cylindrical and exact models (see Figure B-5). The flux ratios at the interface between the inner and outer buffer (13 lattice pitches) are quite sensitive to the loading of U-235 in the driver. Since the driver loading for criticality differed somewhat from the experiment, the flux ratios do not agree as well at this position. A more accurate comparison between calculation and measurement would require three-dimensional analysis to obtain better agreement for the driver loading. However, since the flux shapes in the test region dictate the error due to spectral mismatch and since agreement is good in this region, the analytical method for predicting flux shapes may be judged adequate.

Table B-1. Comparison of Calculated and Measured Radial Flux Shapes

Parameter	Flux group	Unpoisoned test		Poisoned test	
		Calculated	Measured	Calculated	Measured
$\phi(6)/\phi(0)$	4	0.96	0.96	1.12	1.10
$\phi(6)/\phi(0)$	3	0.96	0.96	0.99	0.99
$\phi(13)/\phi(0)$	4	0.80	0.84	~1.11	~1.05
$\phi(13)/\phi(0)$	3	0.84	0.86	~0.91	~0.97

2. Extent of Asymptotic Region

Both calculations and measurements show that the spectrum is asymptotic to a radius of 9 to 10 lattice pitches when the test and buffer regions are unpoisoned and to a radius of only about one lattice pitch when only the test region is poisoned. For the case in which both the buffer and test regions are poisoned, evidence that the neutron spectrum is asymptotic at the center of the test region is furnished by the agreement between the measured and calculated ratios $(1 + \delta_{25})/(1 + \delta_{25})_p$ and between the SLE and critical experiment measurements of ρ_{28} and δ_{25}.

3. Intracell Flux Distributions

Although an extensive program to calculate accurate intracell flux distributions was not warranted because of the small dependence of k_∞ on the flux ratios, some approximate values were obtained by simple P-3 calculations in which the cell was represented in slab geometry. The results, compared below, show that no gross error should exist in measurements.

Flux ratio	Calculated	Measured
$\bar{A}_p/A_p^s$	0.998	0.993 ± 0.004
A_p^s/A_f^s	1.00	0.998 ± 0.007
$A_f^s/\bar{A}_f$	1.06	1.06 ± 0.01

4. Sensitivity

Calculations of the sensitivity, or reactivity difference between the unpoisoned test region and a void, were performed in spherical geometry. This limits the validity of the comparison somewhat, because the spherical model is a poor approximation of the experiment. When the buffer was unpoisoned, the following values of k_{eff} were calculated in spherical geometry:

Test region	k_{eff}
Unpoisoned	1.0175
Poisoned	1.0085
Void	1.0091

The reactivity difference is 0.0084, or about 118 cents if $\beta_{eff} = 0.0071$, which is approximately 35% larger than the measured value of 87 cents. This difference, which can be attributed to the inadequacy of the spherical model, furnishes an empirical method of correcting future reactivity calculations in spherical geometry. However, the calculations could be done in two- or three-dimensional geometry if the required accuracy warranted the extra cost and effort. Both calculations and measurements show that the sensitivity is slightly reduced when the buffer is poisoned.

5. Correction for Aluminum Void Can

The effect of aluminum in the void region was computed in spherical geometry, as a function of effective aluminum density, using BPG-generated four-group constants. Figure B-8 shows the results for two cases that bracket the conditions of the experiment. The values of k_{eff} are tabulated below.

Test region	Unpoisoned buffer region	Poisoned buffer region
Unpoisoned	1.0175	0.95527
Poisoned	1.0085	0.94794
Void	1.0091	0.94539

The effective aluminum density for 12 vol % aluminum in the void can is about 0.3 gm/cm^3. Equivalence in grams of Binal is calculated by the following equation:

$$\frac{k_{void} - k_{Al}}{k_{unp} - k_{void}} \times M_p \text{ (null-reactivity)}$$

The reactivity worth of the aluminum in the void can is approximately 18 gm of Binal for the unpoisoned buffer and about 11 gm for the poisoned buffer, or -(14 ± 5) gm of Binal for the conditions of this experiment. As discussed earlier, this reactivity worth is about three times larger than measured, although the measured value is actually only a lower limit. In view of the minor importance of this correction, the analytical model should be adequate for future design purposes, providing the volume fraction of aluminum is not substantially increased.

6. Effect of Moderator Displacement

The displacement of moderator by the addition of the Binal poison foils decreases the resonance escape probability by a substantial amount (≈2%) in addition to the decrease caused by absorptions in the boron. To judge the accuracy of the model in computing this extra effect, the reactivity worth of moderator displacement by pure aluminum was calculated and compared to the experimental value. The change in k_∞ from an infinite medium BPG calculation was found to be 0.0083 when the volume fraction of the moderator was reduced by the equivalent displacement of 25 Binal foils in the test region. This displacement corresponds to a reactivity change in the SLE of

$$\frac{0.0083}{0.133} \times 65 = 4.05 \text{ cents},$$

or a moderator coefficient of 0.29¢/in.^{3}. This value agrees very well with the measurement (0.24 ± 0.05)¢/in.^{3} reported earlier.

7. Error Due to Spectral Mismatch

This topic has been covered in Appendix A, where satisfactory agreement between measurements and calculations was shown.

Figure B-1. Spherical Model for SLE Calculations

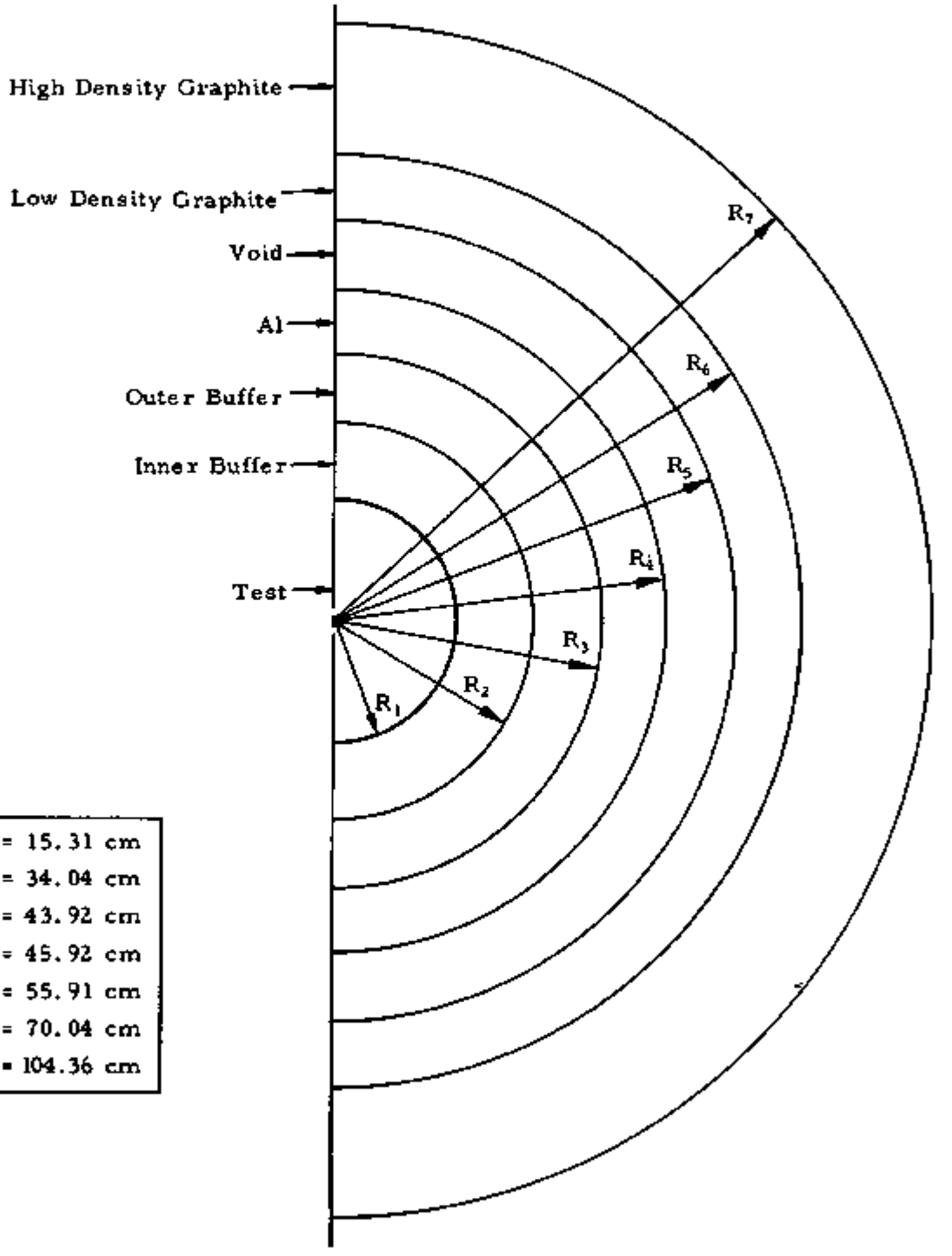

R_1	= 15.31 cm
R_2	= 34.04 cm
R_3	= 43.92 cm
R_4	= 45.92 cm
R_5	= 55.91 cm
R_6	= 70.04 cm
R_7	= 104.36 cm

Figure B-2. Cylindrical Model for SLE Calculations

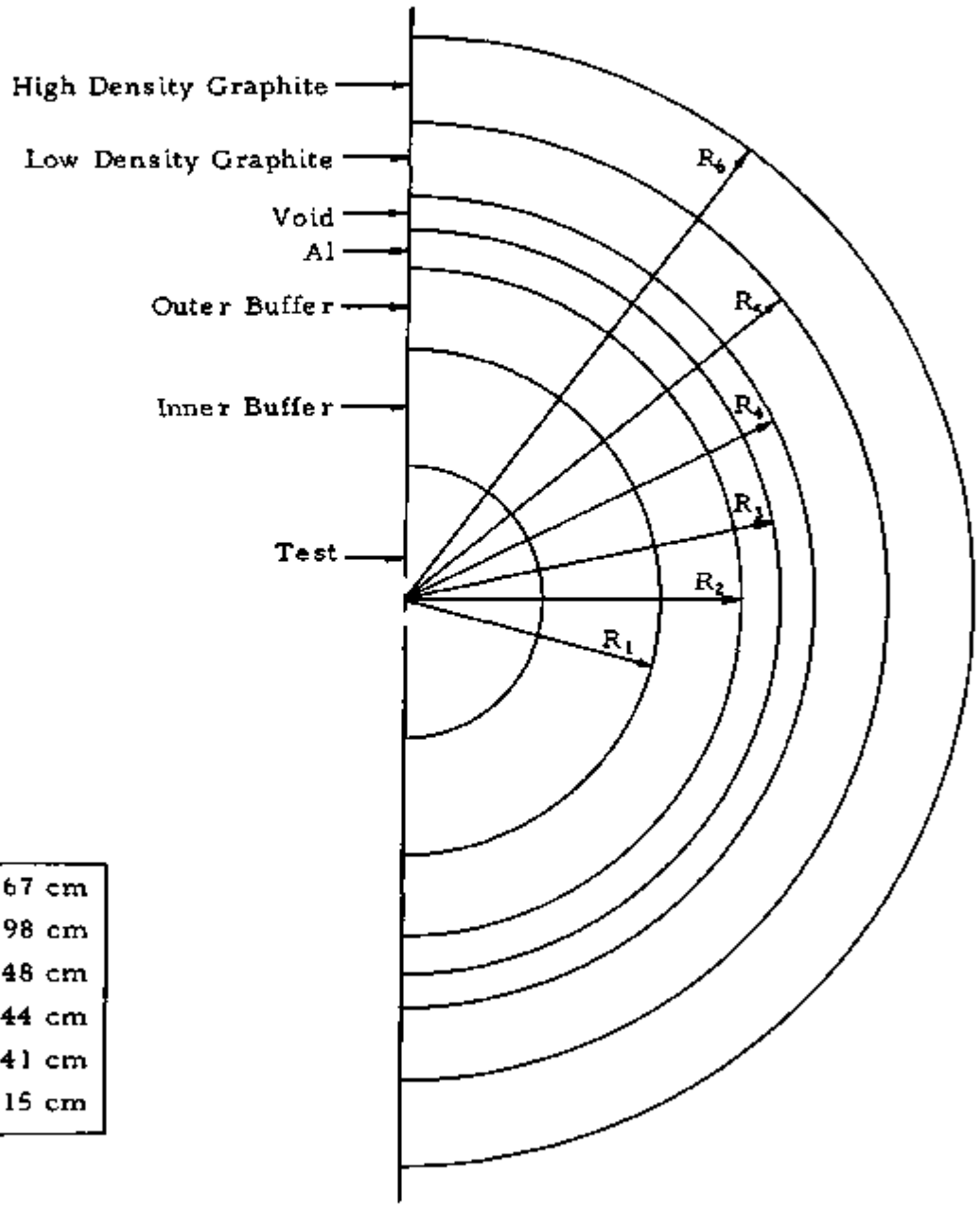

R_1 = 19.67 cm
R_2 = 27.98 cm
R_3 = 30.48 cm
R_4 = 36.44 cm
R_5 = 47.41 cm
R_6 = 81.15 cm

Figure B-3. Two-Dimensional Model for SLE Calculations (X-Y Geometry)

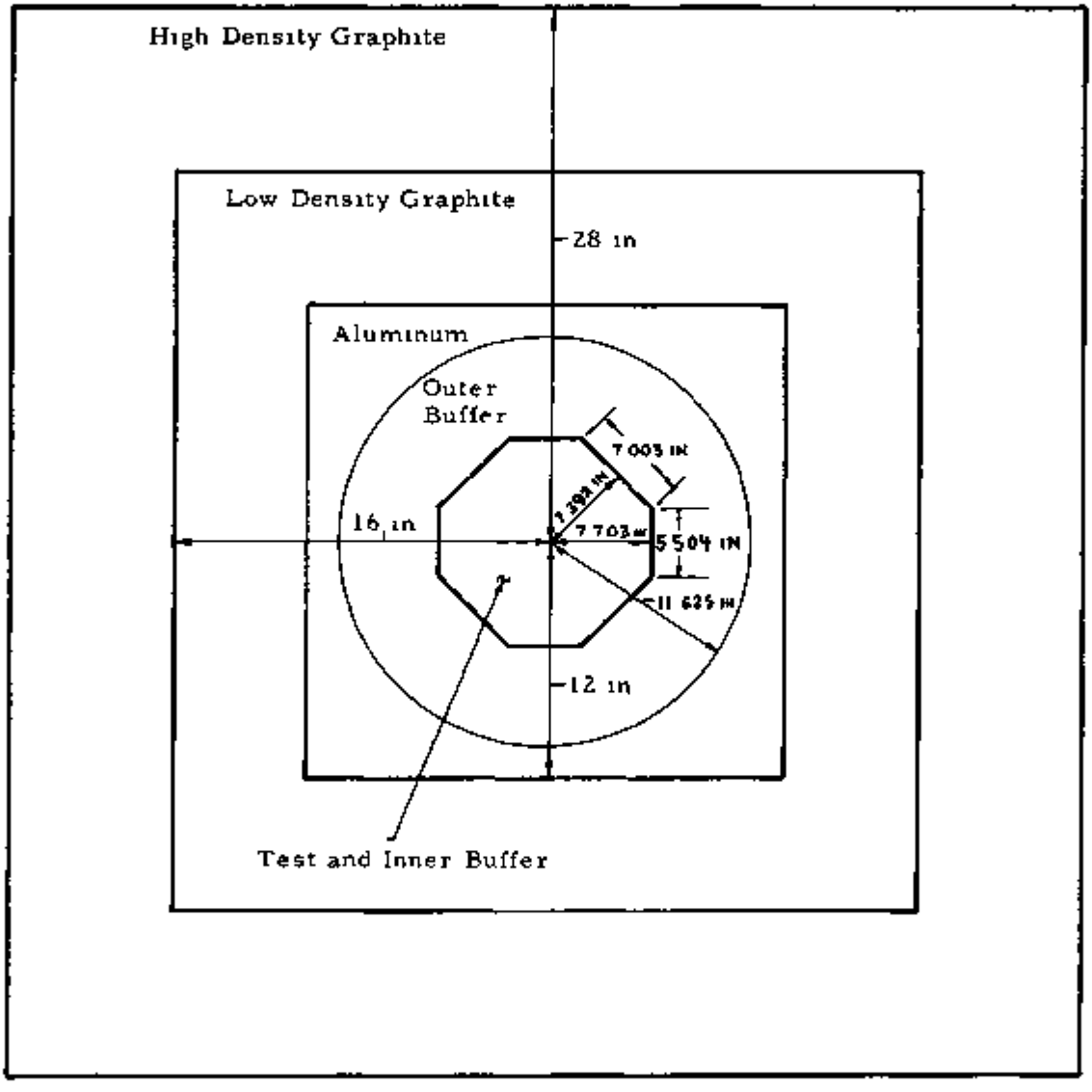

Figure B-4. Two-Dimensional Model for SLE Calculations (R-Z Geometry)

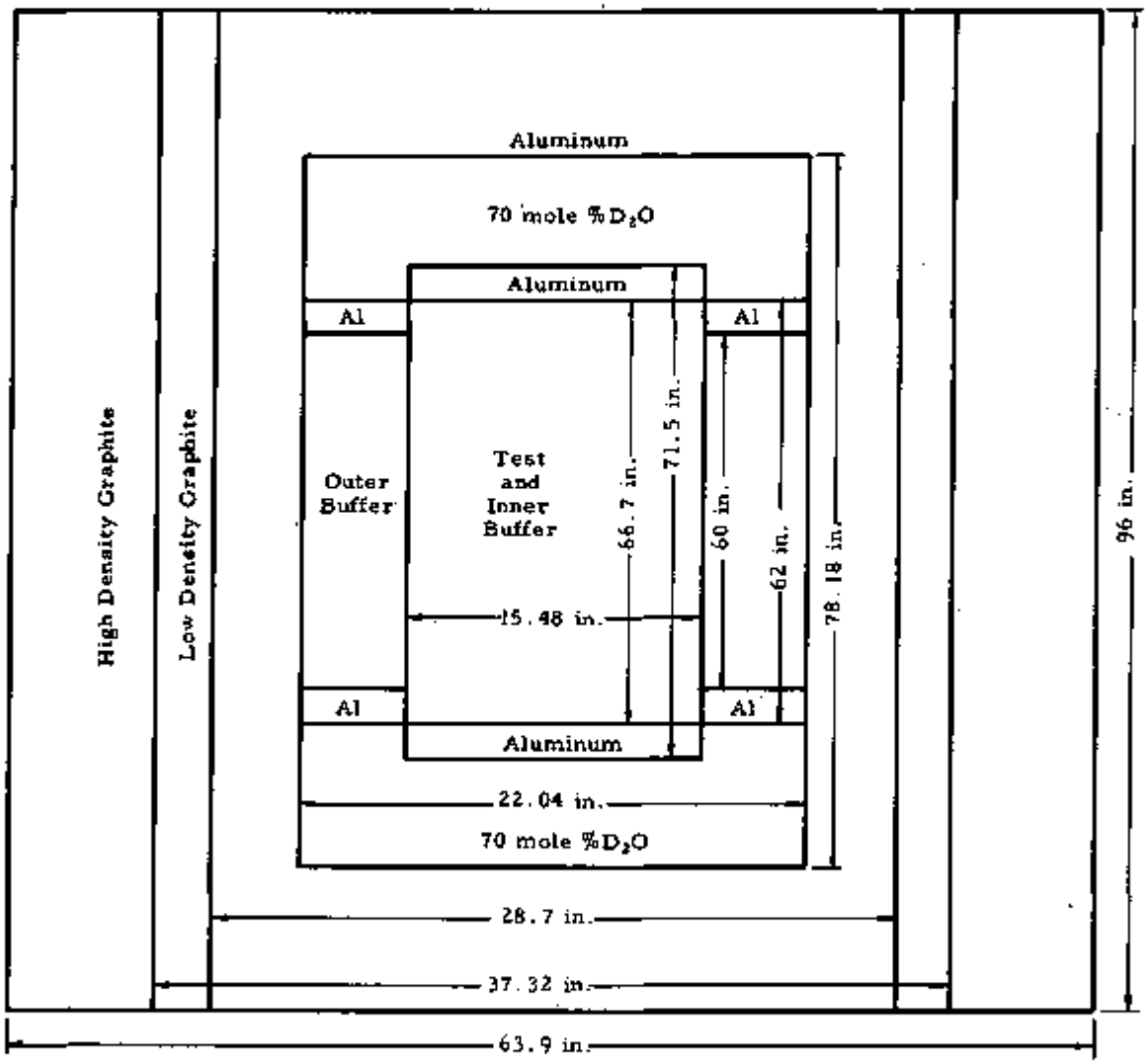

Figure B-5. Thermal Flux Distribution in Unpoisoned Test Region

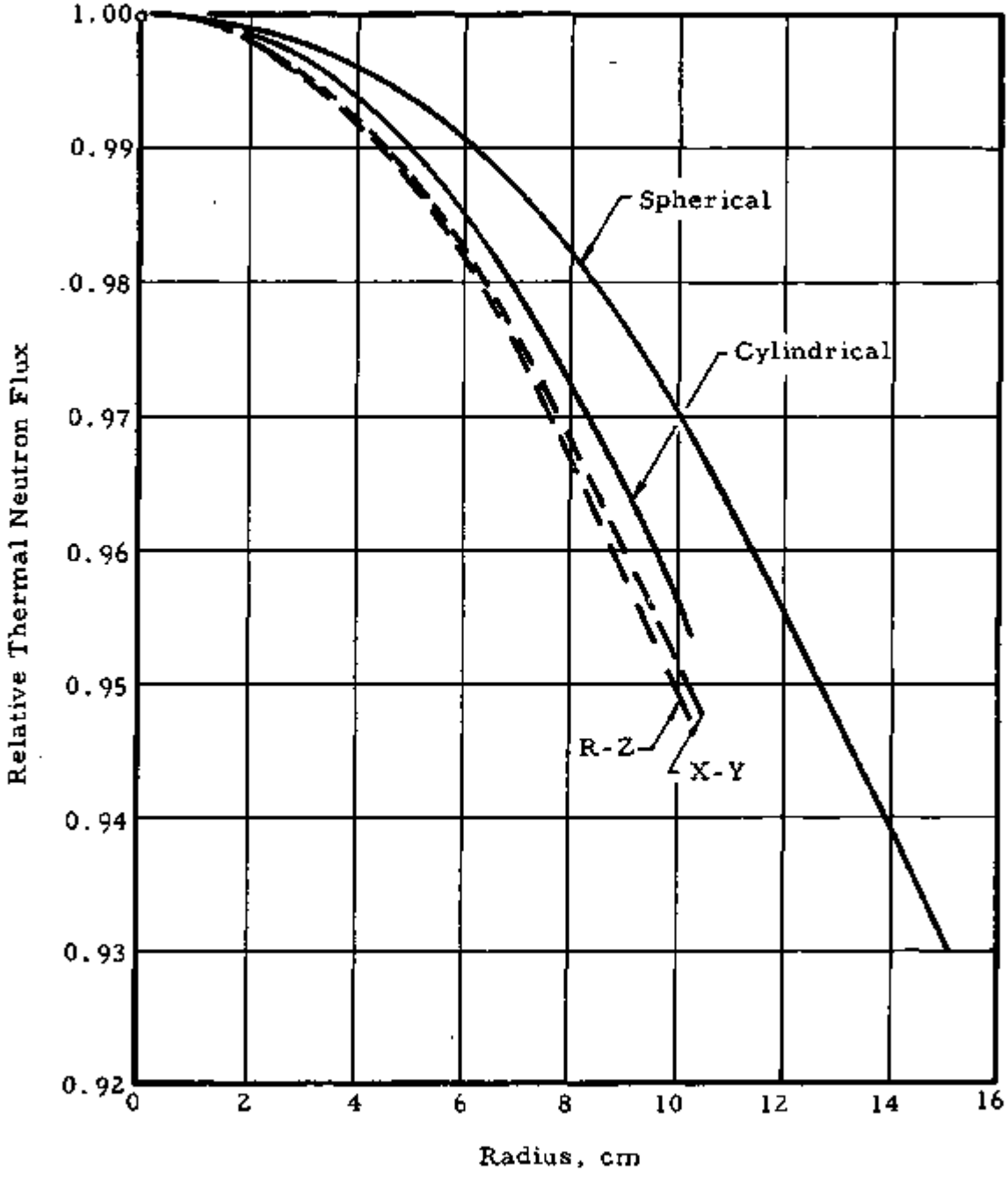

Figure B-6. X-Y Flux Distribution (Unpoisoned Test)

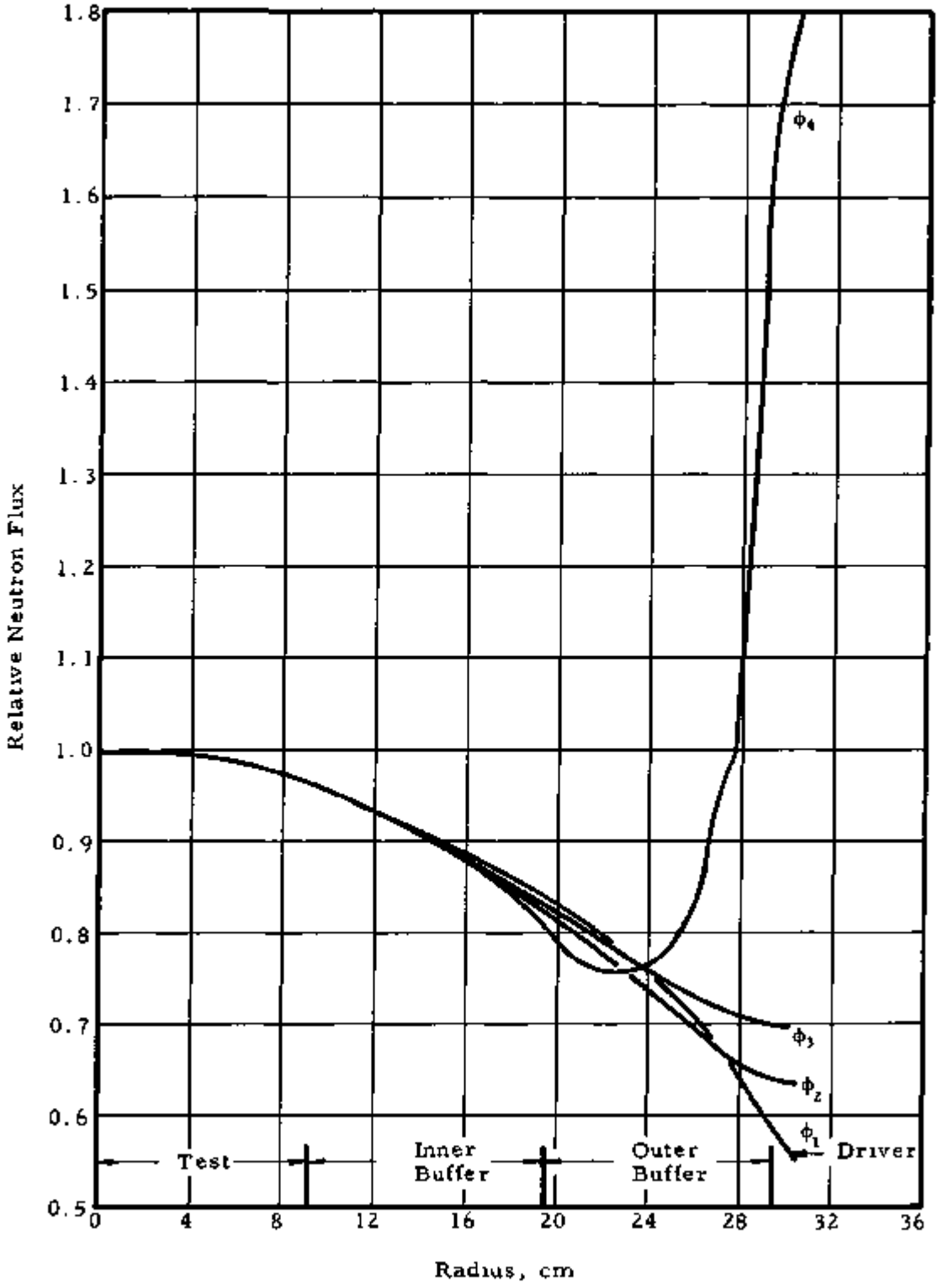

Figure B-7. Cylindrical Flux Distribution (Poisoned Test)

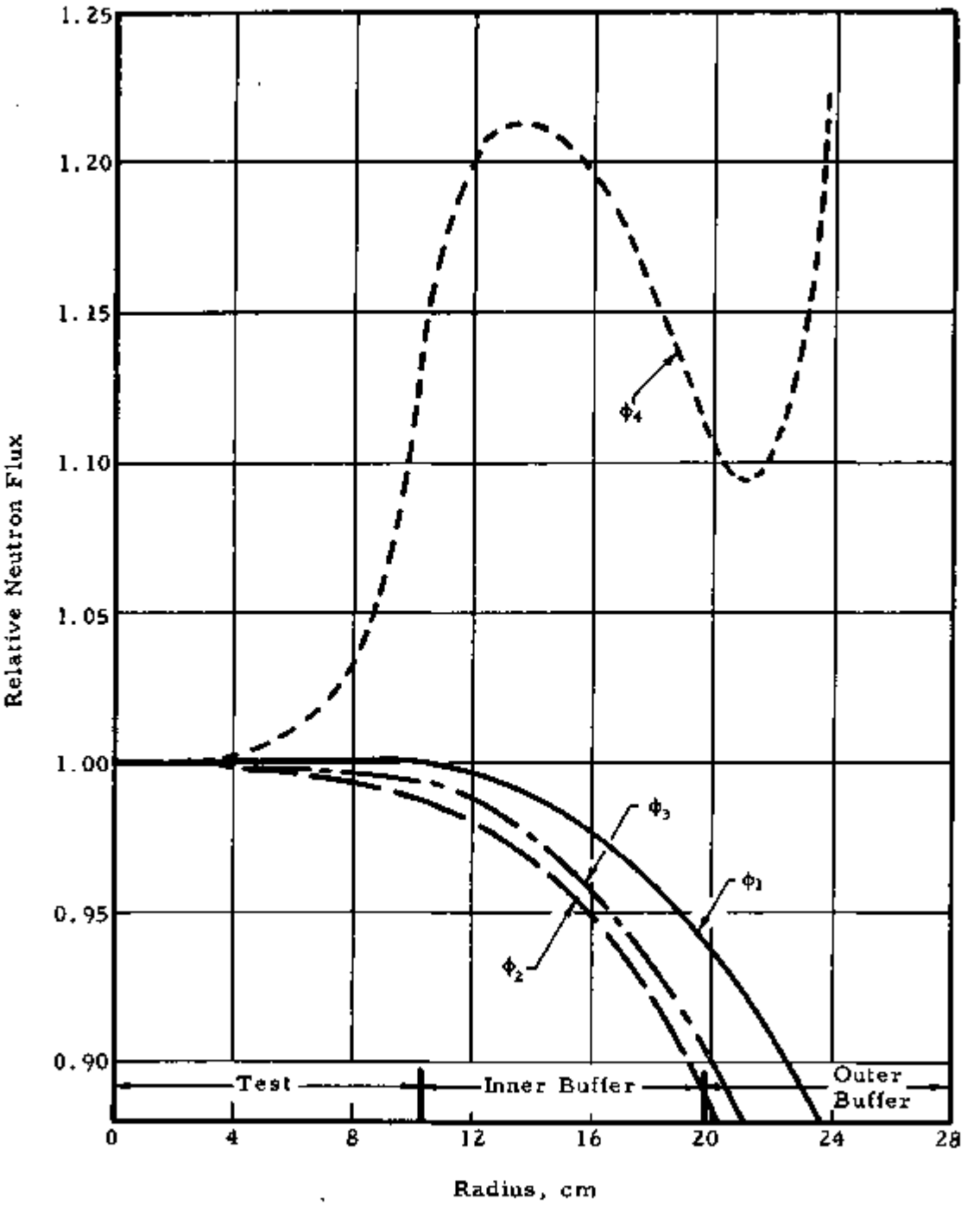

Figure B-8. Calculated Correction for Aluminum in Void Can

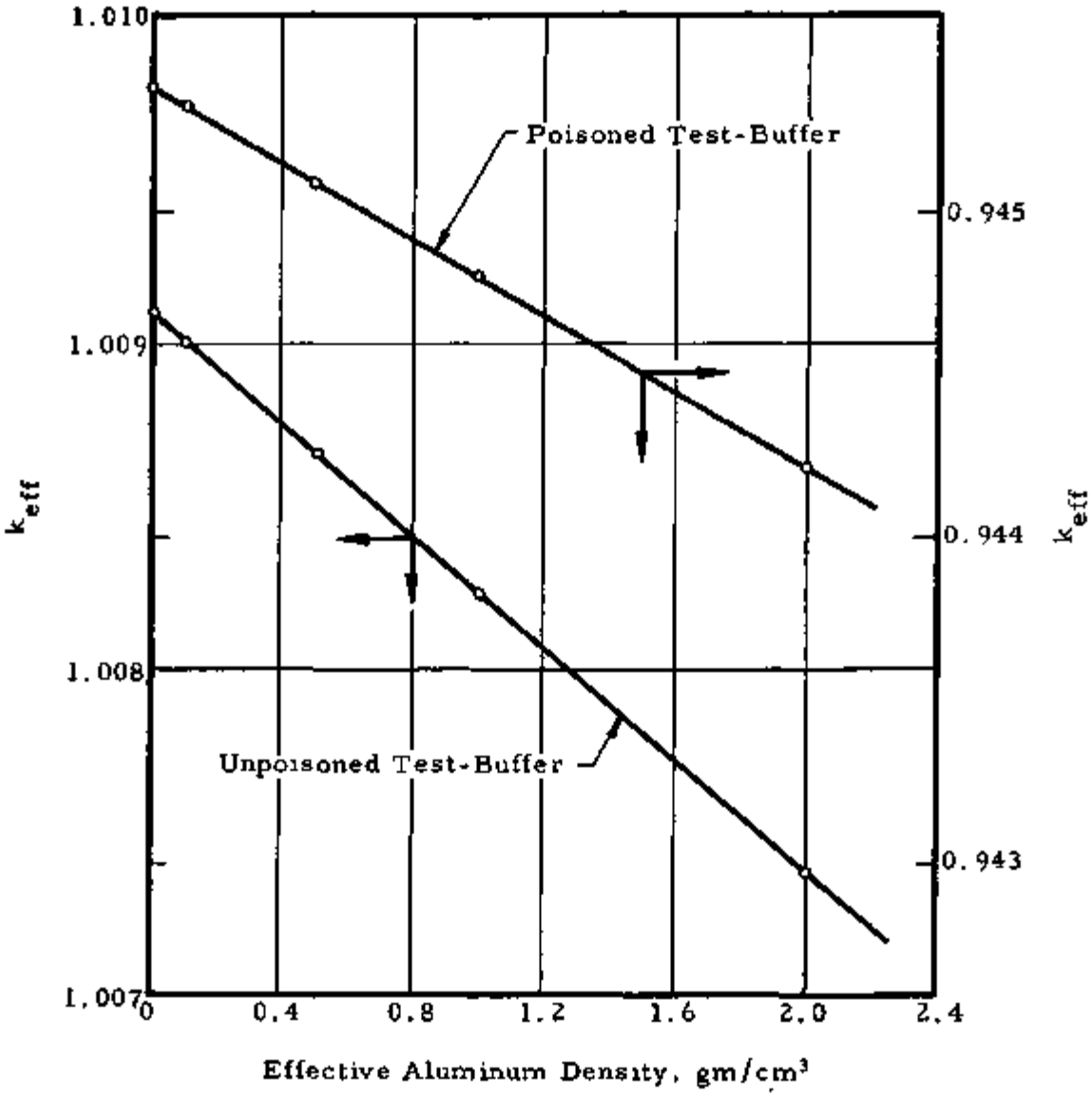

APPENDIX C

Measurements in Equivalent Critical Experiment

APPENDIX C

Measurements in Equivalent Critical Experiment

1. Description

A critical experiment having properties identical to those of the 4.02%-enriched UO_2 test region lattice described in Section 4 was assembled to provide a direct comparison of the equivalence of small lattice and critical experiment data. The critical experiment had identical fuel rods, lattice pitch, and moderator concentration; it differed, of course, only in size. A description of the facility used for these experiments and experimental details are given in Reference 3. Pertinent properties of the critical experiment are listed below:

Type of fuel	4.02%-enriched UO_2
Fuel rod outer diameter	0.4755 inch
Lattice pitch	0.595 inch
M/W ratio	1.006
D_2O concentration	69.7 ± 0.1 mole %
Number of fuel rods	2252
Core radius	40.46 cm
Reflector thickness	35.74 cm
Moderator height	151.0 cm
Radial buckling	15.13×10^{-4} cm^{-2}
Axial buckling	3.47×10^{-4} cm^{-2}
Critical buckling	18.60×10^{-4} cm^{-2}

2. Derivation of k_∞

The following procedure was used to derive k_∞ from the critical experiment data. Using the BPG-II code, k_{eff} was calculated with the buckling set equal to zero, i.e.,

$$k_\infty (BPG) = 1.12894$$

The calculation can be improved considerably by forcing the calculational model to match the experimental data. This is done by repeating the same calculation using the measured buckling. Then

$$k_{eff}\,(\text{BPG}) = 1.00218$$

For this case,

$$k_{eff}\,(\text{measured}) = 1.00000.$$

Therefore, normalizing the calculation to match the measured critical condition, the best value of k_∞ is

$$k_\infty = k_\infty\,(\text{BPG}) \times \frac{k_{eff}\,(\text{measured})}{k_{eff}\,(\text{BPG})} = 1.12648.$$

Another approach[14] can be taken that depends almost exclusively on experimental data. When the assembly is critical,

$$k_\infty = 1/P_{NL}$$

where P_{NL} is the buckling-dependent nonleakage probability. Although this expression is not rigorously correct, the more accurate representation

$$k_{eff} = (1 - \beta)\,k_\infty P_{NL}\,(\text{prompt}) + \frac{k_\infty}{\epsilon}\beta\,P_{NL}\,(\text{delayed})$$

leads to the same result within the accuracy desired. P_{NL} can be derived from the measured buckling and measured $\partial k/\partial B^2$ providing the leakage model is known. The measured value of $\partial k/\partial B^2$ was $-(7.7 \pm 0.2) \times 10^5$ ¢ - cm^2, or $-(60 \pm 3)$ cm^2 converted to absolute units using a calculated value of $\beta_{eff} = 7.8 \times 10^{-3}$ (accurate to about 5%). Using the two-group model,

$$P_{NL} = \frac{1}{(1 + L^2B^2)(1 + B_\tau^2)},$$

the measured $\partial k/\partial B^2$, and the measured buckling,

$$P_{NL}\,(\text{2-group}) = 0.888 \pm 0.004.$$

This value compares very well with the foregoing BPG calculation, based on the measured buckling

$$P_{NL}\,(\text{BPG}) = 0.88772$$

(Using a Gaussian kernel, which should be less applicable to these lattices, P_{NL} (Gaussian) = 0.894.)

The best value of k_∞ for the critical experiment depends on the choice of the leakage model. The multigroup BPG model is preferred on theoretical grounds and also because it matches k_{eff} and $\partial k/\partial B^2$ measurements in other D_2O-H_2O moderated critical experiments[3], as well as neutron age measurements in D_2O-H_2O mixtures[6]. The close agreement with the simpler two-group model (and even the Gaussian model) lends additional confidence in the validity of the BPG model. The uncertainty in k_∞ for the critical experiments is more difficult to estimate, but the choice is not crucial because of the close agreement with the SLE-derived k_∞. One estimate is the difference between the measured and BPG-calculated values of k_{eff}, or 0.002. Since this close agreement may be fortuitous, a more conservative estimate can be based on the uncertainty in P_{NL} (2-group) derived from the measured B^2 and $\partial k/\partial B^2$.

Therefore, the best value of k_∞ for the equivalent critical experiment is

$$k_\infty = 1.126 \pm 0.005.$$

3. Lattice Parameters

The thermal disadvantage factor $\overline{\phi}_m/\overline{\phi}_f$ and the cadmium ratios of U-235 and U-238, C_{25} and C_{28}, were measured in the central cell of the equivalent critical experiment to provide another basis for comparison with the small lattice experiment results. The measurements were made in Fuel Rod a using the same techniques described in Section 4.

$$\overline{\phi}_m/\overline{\phi}_f = 1.157 \pm 0.009$$

$$C_{25} = 2.434 \pm 0.012$$

$$C_{28} = 1.087 \pm 0.004$$

REFERENCES

[1] Heineman, R. E., Second UN International Conference on Peaceful Uses of Atomic Energy, A/Conf 15/P/1929, Geneva, 1958.

[2] Brooks, W. L., et al, PLATR-Test Report No. 1, United Nuclear Corporation, NDA-2131-40, June 1961.

[3] Engelder, T. C., et al, Measurement and Analysis of Uniform Lattices of Slightly Enriched UO_2 Moderated by D_2O-H_2O Mixtures, The Babcock & Wilcox Company, BAW-1273, Lynchburg, Virginia, November 1963.

[4] Engelder, T. C., et al, Measurement and Analysis of Perturbed Lattices of Slightly Enriched UO_2 Moderated by D_2O-H_2O Mixtures, The Babcock & Wilcox Company, BAW-1274, Lynchburg, Virginia, October 1963.

[5] deCoulon, G. A. G., Gates, L. D., Worley, W. R., SSCR Basic Physics Program, Theoretical Analysis, Part II, The Babcock & Wilcox Company, BAW-1230(II), Lynchburg, Virginia, March 1962.

[6] Wehmeyer, D. B., et al, SSCR Basic Physics Program, Theoretical Analysis, Part I, The Babcock & Wilcox Company, BAW-1230(I), Lynchburg, Virginia, March 1962.

[7] Engelder, T. C. and Doederlein, J. M., SSCR Basic Physics Program, Small Lattice Experiment Hazard Evaluation, The Babcock & Wilcox Company, BAW-1248, Lynchburg, Virginia, May 1962.

[8] SSCR Basic Physics Program, Quarterly Technical Report No. 7, The Babcock & Wilcox Company, BAW-1259, Lynchburg, Virginia, September 1962.

[9] SSCR Basic Physics Program, Quarterly Technical Report No. 8, The Babcock & Wilcox Company, BAW-1262, Lynchburg, Virginia, December 1962.

[10] SSCR Basic Physics Program, Quarterly Technical Report No. 9, The Babcock & Wilcox Company, BAW-1266, Lynchburg, Virginia, April 1963.

[11] SSCR Basic Physics Program, Quarterly Technical Report No. 10, The Babcock & Wilcox Company, BAW-1271, Lynchburg, Virginia, July 1963.

[12] Lewis, R. H., et al, Thermal Activation Method for ρ_{28} Measurements in Slightly Enriched UO_2 Lattices, The Babcock & Wilcox Company, BAW-1268, May 1963.

[13] Valarde, G., "Effective Diffusion Coefficient in Void Regions", Letter to the Editor, Nucl Sci & Eng 13, No. 2 (June 1962).

[14] Michalczo, J. T. and Neely, V. I., Nucl Sci & Engr 13, No. 6 (1962).

DISTRIBUTION

1. TID-4500, UC-80, 23rd Edition (619)

2. United States Atomic Energy Commission, New York Operations Office (5)

   Behmer, RE (3)
   Catalano, JJ
   Potter, HS

3. United States Atomic Energy Commission, Washington 25, D. C. (5)

   Hall, EE (2)
   Voigt, WR (3)

4. Brookhaven National Laboratory (2)

   Hellens, R
   Kouts, HJC

5. Hanford Atomic Products Operation

   Heineman, RE

6. Norwegian Atomic Energy Commission

7. The Babcock & Wilcox Company (65)

   Allen, RK
   Alliance Library
   Ball, RM
   Barberton Library
   Barringer, HS
   Blaser, RU
   Breazeale, WM
   CEL File (10)
   Central Files (10)
   Clark, RH
   Deuster, RW (3)
   Edlund, MC
   Engelder, TC (5)
   Fairburn, GT
   Gumprich, WC/Mumm, JF
   Hallam, JW
   Happell, JJ
   Harrison, RH/Moore, WT
   Hostetler, DR
   Jones, CE
   Landis, JW
   Lewis, RH
   Library, AED (2)
   Littrell, LW (2)
   Markert, W
   Pettus, WG
   Plunkett, DA
   Poor, HH
   Roberts, DM
   Roy, DH

7. The Babcock & Wilcox Company (Cont'd)

Schomer, RT
Schuler, TM, Jr.
Schutt, PF
Snidow, NL
Travis, CC/TRG
Webb, RA/Project File
Wehmeyer, DB
Williams, DVP
Woodhall, CB